REACHING QUANTUM POLARITONS

BLANCA SILVA FERNÁNDEZ

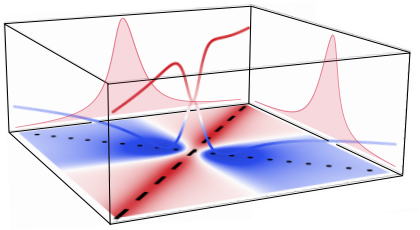

Advisors
Dr. Fabrice P. Laussy
Dr. Daniele Sanvitto

A dissertation submitted for the degree of
Doctor of Philosophy

Universidad Autónoma de Madrid
October 2016

To my family
They are always there for me

PREFACE

In this thesis I present the main results obtained during my PhD. The purpose of this work was the arrival to the quantum polaritonic limit for which two main methods were used. Although the first of them did not lead us to our final purpose, it did lead us to an expansion of the Hanbury Brown-Twiss effect (chapter 4). With the second approach we finally reached our initial goal: the arrival to the quantum polaritonics level.

The thesis is organized as follows:

The first chapter is a general introduction to polaritons and all the basic concepts of optics and photon correlations used along the thesis.

The second chapter is a state of the art chapter with deeper introduction of the experimental and theoretical methods.

For the first studies mentioned above we developed a new experimental setup for the measurement of the second-order correlation function with energy discrimination. This setup was based on a recent method for the measurement of this parameter by means of a streak camera.

Chapter three is a theoretical study of the streak camera: methods of data analysis, effects on the results of experimental unavoidable effects such as detector deficiencies, modulations on the signal, random noise, gravity peak and timing jitter. We managed to see the effect of each of them on the final result and, when possible, we backed-up our results with a theoretical model.

Chapter four includes the studies done on frequency filtered photon correlations of the emission of a condensate of exciton-polaritons. For this first attempt to reach the quantum limit we designed a new more efficient setup for the measurements of $g^{(2)}(\omega_1, \omega_2; \tau)$ and found an intrinsic property of bosons which we denominated *the form factor*, which we managed to explain both from a classical and a quantum point of view.

Finally chapter five includes our latest studies on quantum polaritons for which we made a new approach: single-photon excitation instead of classical excitation by means of a laser. With one entangled photon we were able to do this single excitation of the microcavity. This way we finally achieved the genuine quantum regime, both by proving single polaritons and by entangling polaritons with external photons. In addition, we also studied the polariton-polariton interaction, which showed the suppression of the entanglement as it increased.

"...we never experiment with just one electron or atom or (small) molecule. In thought experiments we sometimes assume that we do; this invariably entails ridiculous consequences... In the first place it is fair to state that we are not experimenting with single particles, any more than we raise ichthyosauria in the zoo" **Schrodinger, 1952**

ACKNOWLEDGMENTS

First, I'd like to thank my legs, for supporting me,
my arms, for always being by my side,
and my fingers, I could always count on them.

also..

First of all, I would like to thank Fabrice Laussy. He gave me an opportunity and for that I can not thank him enough.

Of course, I would also like to thank Daniele Sanvitto. He introduced me into the world of burning lasers and gave me the chance to work in one of the greatest laboratories.

After this thesis, I have grown to admire both of them. They are definitely some of the brightest scientists I have ever met and wonderful friends. I believe that I have been in one of the most important moments of their lives (they both became parents while I was doing the PhD) just like they have been in mine. Both Fabrice and Daniele have not only been wonderful thesis directors, but also friends and we have enjoyed together so many stories (the "orangefest", the cineforum, ...) that will remain in my heart forever.

Having two directors in two different cities (Fabrice in Madrid and Daniele in Lecce) implied going back and forth between both places, meeting lots of people in each of them and trying for the first time the experience of being alone in a new city, in a new country, with a new language, and it was a wonderful experience.

There are lots of people to thank in Madrid. I shall start with Carlos Sánchez. We started the degree together, afterwards the master and now we are finishing the PhD together; I have known him for 10 years already and owe him a lot; he is an incredible scientist and even more incredible person, for all that I will always be grateful. I also want to thank David (who just finished his PhD and will miss the Spanish lifestyle for sure), Juan Pablo (the kind of happy person that is good to have around), Camilo (who still has half his PhD left and has already achieved enormous results), Eduardo (the bassman) and Elena (who is not only a wonderful person, but also a bright scientist and a lovely mother). I

also want to thank all my friends from the office: Javi, Miguel and Diego, and my friday's "lunchteam", with whom I have laughed so much at the end of every week.

In Lecce I have met lots of incredible people (who managed to learn *Blanchiano* just to talk with me). I would like to thank the rest of the PhD students (some of them already doctors): Antoñete (whom you can make happy just by talking about funghi), Antonio (who makes *me* happy by means of burrata), Daniel (the youngest of all, to whom I wish a wonderful PhD), Francesco (la sala grossa!), Gianni (a very clever person who always managed to be in delay), Ste (with whom I learned a new way of dealing with the stress). Of course, I can't forget Dario, Lorenzo and Milena, they have taught me much more than they are aware of and made all the results possible. And last, but not least, Paolo, the technician of the lab, without whom everything becomes a total chaos! But Lecce was not only the laboratory, I also got to meet Rocío; a good friend and beautiful person. She managed to make the transition Spain-Italy easy (and introduced me to the spritz world!). And of course Luci, the cutest girl I've met.

During this thesis I worked with people from Rome (Álvaro Cuevas, Fabio Sciarrino, Paolo Mataloni, Luca Leuzzi and Fabrizio Antenucci) and from Napoli (Filippo Cardano and Lorenzo Marrucci); it was a pleasure meeting and working with all of them. I was also lucky enough to work with Alejandro González Tudela, nice, clever and hardworker.

I would like to thank specially Davidiño for so many things... for taking me to Porto Cesareo, for teaching me Italian and how to cook risotto, for being there when I needed him and so many others, but mainly for doing the PhD. Grazie Pu!

I would like to thank again Lorenzo Dominici and Alejandro Gonzalez Tudela for their additional revision of the thesis for the application for the international PhD.

Finally, there are three people I can not forget: my parents, wise, caring and loving; and my sister, strong and supporting, who will become a wonderful doctor.

CONTENTS

LIST OF FIGURES

ACRONYMS

APD Avalanche Photon Detector

BEC Bose-Einstein Condensate

BS BeamSplitter

CCD Charge-Coupled Device

CSI Cauchy-Schwarz inequality

CW Continuous Wave

DBR Difractive Bragg Reflector

DM Dichronic Mirror

EMW ElectroMagnetic Wave

F Focal length

FP Fabry-Pérot

FWHM Full Width at Half Maximum

HBT Hanbury Brown-Twiss

HO Harmonic Oscillator

HWP Half WavePlate

LASER Light Amplification by Stimulated Emission of Radiation

LPB Lower Polariton Branch

MASER Microwave Amplification by Stimulated Emission of Radiation

meV Milli-electron volt

n Refractive index

OPO Optical Parametric Oscillator

PBS Polarized BeamSplitter

PH PinHole

PM PhotoMultiplier

PPKTP Periodically Polarized KTP

Q Quality factor

QW Quantum Well

QWP Quater WavePlate

R Reflectivity

RIE Reactive Ion Etching

SHG Second Harmonic Generator

T Temperature

UPB Upper Polariton Branch

W Watt

2LS Two-level system

RESUMEN (CASTELLANO)

Los polaritones de tipo excitónico son quasipartículas generadas por la interacción de fotones con excitones (parejas de electrón-hueco) en un material semiconductor. Han recibido gran atención desde su descubrimiento en 1992 ya que unen el estado sólido, la materia condensada y la física atómina y de QED en cavidades. Su interés ha crecido exponencialmente con con la observación de efectos tales como la condensación de Bose-Einstein (año 2006), su propagación superfluida (2009), sus propiedades cuánticas hidrodinámicas y solitónicas (2010-2012) y más recientemente fases exóticas, ingeniería de bandas, puntos excepcionales (2015) y otros efectos topológicos. Puesto que los polaritones se obtienen como el autoestado del hamiltoniano polaritónico (siendo por lo tanto una superposición cuántica fotón-excitón) siempre han sido tratados como el ejemplo máximo de los objetos cuánticos, con propiedades tales como el entrelazamiento y otros tipos de correlaciones cuánticas. Sin embargo, esta concepción supone un abuso de la terminología, puesto que ha sido demostrado (y aceptado) que todos los resultados experimentales hasta el día de hoy pueden igualmente ser descritos de forma clásica. Pese a esto, una de las prioridades actuales del campo polaritónico es el alcance de su nivel cuántico, ya que los polaritones aportan los tan buscados fotones con la capacidad de interaccionar, necesarios para el desarrollo de la información cuántica. Varios grupos de investigadores han intentado llegar a este régimen por más de una década sin obtener resultados positivos. La causa principal de estos intentos fallidos se encuentra en los cimientos de la teoría, puesto que siempre se ha asumido que serían las interacciones polaritón-polaritón las que permitirían transformar un campo incidente clásico en uno cuántico.

Esta tesis explora nuevas fronteras, combinando teoría y experimento, para alcalzar el nivel cuántico de los polaritones. Para ello, se emplean sistemas con grandes correlaciones tales como configuraciones OPO y nuevas técnicas experimentales para el estudio de correlaciones entre fotones con discriminación energética usando una streak camera. Paralelamente, se han desarrollado modelos teóricos para explicar los resultados y la comprensión y contro de las incertezas experimentales y falta de eficiencia en las medidas. Pese a que el primer compendio de medidas no permitió alcanzar el régimen quántico, el estudio de las correlaciones entre dos fotones con discriminación en frecuencias a lo largo de todo el espectro nos proporcionó nuevas perspectivas en el estudio del efecto de Hanbury Brown-Twiss, expandiéndolo al reino de los bosones coloridos, que muestran anticorrelaciones junto con el bien conocido bunching (correlaciones positivas).

En un segundo intento de alcanzar el régimen cuántico polaritónico, desarrollamos otro experimento basado en la excitación del sistema directamente con luz cuántica. Es decir, en vez de autogeneración de estados cuánticos, facilitamos el proceso imponiendo una excitación con un único fotón. De este modo superamos el objetivo principal de esta tesis: creamos por primera vez polaritones en el régimen cuántico. Es más, la obtención de estos únicos polaritones involucraron también el entrelazamiento entre un polaritón y un fotón externo, demostrando también no localidad en un nivel macroscópico. Finalmente demostramos el interés del alcance de este régimen cuántico a partir del estudio de interacciones polaritón-polaritón introduciendo un único polaritón en un condensado de polaritones creado con excitación clásica, siendo ésta la primera medida de espectroscopía cuántica.

ABSTRACT (ENGLISH)

Exciton-polaritons are quasiparticles that arise from the interaction of photons with excitons (electron-hole pairs) in a semiconductor material. They have enjoyed a considerable attention since their discovery in 1992, since they bring together solid state, condensed-matter, atomic and cavity QED physics. Interest has been growing exponentially with subsequent reports of their Bose–Einstein condensation in 2006, of their superfluid propagation (in 2009), of their quantum-hydrodynamics and solitonic attributes (2010-2012), and, more recently, exotic phases, band-engineering, exceptional points (2015) and other topological features. Since polaritons, as eigenstates of the polariton Hamiltonian, are quantum superpositions of a photon and an exciton, they have always been regarded in the field as the epitome of quantum objects, featuring entanglement and other types of quantum correlations. This is however a (known and accepted) misuse of terminology as all the experimental findings so far can be equally accounted for by purely classical descriptions. Nevertheless, quantum polaritonics—bringing polaritons at the quantum-level—has remained a top priority of the field, for benefits such as providing the long-sought strongly interacting photons necessary for optical quantum information processing. While such attempts have been pursued by several groups for over a decade, they failed due to their relying on polariton-polariton interactions as the mechanism to turn an incident classical field into a quantum one.

This thesis explores new directions, combining theory and experiment, to reach the genuine quantum regime of polaritons, using strongly-correlated systems such as the OPO configurations and new experimental techniques, designed for the measurement of photon correlations with energy discrimination by means of a streak camera. Ad hoc theoretical models have been developed to explain the obtained results as well as to understand and control the effect

of the experimental uncertainties and deficiencies on the measurements. Although the first set of experiments did not achieve the quantum polaritonic regime, the measurement of the full frequency-frequency two-photon correlation spectrum provided us with a new perspective on the celebrated Hanbury Brown-Twiss effect, extending it to the realm of colored-bosons that also features anti-correlations in addition to the well-known bunching (positive correlations).

In a second attempt to reach the genuine quantum regime of polaritons, we pursued another method consisting in exciting directly the system with quantum light. That is to say, instead of self-servicing the generation of quantum states from within, we assisted this step by means of single-photon excitation. With this experiment, the main objective has been fulfilled: polaritons have been created and observed in the genuine quantum regime for the first time. Furthermore, this involved the entanglement of a polariton to a single external photon, and therefore also demonstrates nonlocality at a macroscopic scale. Finally, the interest of reaching such a quantum regime has been demonstrated through the studies of the polariton-polariton interaction, by injecting a single polariton into a condensate of exciton-polaritons obtained by classical excitation, thereby realizing one of the first instance of quantum spectroscopy.

ABSTRACT (ITALIANO)

I polaritoni eccitonici sono quasiparticelle che vengono a formarsi mediante l'interazione fra fotoni ed eccitoni (le coppie elettrone-lacuna) in un materiale semiconduttore. Essi hanno attratto una considerevole attenzione sin dalla loro scoperta nel 1992, fondamentalmente grazie alla loro capacità di unire la fisica dello stato solido, della materia condensata, atomica e della QED di cavità. L'interesse attorno ad essi è cresciuto esponenzialmente con le successive osservazioni della loro condensazione di Bose Einstein nel 2006, della propagazione in regime superfluido (nel 2009), della loro idrodinamica quantistica e la loro caratteristica solitonica (2010-2012) fino ad arrivare, più recentemente, alle fasi esotiche, punti eccezionali (2015) e altre proprietà topologiche.

Siccome i polaritoni, in quanto autostati dell'Hamiltoniana polaritonica, rappresentano la sovrapposizione di un fotone e un eccitone, essi sono sempre stati considerati nel campo il paradigma dell'oggetto quantistico, con capacità di entanglement e altri tipi di correlazioni quantistica. Ad ogni modo questo è un abuso, seppur noto e accettato, di terminologia essendo tutti gli esperimenti realizzati fin ora ugualmente spiegabili mediante descrizioni puramente classiche.

Ciò nonostante, la polaritonica quantistica—che porterebbe quindi i polaritoni al livello quantico—rimane un'assoluta priorità nel campo, in quanto permetterebbe di trovare i tanto a lungo cercati fotoni fortemente interagenti, componenti necessari allo sviluppo dell'elaborazione quantistica dell'informazione.

Nonostante per più di un decennio vari tentativi in questa direzione siano stati effettuati da diversi gruppi, essi sono falliti a causa delle interazioni polaritone-polaritone su cui erano basati per la promozione del campo incidente da classico a quantistico.

Questa tesi esplora nuove direzioni, ricombinando teoria ed esperimento, al fine di raggiungere un genuino regime quantistico polaritonico, mediante l'utilizzo di sistemi fortemente correlati come le configurazioni OPO e nuove tecniche sperimentali, designate appositamente per la misura delle correlazioni fotoniche con capacità di risoluzione in energia grazie all'utilizzo di una streak camera. Sono stati sviluppati modelli teorici appositi per spiegare i risultati ottenuti e al fine di capire e controllare l'effetto dell'incertezza sperimentale e delle carenze delle misure. Sebbene il primo set di esperimenti non abbia raggiunto il regime quantistico polaritonico, la misurazione dell'intero spettro di correlazione frequenza-frequenza a due fotoni, ci ha portato a nuove prospettive sul celebrato effetto di Hanbury Brown-Twiss, con la sua estensione al reame dei bosoni colorati e la conseguente anti-correlazione in aggiunta al ben noto bunching (correlazione positiva).

In un secondo tentativo di raggiungere il regime quantistico dei polaritoni, abbiamo approfondito un diverso metodo consistente nell'eccitare direttamente il sistema con luce quantica. Con questo si vuole dire che, al posto di provvedere alla generazione di uno stato quantico dall'interno, l'abbiamo assistito passo passo per tramite dell'eccitazione di un singolo fotone. Con questo esperimento, il principale obiettivo è stato soddisfatto: i polaritoni sono stati creati e osservati in un regime quantistico genuino per la prima volta. Per di più questo ha comportato all'osservazione dell'entanglement di un polaritone con un singolo fotone esterno, e ha dimostrato la nonlocalità su scala macroscopica.

Infine, l'interesse nel raggiungimento di questo regime quantico è stato dimostrato attraverso lo studio dell'interazione polaritone-polaritone, iniettando un polaritone singolo in un condensato di polaritoni ottenuto eccitando classicamente il sistema, realizzando, di fatto, uno dei primi esempi di spettroscopia quantistica.

1 INTRODUCTION

1.1 MICROCAVITY POLARITONS

1.1.1 *Microcavities*

A microcavity brings to the micrometer scale the concept of a "cavity" that is a trap for light and which allows to study interactions of light with matter in a controlled environment, a field known as cavity Quantum Electro-Dynamics. Specifically, a microcavity is an optical resonator close to, or below the dimension of the wavelength of light. There are two different ways to confine light: reflection off a single interface, as a metallic surface or at the boundary between two dielectrics. This method is the one used for micrometer-size or smaller cavities. The second way uses microstructures periodically patterned on the scale of the resonant optical wavelength, such as planar Distributed Bragg Reflectors (DBRs) or photonic crystals.

There are several types of microcavities: spherical, pillars, planar, stripes, etc. For the purpose of this work, the microcavities will be *planar* ones. They typically consist of a 2D-quantum well (the active part that traps material excitations) between two groups of DBRs. Their total reflectivity shows a broad spectral region of total reflectivity called *stop-band* (see Fig. 1a). These DBRs are designed such that, with a and b the thickness of the layers:

$$n_a a = n_b b = \frac{\bar{\lambda}}{4} \tag{1}$$

where $\bar{\lambda}$ is the central wavelength of the stop-band of the mirror. The cavity can be seen as a defect in the periodic structure of a DBR, opening a gap appear at the stop-band (see Fig. 1b), that is the *cavity mode*. For microcavities, the length of the cavity L_c is small (typically 0.2-0.4 μm) and there is only one cavity mode inside the stop-band (unlike in cavities, in which many cavity modes can be found in the stopband). Typically, L_c is an integer number of times larger than the width of one layer in the DBRs, such that $k_z L_c = j\pi$ for $\omega_c = \bar{\omega}$. Inside the microcavity, there are the longitudinal modes $\omega_c = n\lambda/2$ (with n an integer number) and transversal modes, with different spatial shapes.

Several properties are important for the characterization of a microcavity:

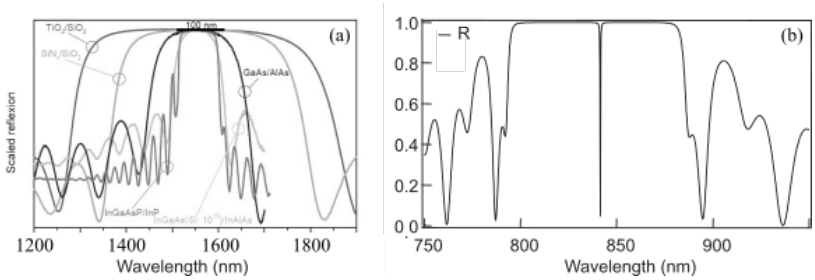

Figure 1: Two examples of stop-band. (a) Stop-band of DBRs of various materials. (b) Stopband for a DBR with a QW, a dip in the center of the stopband appears. (Adapted from from Ref. [67]).

- **Q-factor (or Quality Factor)**: the rate at which the optical energy decays from within the cavity (due to absorption, scattering or imperfect mirrors)

$$Q = \frac{\omega_c}{\delta\omega_c},$$

- **Finesse**l

$$F = \frac{\Delta\omega_c}{\delta\omega_c} = \frac{\pi\sqrt{R}}{1-R},$$

- **Lifetime of the photons**:

$$\tau = \frac{Q}{\omega_c},$$

where ω_c is the frequency of resonance of the cavity, $\delta\omega_c$ is the FWHM of the cavity mode, R the reflectivity and $\Delta\omega_c$ is the frequency separation between consecutive longitudinal cavity modes, defined as $\Delta\omega_c = 2\pi c/L$, with L the size of the cavity.

1.1.2 *Light-matter coupling*

As already mentioned, microcavities typically contain a 2D quantum well. When placed at the center, it sits at the antinode of the optical field and thus maximises the interaction with the light trapped by the cavity and the material excitation of the quantum well. When an electron in the valence band of the latter is excited to the conduction band by the standing mode of light, it leaves a hole in its initial band. This hole can bind with the original electron due to Coulomb interations (this depend on the material), creating correlated electron-hole pairs called *excitons*.

Figure 2

Assuming that the QW is made from a material having an excitonic transition at the frequency ($\tilde{\omega}_0$) close to the eigenfrequency of the photonic mode of the cavity (ω_c), the polaritons can be modeled by two coupled harmonic oscillators, the exciton and the cavity:

$$(\tilde{\omega}_0 - \omega - i\gamma)(\omega_c - \omega - i\gamma_c) = V^2\,, \tag{2}$$

where γ_c are the radiative losses of the cavity and V is the coupling between the exciton and the cavity given by:

$$\begin{aligned} \gamma_c &= \frac{1-\bar{r}}{\bar{r}\frac{n_c}{c}(L_{DBR}+L_c)}\,, \\ V^2 &= \frac{1+\bar{r}}{\bar{r}}\frac{\Gamma_0 c}{n_c(L_{DBR}+L_c)}\,. \end{aligned} \tag{3}$$

Diagonalization of equation 2 leads to:

$$\begin{aligned} \omega_{1,2} = {} & \frac{\omega_0+\omega_c}{2} - \frac{i}{2}(\gamma+\gamma_c) \\ & \pm\sqrt{(\frac{\omega_0-\omega_c}{2})^2 + V^2 - (\frac{\gamma-\gamma_c}{2})^2 + \frac{i}{2}(\omega_0-\omega_c)(\gamma_c-\gamma)}\,. \end{aligned} \tag{4}$$

This equation has two different regimes: the weak coupling and the strong coupling. In the weak coupling regime, $V < |\frac{\gamma-\gamma_c}{2}|$ leading to a crossing between the photon and the exciton bare bands while the decay rate of the exciton is enhanced. On the other hand, in the strong coupling regime, $V > |\frac{\gamma-\gamma_c}{2}|$, there is

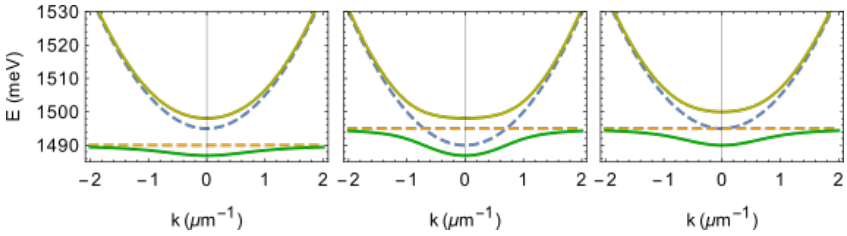

Figure 3: Energies of polaritons for three different regimes: (a) positive detuning, (b) negative detuning and (c) zero detuning. The dark green line corresponds to the UPB, the blue dashed to the cavity mode, the yellow dashed to the exciton and the bright green to the LPB.

an anticrossing and, in particular, a splitting of the eigenfrequencies when the bare frequencies are at resonance. This is known as the *Rabi splitting* and is one of the most important qualitative feature of strong light-matter coupling. Its magnitude is $\Omega = \sqrt{4V^2 - (\gamma - \gamma_c)^2}$. This gives rise to new bands, known as the upper polariton branch (UPB) and the lower polariton branch (LPB). Figure 3 displays the corresponding dispersions as a function of an in-plane momentum k, that make interact an exciton and a photon of different energies since their bare dispersions are very different. Indeed, the photon dispersion E_C appears to be essentially parabolic, and therefore massive, due to confinement in the microcavity axis, while the exciton dispersion E_X on such a scale is essentially flat, since it has a much heavier mass than the confined photon. The energy difference between the two dispersions minima is known as the detuning $\Delta = \omega_c - \omega_0$, and the figure depicts the eigen-energies for the polaritons for three different detunings, the last case corresponding to resonance where the coupling is maximum at $k = 0$. The second case realizes the resonant condition for a finite k while the first case is always out of resonance. Note that various dispersions with different types of light-matter interaction can be realized in this way.

The above considerations were entirely classical. Polaritons, as resonances of coupled oscillators, can be given a quantum flavour and interpreted as quasiparticles by casting them in a quantum formalism. Namely, we write a light-matter coupling Hamiltonian, to be evolved by the Schrödinger equation:[1]

1 Dissipation is an important attribute of polaritons, and this is accurately described by a Liouville—von Neumann equation, but a straightforward and often effective shortcut still within a Schrödinger equation is to turn to a non-Hermitian Hamiltonian:

$$\hat{H} = \begin{bmatrix} E_c - i\gamma_c(k) & \Omega/2 \\ \Omega/2 & E_x - i\gamma_x(k) \end{bmatrix}. \tag{5}$$

$$\hat{H} = \begin{bmatrix} E_c & \Omega/2 \\ \Omega/2 & E_x \end{bmatrix} . \tag{6}$$

In this way, polaritons arise as eigenstates of this 2×2 matrix and, in the quantum formalism, read:

$$|\Psi\rangle = \chi_c |1,0\rangle \pm \chi_x |0,1\rangle , \tag{7}$$

with χ_c and χ_x the so-called *Holpfield coefficients* that weight the polaritons with their photon and exciton component, and $|n_a, n_b\rangle$ the number of photon (n_a) and exciton (n_b), respectively. At resonance (3rd case of figure 3), the admixture is maximum and polaritons are two of the maximally entangled Bell states:

$$|U\rangle = \frac{1}{\sqrt{2}}(|1,0\rangle + \chi_x |0,1\rangle) , \tag{8a}$$

$$|L\rangle = \frac{1}{\sqrt{2}}(|1,0\rangle - \chi_x |0,1\rangle) . \tag{8b}$$

With a very modest theoretical background, we have already reached deep quantum waters. This is a well-known feeling in quantum-optics, that was recently captured by Jaynes' Ph. D student who reminisced on one of the most important result of the field—a slightly more involved variation of the above one—in these terms: "*Get your name in print: Diagonalize a* 2×2." [35].

Equations 8 immediately highlight the strong potential of polaritons for quantum physics. They are the molecules of a modern technology where the components are present but not at the same time. They are half-light, half-matter objects which, one can surmise, combine the best of two words: the high coherence of light with the strong interactions of matter. They are fascinating objects that drive a growing branch of solid-state optics, semiconductor physics and, since the report of their Bose–Einstein condensation in 2006 [63], condensed matter and quantum field theories.

The strong-coupling regime, and its associated Rabi splitting, has been predicted theoretically by various groups in the context of cavity QED, coupling an atomic transition to the single-mode of a cavity. From the start, this made a similar strong impression, strongly versed in the quantum regime [2, 95]. With the first report in 1990 of the strong-coupling between various atoms and a cavity mode by Zhu et al [123], it was however already clarified that the results were within the realm of classical optics in the linear regime (discarding second order elements such as intensity), as the transmission of an Electromagnetic wave passing through two identical mirrors and modeling the atoms as Lorentz oscillators. In the words of the authors:

> This splitting, termed the vacuum Rabi splitting, has attracted the attention of the quantum-optics community because it is considered

> to be an important manifestation of the quantum nature of the electromagnetic field. [...] We find that our experimental results are in excellent agreement with a *completely classical* model in which the cavity transmission function is derived using the standard concepts of multibeam interference applied to a cavity containing atoms displaying *linear* absorption and dispersion. This approach to calculating the cavity's transmission function is dramatically different from the one employed in QED descriptions of the problem. The success of a totally classical model indicates, contrary to popular belief that the vacuum Rabi splitting is not an inherently quantum phenomenon.

Here we have a perfect example of a result that can be equally well described by both the classical and the quantum theory. More than the approach, what is dramatically different is the interpretation of the state that takes place in the cavity. On the one hand, the epitome of quantum physics, a one-particle counterpart of Schrödinger's cat who came to life (no pun intended) to supposedly demonstrate the absurdity of the concept of entanglement, on the other hand, a rather innocent if not trivial concept of "normal modes" of two coupled oscillators.

We will come back repeatedly to the use (and abuse) of such a quantum character of the polaritons.

Two years after the atomic case, in 1992, Weisbuch *et al.* [119] managed to observe strong-coupling between microcavity-photons and excitons by introducing an increasing number of QWs inside a Fabry-Pérot (FP) resonator at the wavelength of the excitons. More quantum wells allow a stronger exciton-photon coupling and leads to the strong coupling (in this specific case with a minimum of 5 QWs). To model their results, they used the theory of Zhu *et al.* with excitons (also modeled as Lorentz oscillators). While in these times, even the cavity was called a "quantum microcavity", it was therefore appreciated that the phenomenon was intrinsically (still) within the confines of classical physics.

1.1.3 *What are polaritons good for?*

Another breakthrough for polaritons came with the report by Savvidis *et al.* from a collaboration between the groups of Southampton and Sheffield [99] of the Bose stimulation of polaritons in a pump-probe experiment. This demonstration of bosonic effects put polaritons in a new light. Being a mixture of light and matter, polaritons can combine the advantages of both photons and excitons. Thanks to the excitonic component, strong nonlinearities are possible, while thanks to the photonic component, the effective mass of the polaritons

can be $\sim 10^4 - 10^5$ times lower than the one of an electron. Being bosons, polaritons have the prospect of undergoing Bose condensation, in which all the particles have relaxed to the ground-state to form a macroscopic state. This happens at a critical temperature inversely related to the mass. Polaritons therefore appear as ideal particles for Bose-Einstein condensation (BEC) in the solid state [39, 63] and indeed the outstanding claim of room temperature Bose–Einstein condensation has been made [18] [2]. There are a few big differences with other bosonic particles though.

First of all, polariton condensates are typically strongly out-of-equilibrium due to their short lifetime ($\sim 2-4$ ps), and require continuous pumping to regenerate the polaritons that constantly exit radiatively from the microcavity as photons [67]. In several cases, condensation takes place not in the ground state but in an excited state. To overcome this, microcavities can be designed with higher Rabi splittings by changing the materials or by increasing the number of QWs [67]. It is only recently that "true equilibrium" polariton BECs started to emerge thanks to cavity with very long lifetimes, exhibiting the expected textbook Bose–Einstein distribution. Second, polaritons behave as bosons for small concentrations of particles. Their composite nature makes the problem of their interaction tricky as it is dominated by exchange terms of the underlying fermions (electrons and holes) and it has be argued that one cannot speak of several excitons but must deal with a multi-excitonic complex more akin to a BCS phase than to a superposition of structureless bosons. Finally, the light (photonic) part of the polariton makes it arguable that a concept for material particles should hold and that an interpretation in optical terms is not more adequate [70]. This debate is in some respects for BEC what our previous discussion is for the classical/quantum character of polaritons.

Nowadays, it appears that the 2006 Kasprzak *et al.*'s claim [63] has gathered a wide consensus, opening new perspectives for these particles. This condensation can lead to other important effects such as superfluidity [5, 7, 29, 66, 98], itself dragging along a rich dynamics of vortices [75, 76, 92, 98]. More recently, the field has enjoyed a fruitful activity surrounding solitons [8, 30, 44, 58, 103, 109, 117] (also coming with its share of controversies [6, 32]) and also joined the thriving field of topological order [45, 62, 85, 86, 111, 112]. An always promising support for any given field is that of applications, and here as well polaritons seem to promise worth-pursuing implementations [33, 46, 80, 102, 108]. Last but not least, even though their connection to, and their prospects for, quantum physics is rooted in their very fabric, polaritons are just recently emerging as candidates for quantum information processing and/or simulation [27, 38, 74, 79].

2 As "room temperature BEC" might have seemed too strong for the title, the denomination of "polariton lasing" was used there instead but Bose–Einstein condensation is back already in the abstract. The claim is substantiated by symmetry breaking, in this case, of the polarization.

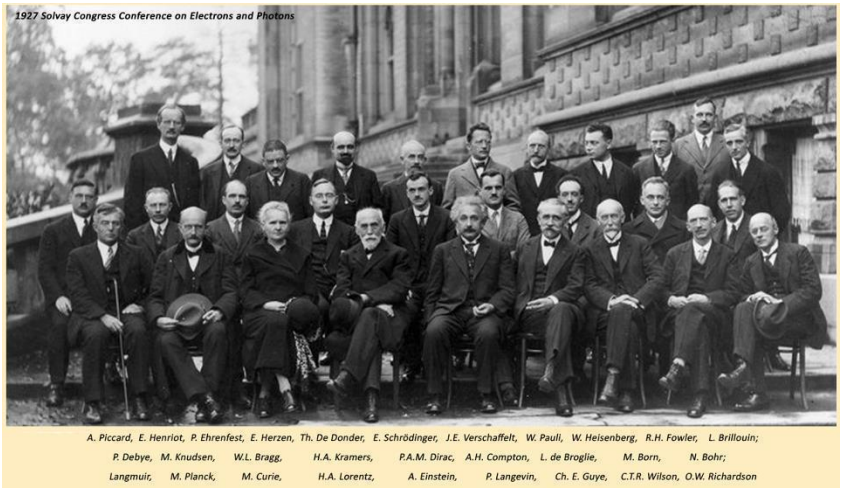

Figure 4: Photo taken during the Fifth Solvay conference: "Electrons and photons", to which all creators of quantum physics assisted for the unification of the definition.

Overall, it is clear that polaritons present considerable interest in all the branches of physics, at both a fundamental and applied level. Their most exciting promises remain those that take advantage of their quantum predisposition. We now focus on this aspect in more details.

1.2 WHAT IS QUANTUM PHYSICS?

When we look for the definition of "Science", we find (Oxford dictionary):

> The intellectual and practical activity encompassing the systematic study of the structure and behaviour of the physical and natural world through observation and experiment.

With such a definition, quantum physics must be seen as one of the prime examples of the scientific method, since it has been like no other field be jolted back and forth between experiment and theory.

The first observations of "strange behaviors" with a quantum flavor were made in the 17th and 18th centuries, when a description of a wave-like behavior of light was put forward, at the same time that a corpuscular theory seemed to be equally fit to account for other optical observables. Maxwell championed the wave worldview for light in the 19th century, at the same time that the corpuscular theory was coming back in force with the discovery of electrons by means of the cathode rays (Michael Faraday), the study of black body radiation

(Gustav Kirchhoff) and the proposal of discrete energy (Ludwig Boltzmann). Based on these results, Max Plank formulated his law that describes the spectral density of electromagnetic radiation emitted by a black body in thermal equilibrium at a given temperature T, involving a "quantization" of energy transfers. These results brought Einstein to the daring re-introduction of corpuscular worldview for light itself, which allowed his successful and correct interpretation of the photoelectric effect in 1905 [41], for which—rather than for any form of relativity (but along with "his services to theoretical physics")—he was attributed the Nobel prize. This made him study the concept of wave-particle duality, according to which electromagnetic waves can also be seen as particles (photons) with an energy defined by their frequency (the concept was generalized to all particles by de Broglie). In the mean time, several studies on atoms were taking place, and Bohr gave his famous "old-school" description of their structure, which basics were experimentally verified by Henry Moseley and Peter Debye. Niels Bohr took very strong views on quantum mechanics and brought Einstein's duality into a highly controversial concept of "complementarity". Along with a visiting Werner Heisenberg, he formulated the Copenhagen interpretation of quantum mechanics, which has proved to be one of the most popular interpretations for its practical aspects, although it is also one of the most decried. In this intepretation, the wavefunction Ψ (that since Born gives a probabilistic representation of the system) includes all the information that can be known on the system before a measurement is made to retrieve it, at which point the wavefunction collapses to an eigenstate of the observable (like opening the Shrodinger's box to see if the cat is alive or dead). Until this measurement, the system evolves smoothly and deterministically according to the Schrödinger equation:

$$i\hbar \frac{\partial}{\partial t} \Psi(\mathbf{r}, t) = \hat{H}\Psi(\mathbf{r}, t)\,. \tag{9}$$

A single measurement spoils completely this deterministic evolution so as to render it, in most cases, useless. It is only when repeating the same experiment (with the same wavefunction) several times that a consistent picture emerges, in terms of averages over the wavefunction. These follow Heisenberg's uncertainty principle (which limits the precision with which pairs of complementary variables can be measured). The wavefunction thus embeds as a particular case the wave–particle duality (i.e. the elementary particle behaves simultaneously as a particle and as a wave) depending on which observable is used to probe the system. Finally, when the quantum numbers are large, one reaches the classical limit, which is known as the correspondence principle. In this case, quantum "weirdness" is supposed to have faded out, which is why we experience a classical world. Although initially quantum physics was centered on the description of the behavior at the single-particle level, it quickly extended to "large-size"

object, at first conceptually with Schrödinger's cat as the first to have suffered the conundrum of quantum physics, until its realization in the laboratory, with superpositions of coherent states of light. Overall, one could enumerate four phenomena that classical physics cannot describe: the quantization of certain physical properties, entanglement, the principle of uncertainty and quantum superposition. The popular wave-particle duality is a particular case of those. From the very beginning, the theory sparked several controversies between the creators of this new science. For example, Einstein, resolutely in favour of both locality and causality, that both subtend relativity, famously claimed that *"God does not play dice"*. His thought experiment assuming local realism led him, with Podolsky and Rosen [42], to the famour EPR paradox, supposedly demonstrating on logical grounds that there are hidden variables (baring a "spooky action at a distance"). With an elegant, technically simple (in the formulation of Bohm) but exceptionally far-reaching reasoning on the consequences of local realism, Bell brought the problem from the realm of philosophical debates and "Gedankenexperiment" to that of a falsifiable experiment, by finding inequalities (*Bell's inequalities*) that are violated according to quantum mechanics but are satisfied according to a classical (non-local realistic) theory involving hidden variables to encode the informations that escape the wavefunction. In the tradition of Science, the experiment was then performed to referee on the issue, by Aspect *et al.* [10] and quantum mechanics was found to be correct. Bell commented about his findings: "*My theorem answers some of Einstein's questions in a way that Einstein would have liked the least*". Other noteworthy reactions from before or after this consecration of quantum mechanics include Schrödinger himself: "*If we are going to have to put up with these damn quantum jumps, I am sorry that I ever had anything to do with quantum theory*". Jaynes, one of the forefathers of quantum optics, who first fully quantized the light-matter interaction problem to show that quantization of light was not, in fact, necessary (a view that fell out of favour today), had hard words for "*Bohr's vague, puzzling sentences always groping for the right word, never finding it*" or Oppenheimer who "*always wanted to make the world still more mystical, and less rational*", what Jaynes considered as "*an anomaly, a basically anti-scientific attitude in a person posing as a scientist*". Even a promoter and champion of quantum theory, such as Richard Feynman, once said: "*I think I can safely say that nobody understands quantum mechanics*". One of the elegant interpretation of the quantum theory came from Hugh Everett, who arrived at the conclusions of multiple-universes each inheriting the various versions of reality, thereby getting rid of the less agreeable aspects of the alternative interpretations, as summarized by Everett himself in a 1957 letter to Bryce DeWitt:

> *The hidden variable theories are, to me, more cumbersome and artificial—while the Copenhagen interpretation is hopelessly incomplete because*

> *of its a priori reliance on classical physics [...] as well as a philosophic monstrosity with a "reality" concept for the macroscopic world and denial of the same for the microcosm.*

This comes at the price, however, of another "conceptual monstrosity" that everything that can happen does, in a parallel universe! This view was taken seriously by several prominent contemporary physicists, including David Deutsch, of "quantum computation" fame. He observes that computing is a real resource, and the massive parallelism implied by (some versions of) quantum computation ought to take place somewhere, and where-else than in the several universes running in parallel, each undertaking a copy of the the computation, that is completed by an ultimate interference bringing back the result to the one-universe of interest: that of the user of the quantum computer.

Still, quantum theory has long been admired and respected, chiefly for its exceptional accuracy and predictive power. In 1927 the Fifth Solvay International Conference on Electrons and Photons took place, where the world's most notable physicists met to discuss the newly formulated quantum theory. The leading figures were Albert Einstein and Niels Bohr. Seventeen of the twenty-nine attendees were or became Nobel Prize winners. It remains today one of the most important discipline in physics, both at an applied and fundamental level. Its promises for quantum technology made it an extremely topical problem, benefiting from an ever-increasing task-force and funding, to the point that quantum effects are sometimes advertised to an extent that is not fully justified. We will now give a brief overview of the opposite standpoint, that consists in tracking classical counterparts to supposedly quantum effects.

1.3 PHOTON CORRELATIONS

Classically, light is an electromagnetic wave, and it must follow Maxwell's equations [118]. In the ideal case, it would be a sinusoidal wave with well-defined frequency ω, amplitude E_0 and phase ϕ propagating along some axis (for simplicity we will set it to x) with a wavevector $k = \omega/c$:

$$E(x,t) = E_0 e^{i(kx-\omega t+\phi)} \tag{10}$$

Of course, there are several effects that destroy the simplicity of this assumption, such as temperature, the finite lifetime of the emitter, superposition of wavetrains, etc.

Coherence accounts for these effects. Coherence can be either temporal or spatial, being the temporal/spatial one the ability of inferring the signal at remote locations (time or space) from its knowledge at a given point. The temporal/spatial interval of coherence is called the coherence time (τ_c))/length (l_c).

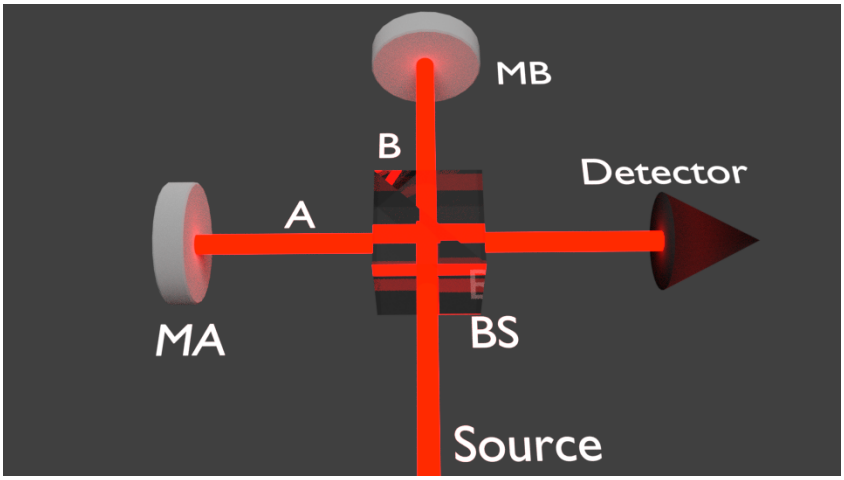

Figure 5: Michaelson interferometer: light arrives to the beamsplitter (BS) and is divided into two beams (A,B) that are reflected by two mirrors (MA,MB) and sent back to the BS, where they interfere and exit to the detector. The temporal delay τ can be modified by changing the distance between the mirrors and the beamsplitters.

This describes the *first-order coherence*, giving deep information about the light, but yet not enough. Since it is a correlation between signal at different times/positions, it's a *correlation*. Since the correlation is between the signal and itself, it's refered to as *autocorrelation*.

In the case of the temporal coherence, to study the information given by $E(t_0)$ about other times $E(t)$, the product $E(t_0)E(t)$ must be studied and averaged over several measurements, $\langle E(t_0)E(t)\rangle$. When this value is studied, normalizing in order to avoid the dependence on the absolute amplitude, the *first-order coherence degree* is defined:

$$g^{(1)}(t,\tau) = \frac{\langle E^*(t)E(t+\tau)\rangle}{\langle |E(t)|^2\rangle} \tag{11}$$

being $\tau = t_0 - t$. This parameter gives information about the coherence of the signal, being equal to 1 in coherent one. On the other hand, being A and B independent signals $\langle AB\rangle = 0$. Hence, for incoherent signal $g^{(1)}$=0.

Experimentally, this correlation can be measured by means of the Michaelson interferometer. As can be seen in Fig. 5, the signal emitted by the source is sent to a beam splitter that will divide it into two equal beams(A and B). Both of them will go to two mirrors (MA and MB) that reflect them back to the initial BS, in which they will interfere and exit together from the 4th face of the BS to

get to a detector. The interference will build up fringes with visibility defined as:

$$\mathcal{V} = \frac{I_{max} - I_{min}}{I_{max} + I_{min}}, \tag{12}$$

with I_{max} the maximum intensity of the fringes and I_{min} the minimum one. This visibility is related to the first-order correlation by means of:

$$\mathcal{V} = |g^{(1)}(\tau)| \tag{13}$$

1.3.1 *Hanbury Brown-Twiss effect*

At the beginning of the 1950's Michaelson interferometer was used with the radar to measure star sizes. Yet, it implied huge space for the entire setup depending on the size. Hanbury Brown realized that intensity correlations should be able to give the same information in smaller setups "*if the radiation received at two places is mutually coherent, then the fluctuation in the intensity of the signals received at those two places is also correlated*" [24]. Based on this idea, he proposed a new type of interferometer for the radio astronomy [25] with the help of the mathematician Richard Twiss, in order to analyze the intensity correlations.

To prove the correct operation of this intensity interference, he used it in 1950 to measure the radius of the sun with two radio telescopes, which could have been done in a simpler way by means of the Michaelson interferometer (he said that it had been like "*building a stream roller to crack a nut*").

Despite this correct behavior of the intensity correlations for radio waves (classical fields), it was not obvious that it could also be applied to light. To test this idea, they used a beam from a lamp of mercury and a silvered mirror to split the beam in two, each of them sent to one detector. The found that these correlations increased as the delay between beams (modified by changing the length of one of the arms) τ decreased, showing that photons from a thermal source tend to be detected in pairs.

These counter intuitive results were criticized by various groups that tried to prove its incompatibility with quantum physics [23]. It was at the end of 1956 when Purcell managed to prove that, not only these results were as predicted by classical physics, but could also prove a connection between classical and quantum physics [91], opening a new study of physics: quantum optics.

In 1956, with Purcell's demostration in hand, Robert Hanbury Brown and Richard Twiss used the intensity interferometer [56, 57] for the study of the angular diameter of the star Sirius (sketch of the setup in figure 6). By means of two searchlights (left over from the Second World War) they managed to send the light emitted by the star to two different photomultipliers (PM) which

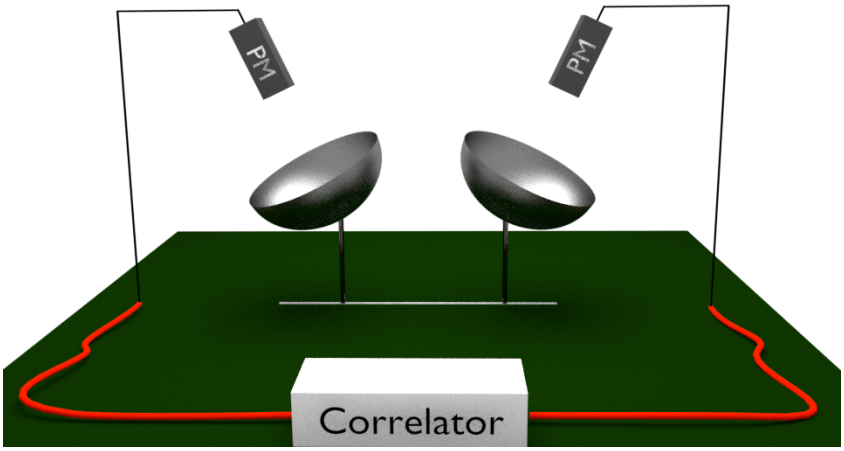

Figure 6: Sketch of the setup used by Hanbury Bronw and Twiss [56] for the measurement of intensity correlations.

had slits to cover the background noise and select only the signal of Sirius. The two detected signals on the PMs were correlated in a correlator as a function of the distance between each PM in order to change the delay between the two signals (τ).

While in the Michaelson interferometer (fig 5) the interference is done *before* the detection (in the BS) and the phase difference must be preserved, in this interferometer the correlation is between two signals, and is given *after* the detection (in the correlator), losing the relative phase. The self-interference of the Michaelson interferometer corresponds to *amplitude* correlation of the field, whereas the Hanbury Brown-Twiss is an *intensity* correlator of the detected signal [55].

When Hanbury Brown and Richard Twiss studied the correlations of the signal of Sirius (the star was selected since it was the only star bright enough to give a workable signal-to-noise ratio), they found the same shocking result: a positive simultaneous correlation of two signals which decreased by increasing the distance between them, and hence increasing the temporal delay τ (see fig 7). [3]

This tendency is easy to understand when thinking of wave superposition [19]. For simplicity, the experiment can be supposed to be of the form of figure 8, in which the initial light beam is considered two close emitters Q_1 and Q_2. And,

3 Curiosity: the entire experiment took 5 months, giving a total observation time of 18 hours, since measurements could only be done at the first and last quaters of the moon to avoid the noise given by the moon.

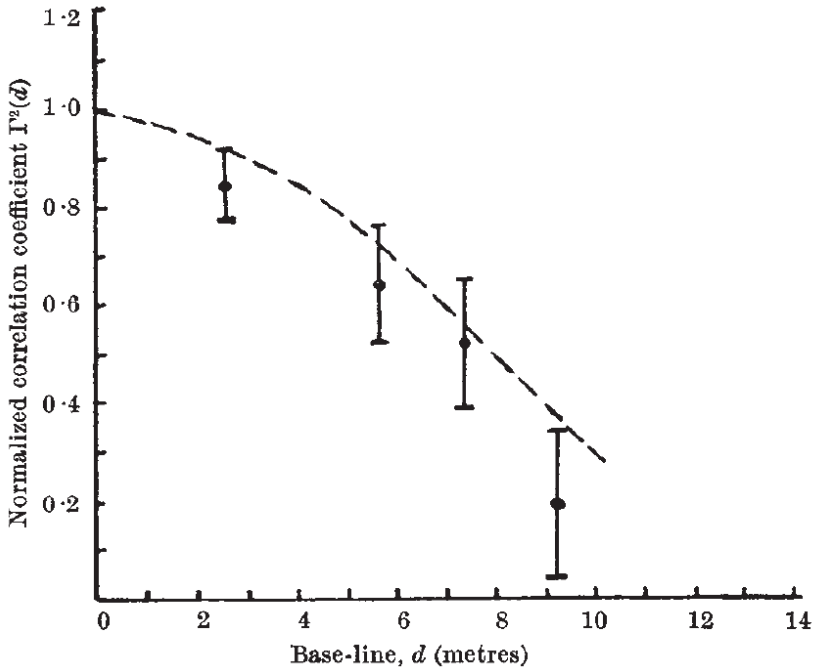

Figure 7: Changes on the correlation as a function of the distance between mirrors with the theoretical expected values for a star of the size predicted by Hanbury Bronw and Twiss [56].

as in the original experiment, the light is detected by two detectors D_1 and D_2. Both Q_1 and Q_2 emit coherent light with the same polarization and wave-number vector $\mathbf{k}_{1,2}$ and amplitude $a_{1,2}$ with random relative phases. Taking into account the signal of both sources, the amplitude in both detectors will be:

$$E_1 = E_{01} e^{i(\mathbf{k}_1 \cdot \mathbf{r}_1)} + E_{02} e^{i(\mathbf{k}_2 \cdot \mathbf{r}'_1)}, \tag{14}$$

$$E_2 = E_{01} e^{i(\mathbf{k}_1 \cdot \mathbf{r}_2)} + E_{02} e^{i(\mathbf{k}_2 \cdot \mathbf{r}'_2)}. \tag{15}$$

With these two definitions, the intensities on each detector will be:

$$I_1 = |E_1|^2 = |a_1|^2 + |a_2|^2 + \Re(a_1^* a_2 e^{i(\mathbf{k}_2 \cdot \mathbf{r}'_1 - \mathbf{k}_1 \cdot \mathbf{r}_1)}), \tag{16}$$

$$I_2 = |E_1|^2 = |a_1|^2 + |a_2|^2 + \Re(a_1^* a_2 e^{i(\mathbf{k}_2 \cdot \mathbf{r}'_2 - \mathbf{k}_1 \cdot \mathbf{r}_2)}), \tag{17}$$

which have an average value of:

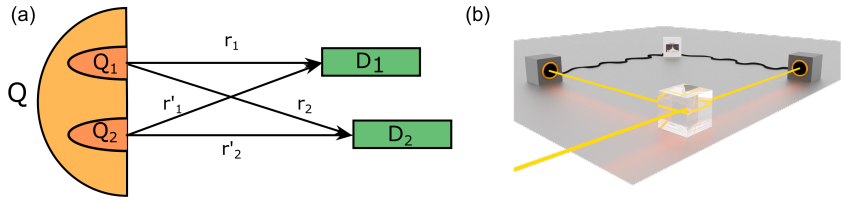

Figure 8: (a) Sketch of the setup considered for the theoretical model: the source Q is taken to be two sources Q_1 and Q_2, which emit the light to be detected in two different detectors D_1 and D_2. (b) HBT interferometer: the source is sent to a BS, which divides the signal into two new signals, each of which arrives to a different detector and finally these detections are correlated to obtain the intensity correlations.

$$\langle I_1 \rangle = \langle I_2 \rangle = |E_{01}|^2 + |E_{02}|^2 \,, \tag{18}$$

leaving no temporal dependence.

On the other hand, the probability of the interference of the signal in each detector is given by $\langle I_1 I_2 \rangle$ which, assuming both of them to be close enough such that $\mathbf{r}_1 - \mathbf{r}_2 = \mathbf{r}'_1 - \mathbf{r}'_2$, has the form:

$$\langle I_1 I_2 \rangle = \langle I_1 \rangle \langle I_2 \rangle + 2|E_{01}|^2 |E_{02}|^2 \cos[\mathbf{p}(\mathbf{r}_1 - \mathbf{r}_2)] \,, \tag{19}$$

with $\mathbf{p} = \mathbf{k}_2 - \mathbf{k}_1$. This function takes on a maximum for $\mathbf{r}_1 = \mathbf{r}_2$, explaining the results of Hanbury Brown and Twiss in which they found maximum interference where the distance difference was zero, which was after explained by Glauber [49] in terms of photon bunching (see section 1.3.2).

By analogy with the correlation function $g^{(1)}$ (see equation 11) defined for amplitude correlations, a new function can be defined: the second-order correlation function $g^{(2)}$, of the form:

$$g^{(2)}(t,\tau) = \frac{\langle E^*(t) E^*(t+\tau) E(t) E(t+\tau) \rangle}{\langle E^*(t) E(t) \rangle \langle E^*(t+\tau) E(t+\tau) \rangle} \,. \tag{20}$$

1.3.2 *Glauber theory*

With the arrival of quantum optics, the basic concepts had to be revised. From all of them the most problematic one was the coherence, which needed a new definition. This was done by Roy Glauber in 1963 [49, 50]. Originally in physical optics the term "coherence" was used to denote the tendency of two values of the field at distantly separated points or at greatly separated times to take on correlated values.

In his studies Glauber used the Heisinberg representation, with field operators $\mathbf{E}(\mathbf{rt})$, which he divided into two components: the positive frequency part ($\mathbf{E}^{(+)}(\mathbf{rt})$) and the negative frequency part ($\mathbf{E}^{(-)}(\mathbf{rt})$). This way $\mathbf{E}(\mathbf{rt}) = \mathbf{E}^{(+)}(\mathbf{rt}) + \mathbf{E}^{(-)}(\mathbf{rt})$, being the two components complex and mutually adjoint. The $\mathbf{E}^{(+)}(\mathbf{rt})$ term was equivalent to the photon annihilation operator (a) and the negative one corresponded to the creation operator ($a^{\dagger}$).

When dealing with quantum mechanics, the average of an observable depends on the density matrix in the way:

$$\{\langle|\, \mathcal{O}\,|\rangle\}_{av} = tr\rho\mathcal{O}\,, \tag{21}$$

where tr accounts for the trace of the matrix. With this in hand he defined the nth-order correlation function as:

$$\begin{aligned} &G^{(n)}(x_1, x_2, ..., x_{n+1}, ..., x_{n+2}) \\ &= tr\{\rho E^{(-)}(x_1)...E^{(-)}(x_n)E^{(+)}(x_{n+1})...E^{(+)}(x_{2n})\}, \end{aligned} \tag{22}$$

where $x_i = \mathbf{r}_i t_i$. The normalization of $G^{(n)}$ leads to the correlation function studied before his modification of the concept of coherence, and is of the form:

$$g^{(n)}(x_1, ...x_{2n}) = \frac{G^{(n))x_1,...,x_{2n}}}{\prod_{j=1}^{2n}\{g^{(1)}(x_j, x_j)\}^{1/2}}\,. \tag{23}$$

He introduced new conditions that should be infinite and should be satisfied by a fully coherent field:

$$\begin{aligned} &|g^{(n)}(x_1, ..., x_{2n})| = 1, \\ &n = 1, 2..., \end{aligned} \tag{24}$$

where x_i denotes a set of position,time variables ($x_i = r_i, t_i$).

Not all the fields that had been described as "coherent" before this new definition followed the condition 24. This lead to the definition of order of coherence. For the nth order of coherence $|g^{(j)}| = 1$ for $j \leqslant n$. Up to this point the coherence had been defined only for the case of $j = 1$, but the arrival of the maser (Microwave Amplification by Stimulated Emission of Radiation), which in principle was coherent to all orders, made this new definition of n-order mandatory.

The HBT effect is a clear example of this definition, since the signal sent to the detectors was coherent from the optical definition ($g^{(1)} = 1$), but the second order correlation function showed non-zero values at short times, known as bunching behavior.

Glauber also noted various times the negative HBT effect [48, 106], known as photon antibunching or the anticorrelation effect. With this last limit, any source of light can be described: for $g^{(2)}(0) > 1$ the signal is said to be bunched (with superpoissonian distribution), typical of classical sources such as thermal light; for $g^{(2)}(0) = 1$ the source is said to be coherentc(with poisonnian distribution), an example would be a laser; finally, for $g^{(2)}(0) < 1$ the source is antibunched (with subpoissonian distribution), which is a characteristic behavior of quantum systems such as the emission of a quantum dot.

These studies on quantum coherence lead to Glauber's nobel price in 2006 [51].

1.3.3 *Other quantum effects*

1.3.3.1 *Violation of Cauchy-Schwarz inequality*

The Cauchy-Schwarz inequality (CSI) for real numbers is of the form:

$$\left(\sum_{i=1}^{n} a_i^2\right)\left(\sum_{i=1}^{n} b_i^2\right) \leqslant \left(\sum_{i=1}^{n} a_i b_i\right)^2 . \tag{25}$$

This theorem has an important role in different branches of modern mathematics including Hilbert spaces theory, probability and statistics, classical real and complex analysis, numerical analysis, qualitative theory of differential equations and their applications [68, 84, 104, 105].

For the purpose of this thesis, we will center our studies of the CSI on optics and the second order correlation function.

In the previous section we defined antibunching as a function of the value of $g^{(2)}(0)$. Yet, a more precise definition is the following: $g^{(2)}(\tau) > g^{(2)}(0)$. This last property can be shown as a violation of CSI in the following way. Given the inequality:

$$2ab \leqslant a^2 + b^2 \tag{26}$$

the averages over t on the numerator and denominator of the $g^{(2)}$ will follow:

$$\left(\frac{E^*(t_1)E(t_1) + ... + E^*(t_n)E(t_n)}{n}\right)^2 \leqslant \frac{(E^*(t_1)E(t_1))^2 + ... + (E^*(t_n)E(t_n))^2}{n}, \tag{27}$$

where the term on the left corresponds to the denominator and the one on the right to the numerator of the $g^{(2)}(0)$, leading to $g^{(2)}(0) \geqslant 1$.

Following the same procedure with the inequality of equation 25:

$$\begin{aligned}&[E^*(t_1)E(t_1)E^*(t_1+\tau)E(t_1+\tau)+...+E^*(t_n)E(t_n)E^*(t_n+\tau)E(t_n+\tau)]^2\\ \leqslant&[(E^*(t_1)E(t_1))^2+(E^*(t_n)E(t_n))^2]\\ &[(E^*(t_1+\tau)E(t_1+\tau))^2+...+(E^*(t_n+\tau)E(t_n+\tau))^2]\,,\end{aligned} \tag{28}$$

which leads to:

$$g^{(2)}(\tau) \leqslant g^{(2)}(0)\,. \tag{29}$$

These two relations have been obtained by means of CSI, which applies to poissonian and superpoissonian photon distributions, hence a violation of 28 corresponds to a subpoissonian limit, i.e. the quantum regime.

1.3.3.2 *Entanglement*

Of all the principles and properties of quantum physics, the hardest to understand (or even accept) is the entanglement, which claims a non-local connection between particles. The most typical example are two entangled electrons with opposite spin. Based on quantum mechanics, if each of them follows a different path, the spin of them can't be identified without measuring it, at which point the wavefunction collapses and sets the spin of the second electron.

Bell states:

$$\begin{aligned}\left|\Psi^{\pm}\right\rangle &= \frac{1}{\sqrt{2}}(\left|H\right\rangle_1\left|V\right\rangle_2 \pm \left|V\right\rangle_1\left|H\right\rangle_2),\\ \left|\Phi^{\pm}\right\rangle &= \frac{1}{\sqrt{2}}(\left|H\right\rangle_1\left|H\right\rangle_2 \pm \left|V\right\rangle_1\left|V\right\rangle_2)\,.\end{aligned} \tag{30}$$

When studying entanglement, the measurement done is of the density matrix ρ. In the specific case of this work, the entangled states (see section 5) used will be the $\Psi^{\pm}$, for which the density matrix has the following form:

$$\mathcal{R}e(\rho^{\pm}) = \frac{1}{2}\begin{pmatrix}0 & 0 & 0 & 0\\ 0 & 1 & \pm 1 & 0\\ 0 & \pm 1 & 1 & 0\\ 0 & 0 & 0 & 0\end{pmatrix}, \tag{31}$$

$$\mathcal{I}m(\rho^{\pm}) = \frac{1}{2}\begin{pmatrix}0 & 0 & 0 & 0\\ 0 & 0 & 0 & 0\\ 0 & 0 & 0 & 0\\ 0 & 0 & 0 & 0\end{pmatrix}. \tag{32}$$

There are several parameters that characterize the purity of an entangled state. Out of all of them, the most important ones are:

- $\hat{\rho} = |\Psi\rangle \langle\Psi|$
- $Tr(\hat{\rho}^2) = 1$
- Entropy $S(\hat{\rho}) = -Tr[\hat{\rho} ln \hat{\rho}] = 0$
- Concurrence $\mathcal{C} = 1$, being $\mathcal{C} = max(0, \lambda_1 - \lambda_2 - \lambda_3 - \lambda_4)$ where λ_i are the eigenvalues of $\sqrt{\sqrt{\hat{\rho}}\tilde{\rho}\sqrt{\hat{\rho}}}$ in decreasing order with $\tilde{\rho} = (\sigma_y \otimes \sigma_y)\hat{\rho}^T(\sigma_y \otimes \sigma_y)$

1.3.3.3 *Bell inequalities*

One of the main laws of Einstein's special relativity is the impossibility of information transport between two points outside of the light cone, which delimits the maximum velocity of transmission to the one of light. This law contrasts with entanglement in the non-locality paradox addressed by Einstein, Podolsky and Roosen (EPR) in 1935 [42] and later by Bohm [21]. EPR proposed an experiment, known as the *gedankenexperiment*, in which a source emits pairs of spin $\frac{1}{2}$ particles in a singlet state. Once these particles are apart, one performs measurements of the spins along arbitrary components $\vec{a}$ and $\vec{b}$, giving either $+1$ or -1. If these two particles are far enough, the measurement of, for example $\vec{a}$ gives information about the particle at $\vec{b}$, at a velocity higher than the one of light with no local connection.

These counter intuitive results of the theory led EPR to the conclusion that quantum physics was an incomplete theory, and explained this non-local information transfer by means of the existence of local "hidden variables" which supplement, and complete, quantum mechanics.

Bell, in 1964, studied this local hidden variable, which showed properties different to the ones predicted by quantum physics, giving a good method for proving the existence or not of these variables.

For his theory, Bell studied the $|\Psi^-\rangle state$ (30) for a type II down-conversion. Considering each photon to leave the crystal with an angle θ (photon 1) and ϕ (photon 2), he recalculated the state as a function of the angles:

$$\begin{aligned} \left|\Psi^-\right\rangle = & \frac{1}{\sqrt{2}}[(cos\theta sin\phi - sin\theta cos\phi)\,|\theta\rangle_1\,|\phi\rangle_2 \\ & + (cos\theta cos\phi + sin\theta sin\phi)\,|\theta\rangle_1\left|\phi^\perp\right\rangle_2 \\ & - (sin\theta sin\phi + cos\theta cos\phi)\left|\theta^\perp\right\rangle_1|\phi\rangle_2 \\ & - (sin\theta cos\phi - cos\theta sin\phi)\left|\theta^\perp\right\rangle_1\left|\phi^\perp\right\rangle_2 \end{aligned} . \tag{33}$$

To reproduce the EPR experiment, Bell defined the correlation function:

$$C(\theta,\phi) = Average[A(\theta)B(\phi)]\,, \tag{34}$$

where A corresponds to particle 1 and B to particle 2. A and B will be one for the photon at θ or ϕ and -1 in the perpendicular directions. This way:

$$\begin{aligned} C(\theta,\phi) =& Pr(|\theta\rangle_1 |\phi\rangle_2) + Pr(\left|\theta^\perp\right\rangle_1 \left|\phi^\perp\right\rangle_2) \\ &- Pr(|\theta\rangle_1 \left|\phi^\perp\right\rangle_2) - Pr(\left|\theta^\perp\right\rangle_1 |\phi\rangle_2)\,, \end{aligned} \tag{35}$$

where $Pr(|\theta\rangle_1 |\phi\rangle_2)$ is the probability of finding the outcomes $|\theta\rangle_1 |\phi\rangle_2$, etc.

Applying this relation to the state of equation 33, the correlation function is found to be:

$$C(\theta,\phi) = -cos[2(\theta-\phi)]\,, \tag{36}$$

which is a straightforward quantum mechanical prediction.

To take into account the theory of the hidden variable (λ), he repeated the same calculations with the additional variable, such that, being $\rho(\tau)$ the probability distribution of the hidden variables:

$$\int \rho(\lambda)d\lambda = 1\,, \tag{37}$$

Applying this distribution to the correlation function:

$$C_{HV}(\theta,\phi) = \int A(\theta,\lambda)B(\phi,\lambda)\rho(\lambda)d\lambda\,, \tag{38}$$

where the HV accounts for "hidden variable". A new parameter is defined as a function of X_1,X_1',X_2,$X_2' = \pm 1$:

$$\begin{aligned} S &= X_1X_2 + X_1X_2' + X_1'X_2 - X_1'X_2' \\ &= X_1(X_2 + X_2') + X_1'(X_2 - X_2') = \pm 2' \end{aligned} \tag{39}$$

which can be rewritten as a function of the correlation function:

$$-2 \leqslant C_{HV}(\theta,\phi) + C_{HV}(\theta',\phi) + C_{HV}(\theta,\phi') - C_{HV}(\theta',\phi') \leqslant +2\,. \tag{40}$$

This is the Bell inequality (can be easily rewritten as $|S| \leqslant 2$), which must be violated in quantum systems. To proof the entanglement, S can be calculated with the definition given in eq. 36 for $\theta = 0$, $\theta' = \frac{\pi}{4}$, $\phi = \frac{\pi}{8}$ and $\phi' = -\frac{\pi}{8}$,

which leads to $S = 2\sqrt{2}$, which clearly violates Bell's inequalities proving the non-locality and absence of hidden variables.

Of course, there is an efficiency on the detectors that must affect the measurements. To avoid this effect, the correlation function is normalized such that:

$$C(\theta, \phi) = \frac{Average[A(\theta)B(\phi)]}{Average[N_1 N_2]}, \tag{41}$$

being N_1 and N_2 the total number of photons in detectors 1 and 2:

$$Average[N_1 N_2] = Pr(\theta, \phi) + Pr(\theta^{\perp}, \phi^{\perp}) + Pr(\theta, \phi^{\perp}) + Ps(\theta^{\perp}, \phi), \tag{42}$$

where $Pr(A, B)$ are the coincidences between A and B.

2

EXPERIMENTAL, THEORETICAL AND NUMERICAL METHODS

2.1 EXPERIMENTS

There are several sources of entangled particles, such as photon cascades or spontaneous parametric down-conversion (SPDC). This thesis is centered on the creation of couples of entangled photons by means of type-II SPDC. In the following, we detail this particular setup.

2.1.1 *Single-photon source: Polarization Sagnac Interferometer*

One of the most efficient setups used to create couples of entangled photons by means of type-II SPDC is the Polarization Sagnac Interferometer (PSI), which emits couples of polarization-entangled photons by means of a "Periodically Poled KTP" crystal (PPKTP). PPKTP is a popular nonlinear material that is the active element transforming classical light into quantum one. Other commonly used crystals are KDP (KD_2PO_4), BBO ($\beta - BaB_2O_4$) [73] The main problem of these nonlinear crystals is their low efficiency. For the purpose of our studies in entangled polaritons (section 5), high signal is needed, making it necessary to use PPKTP crystals which have a higher efficiency (10^5 phot/sec with PPKTP against 10^3 phot/sec in BBOs). A scheme of our setup is shown in Fig. 9 and the generation of entangled signal and idler photons from a laser diode as the classical input proceeds as follows: a single-mode laser of wavelength λ_p is sent to the interferometer. To keep only the single mode of the laser diode (we will call it simply laser from now on), it is sent to a single-mode fiber (SMF). The form of the pump field will have an enormous effect on the final state, and must be set carefully. Let us suppose a classical pump of the form:

$$\vec{E_p} = E_H \hat{e}_H + e^{i\phi_p} E_V \hat{e}_V \,, \tag{43}$$

where $\hat{e}_H$ and $\hat{e}_V$ are the unitary vectors of the horizontal (H) and vertical (V) components and ϕ_p is the relative phase between the two components. This wave goes through a half waveplate (HWP) and polarized beam splitter (PBS1) to select the power and set the polarization (vertical in this case), a quater waveplate (QWP1) and half waveplate (HWP1), which role will be explained further, and a dichronic mirror that reflects the wavelength of the laser and transmit the wavelength of the signal photons. When the laser light arrives to

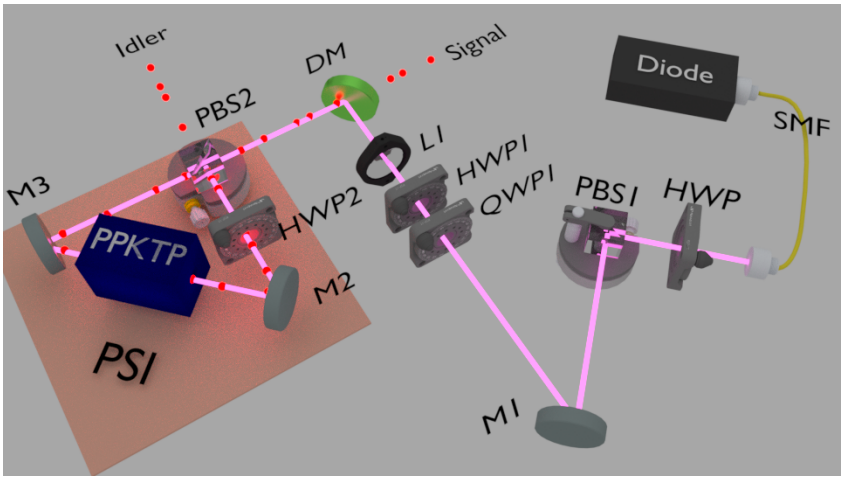

Figure 9: Sketch of the Sagnac interferometer.

the second PBS, the horizontal component goes through the PSI counterclockwise, while the vertical component follows the opposite direction. When the H component gets to the PPKTP, two photons with opposite polarizations in the form $|H_s\rangle|V_i\rangle$ are created, where the subindex s/i denotes signal/idler photon. These photons are rotated 90 degrees in HWP2, such that at the arrival to PBS2, the pair is now $|V_s\rangle|H_i\rangle$, transmitting the signal photon to branch 2, and reflecting the idler one to branch 1. This way the output state at the PBS2 is:

$$|\Psi_H\rangle = e^{i[k_p L_A + (k_s+k_i)L_B + \theta_s + \theta_i]} \eta_H E_H |V_s\rangle_1 |H_i\rangle_2 \,, \tag{44}$$

where L_A and L_B are the distances between PBS2 and PPKTP when passing through M3 and M2, respectively. The effect of the optical path on the phase is thus included in $k_p L_A$ for the laser before arriving to the PPKTP, and $(k_s + k_i)L_B$ for the two photons after the PPKTP, until they arrive to the PBS2. There is also and additional phase on the two photons due to the HWP2 denoted as θ_s and θ_i. Finally, the η_H includes the efficiency of the system due to propagation and absorption of the elements.

With only the horizontal component of the laser, the final state is not entangled. Therefore, we need both components. When E_V gets to PBS2, it is reflected and goes through the PSI clockwise. PPKTP crystals only create couple of photons with horizontal pumping, so the HWP2 rotates the E_V light such that the pumping arrives parallel to the axis of the crystal. This way, once again a pair $|H_s\rangle|V_i\rangle$ is created, which arrives to the PBS2, transmitting the $|H_s\rangle$ component

to branch number 1, and reflecting $|V_i\rangle$ to branch number 2. The output state due to the vertical component is therefore of the form:

$$|\Psi_V\rangle = e^{i[\phi_p + k_p L_B + (k_s + k_i)L_A + \theta_p]} \eta_V E_V |H_s\rangle_1 |V_i\rangle_2 \,. \tag{45}$$

This way, the final state is the required Bell state:

$$|\Psi\rangle \propto (|H_s\rangle_1 |V_i\rangle_2 + e^{i\phi} \beta |V_s\rangle_1 |H_i\rangle_2) \,, \tag{46}$$

where the phase $\phi = \theta_s + \theta_i - \theta_p - \phi_p$ includes the phases given by the horizontal and the vertical components of the incident pumping taking into account the momentum conservation ($k_p = k_i + k_s$), while $\beta = \frac{\eta_H E_H}{\eta_V E_V}$ includes the losses in the interferometer. To get a specific Bell state, both ϕ and β must be set to specific values which can be introduced by means of the PBS1, HWP1 and QWP1.

The final parameter to set in the setup are the energies of the two emitted photons by means of two variables: the energy of the incident laser and the temperature of the crystal. Typically, the crystals are done such that, for and initial ω_p, and a specific temperature, two degenerate photons of energy $\omega_p/2$ are emitted. But changing the temperature of the PPKTP, two non-degenerate photons can be created (always conserving energy) with $\omega_s = \omega_p/2 + \Delta\omega$ and $\omega_i = \omega_p/2 - \Delta\omega$ such that $\omega_p = \omega_s + \omega_i$.

2.1.2 *Spontaneous Parametric Down-Conversion*

We now describe the SPDC, that is the mechanism at the heart of the PPKTP. SPDC stands for "Spontaneous Parametric Down-Conversion". The down-conversion results from a nonlinear interaction of pump radiation with a nonlinear media (the KTP crystal), which results in an instantaneous creation of quantum light in the form of a couple of photons (signal and idler). In this process, both energy and momentum are conserved, a property known as "phase matching". This generation can be degenerate, when $\omega_s = \omega_i = \frac{1}{2}\omega_p$, or non-degenerate when $\omega_s \neq \omega_i$, still following $\omega_s + \omega_i = \omega_p$.

Typically, these nonlinear media are highly anisotropic crystals with a response given by:

$$\hat{P}_i = \chi^{(1)}_{i,j} \hat{E}_j + \chi^{(2)}_{i,j,k} \hat{E}_j \hat{E}_k + \chi^{(3)}_{i,j,k,l} \hat{E}_j \hat{E}_k \hat{E}_l + \cdots \tag{47}$$

where $\chi^{(m)}$ is the m-th order electric susceptibility tensor.[1] With this polarization function, the energy density is of the form $\epsilon_0 E_i P_i$, which gives the following interaction Hamiltonian:

$$\hat{H}^{(2)} = \epsilon_0 \int_V \chi^{(2)}_{i,j,k} \hat{E}_i \hat{E}_j \hat{E}_k \, d^3\mathbf{r} \,. \tag{48}$$

1 Remembering that in tensor calculus, repeated indices imply a sum.

Taking the fields of the form:

$$\begin{aligned}\hat{E}^{(+)}(\mathbf{k}) &= i\sqrt{\frac{2\pi\hbar\omega(\mathbf{k})}{V}}a^{\dagger}(\mathbf{k}),\\ \hat{E}^{(-)}(\mathbf{k}) &= i\sqrt{\frac{2\pi\hbar\omega(\mathbf{k})}{V}}a(\mathbf{k}),\end{aligned} \tag{49}$$

which substituted in Eq. (48), and limiting the results to the case in which the signal and idler modes are initially in vacuum, gives the interaction Hamiltonian:

$$\begin{aligned}\hat{H}_I(t) =& \epsilon_0\int_V d^3\mathbf{r}\int d^3\mathbf{k}_s\, d^3\mathbf{k}_i \chi^{(2)}_{l,m,n}\\ &\times \hat{E}^{+}_{pl}e^{i[\omega_p(\mathbf{k}_p)-\mathbf{k}_p\cdot\mathbf{r}]}\\ &\times \hat{E}^{(-)}_{sm}e^{-i[\omega_s(\mathbf{k}_s t-\mathbf{k}_s\cdot\mathbf{r})]}\\ &\times \hat{E}^{(-)}_{in}e^{-i[\omega_i(\mathbf{k}_i t-\mathbf{k}_i\cdot\mathbf{r})]} + \text{H.c.}\end{aligned} \tag{50}$$

Applying time dependent perturbation theory and assuming the initial states of signal and idler modes to be in vacuum ($|\Psi_0\rangle$), the system evolves to first order as $|\Psi\rangle \approx |\Psi_0\rangle + |\Psi_1\rangle$, where:

$$\begin{aligned}|\Psi_1\rangle =& -\frac{i}{\hbar}\int dt\hat{H}(t)\,|\Psi_0\rangle\\ =& \mathcal{N}\int d^3\mathbf{k}_s\, d^3\mathbf{k}_i\,\delta(\omega_p-\omega_s(\mathbf{k}_s)-\omega_i(\mathbf{k}_i))\\ &\times\delta^{(3)}(\mathbf{k}_p-\mathbf{k}_i-\mathbf{k}_s)a^{\dagger}_s(\mathbf{k}_s)a^{\dagger}_i(\mathbf{k}_i)\,|\Psi_0\rangle\end{aligned} \tag{51}$$

with $\mathcal{N}$ a normalization factor. The delta functions include the phase matching conditions:

$$\begin{aligned}\omega_p &= \omega_s+\omega_i,\\ \mathbf{k}_p &= \mathbf{k}_s+\mathbf{k}_i.\end{aligned} \tag{52}$$

There are two types of SPDC: type-I and type-II. To make this more evident, the interaction Hamiltonian can be rewritten in the form:

$$\hat{H}_I \sim \chi^{(2)}\hat{a}_p\hat{a}^{\dagger}_s\hat{a}^{\dagger}_i + \text{H.c.} \tag{53}$$

In type-I SPDC, the signal and the idler have the same polarization, perpendicular to the one of the pump. In this case the interaction Hamiltonian will be:

$$\hat{H}_I = \hbar\alpha\hat{a}^{\dagger}_s\hat{a}^{\dagger}_i + \text{H.c.} \tag{54}$$

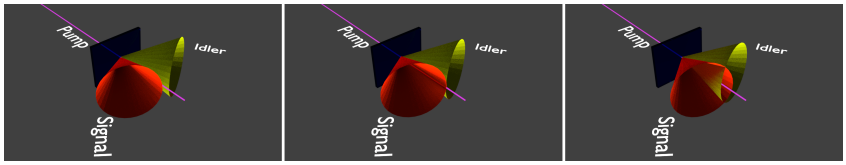

Figure 10: SPDC effect. An initial signal (purple laser) excites the nonlinear crystal, creating couples of photons with opposite polarizations (red and yellow cones). (a) Non-correlated photons. (b) Indistinguishable photons. (c) Entangled photons.

with $\alpha \propto \chi^{(2)} E_p$, where E_p is the amplitude of the classical coherent field. Based on the momentum conservation, both the signal and the idler exit the crystal in opposite sides of two concentric cones centered on the direction of the pump.

On the other hand, for type-II SPDC, the two photons are perpendicular. Like in the previous case, both photons leave in cones, in this case in two opposite directions with an angle θ respective to the laser beam. This way of emission leads to polarization-entangled couples of photons when the two cones intersect, since each intersection presents both horizontal and vertical components and it is not possible to tell from which beam a photon is obtained. The Hamiltonian for the photons coming from such intersections is given by:

$$\hat{H}_I = \hbar\chi(\hat{a}^\dagger_{V_s}\hat{a}^\dagger_{H_i} + \hat{a}^\dagger_{H_s}\hat{a}^\dagger_{V_i}) + \text{H.c.} \tag{55}$$

where $\hat{a}^\dagger_{V_s}$, $\hat{a}^\dagger_{H_s}$, $\hat{a}^\dagger_{V_i}$ and $\hat{a}^\dagger_{H_i}$ are the creation operators of the signal (s) and idler (i) photons, with horizontal (H) and vertical (V) polarization, respectively.

Considering an initial state $|\Psi_0\rangle$, the state vector evolution under the action of H_I leads to:

$$\left|\Psi^+\right\rangle = \frac{1}{\sqrt{2}}(|V\rangle_s |H\rangle_I + |H\rangle_s |V\rangle_i)\,, \tag{56}$$

that is, one of the four Bell states, which describes a polarization-entangled system between two photons: signal (s) and idler (i). Depending on the angle between the laser (which can be either CW or pulsed) and the crystal, the phase matching conditions are modified and the angle between cones is changed, leaving three different options (in type-II SPDC): cut in two lines (which will be entangled), cut in one line (indistinguishability between the two photons but without any entanglement) and no intersection at all. Figure 10 shows a sketch of these two cones for different angles.

2.1.3 *Measurement of quantum observables*

There are various ways to demonstrate entanglement, out of which the most common ones are the measurement of the density matrix by means of tomography, and the study of Bell inequalities. We now discuss these techniques.

2.1.3.1 *Quantum tomography measurement*

Tomography measurements allow the full reconstruction of the density matrix ρ. To understand the procedure, it is easier to begin by the tomography of a single particle, which will after be extrapolated to the case of two particles. For the simplest case of a particle that can take two states (2LS), defining a so-called "qubit", the density matrix is given by:

$$\hat{\rho} = \frac{1}{2}\sum_{i=0}^{3}\frac{S_i}{S_0}\hat{\sigma}_i \tag{57}$$

where $\hat{\sigma}_i$ represents the Pauli matrices, given by:

$$\hat{\sigma}_0 = \begin{pmatrix} 1 & 0 \\ 0 & 1 \end{pmatrix} \tag{58a}$$

$$\hat{\sigma}_1 = \begin{pmatrix} 0 & 1 \\ 1 & 0 \end{pmatrix} \tag{58b}$$

$$\hat{\sigma}_2 = \begin{pmatrix} 0 & -i \\ i & 0 \end{pmatrix} \tag{58c}$$

$$\hat{\sigma}_3 = \begin{pmatrix} 1 & 0 \\ 0 & -1 \end{pmatrix} \tag{58d}$$

These are related in classical optics to the Stokes parameters when taking averages: Eq. 2.1 There are four possible measurements: with a filter that transmits only 50% of the signal (or $1/2$ of the horizontal plus $1/2$ of the vertical) (n_0), the horizontal component (n_1), the diagonal component (n_2) and the right-circularly polarized light (n_3). Thus, the Stokes parameters are obtained as:

$$\begin{aligned} S_o &= 2n_0 \\ S_1 &= 2(n_1 - n_0) \\ S_2 &= 2(n_2 - n_0) \\ S_3 &= 2(n_3 - n_0)\,. \end{aligned} \tag{59}$$

The measurement of these n_i corresponds experimentally to the measurement of the transmission through a given polarizer. Although linear polarizers are

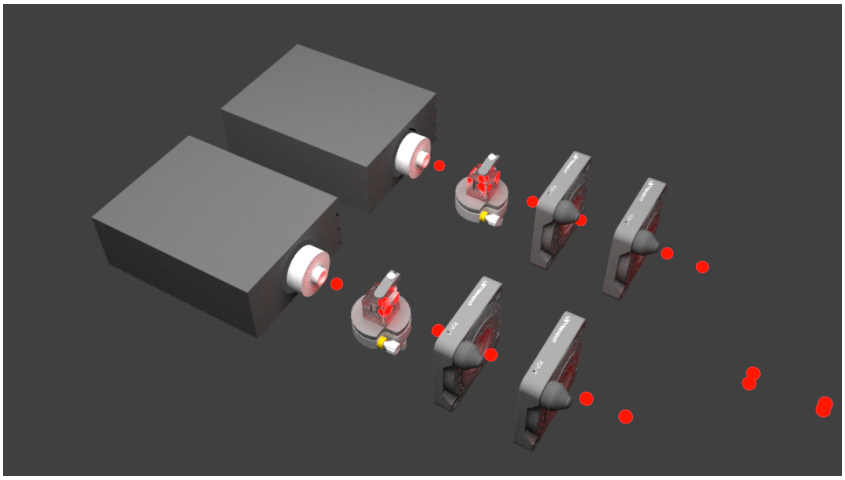

Figure 11: Sketch of a tomography setup for two photons: Each entangled photon goes through one tomography stage, which consists on a QWP, followed by a HWP and a PBS. With the first two plates, any possible polarization can be achieved, and with the PBS the horizontal component of the photon is sent to the APD. The signal of the APDs is analyzed[] to obtain the value of the concurrence and the real and imaginary components of the density matrix.

commercialized, circular ones can only be obtained by means of waveplates and linear polarizers. Based on this, we can define a tomography stage: a QWP, HQP, PBS and APD. By means of the three first elements, all types of polarizers can be done, and with the APD the amount of signal with each of them is measured. This allows the reconstruction of all the S_i coefficients just by means of $|H\rangle$, $|V\rangle$, $|D\rangle$ and $|R\rangle$. Once these four measurements have been done (three independent ones and one to obtain the parameter $\mathcal{N}$), the density matrix of the qubit $\hat{\rho}$ can be reconstructed.

This simple method can be extrapolated for the case of two qubits. In this case, instead of a single tomography stage, two are required (see Fig. 11) and instead of the measurement of the four polarizations, 16 must be done: 15 independent ones and one for the value of $\mathcal{N}$. Calling $|AB\rangle$ the state measured with photon 1 having polarization A and photon 2 having polarization B, the 16 combinations are: $|HH\rangle$, $|HV\rangle$, $|VV\rangle$, $|VH\rangle$, $|RH\rangle$, $|RV\rangle$, $|DV\rangle$, $|DH\rangle$, $|DR\rangle$, $|DD\rangle$, $|RD\rangle$, $|HD\rangle$, $|VD\rangle$, $|VL\rangle$, $|HL\rangle$ and $|RL\rangle$.

For the specific case of two-qubits, the density matrix is given by:

$$\hat{\rho} = \frac{\left(\sum_{\nu=1}^{16} \hat{M}_\nu n_\nu\right)}{\left(\sum_{\nu=1}^{4} n_\nu\right)} \tag{60}$$

with $\hat{M}_\nu$ large 4×4 matrices[2] whose definition can be found in the literature (see for instance [60]), and with the denominator corresponding to $\mathcal{N}$.

This method, although very simple, is not the most precise one, since the final results can fail to retain some of the main properties of the density matrix, such as positivity. A longer but more robust method, that constrains the matrix to remain physical, is the *maximum likelihood estimation*. It consists of three steps:

1. Generation of a formula for an explicitly "physical" density matrix (i.e., obeys normalization, Hermiticity and positivity) of 16 variables: $\hat{\rho}_p(t_1, t_2, ..., t_{16})$.
2. Define the "likelihood function" which quantifies how good the density matrix $\hat{\rho}_p(t_1, t_2, ..., t_{16})$ is in relation to the experimental data. It is denoted as $\mathcal{L}(t_1, t_2, ..., t_{16}; t_1, t_2 ..., t_{16})$.
3. Optimize the t_i $(t_1^{opt}, t_2^{opt} ..., t_{16}^{opt})$ that maximize the likelihood function, leading to $\hat{\rho}(t_1^{opt}, t_2^{opt}, ..., t_{16}^{opt})$.

These functions are of the form (the demonstration and more information can be found in [60]):

$$\hat{\rho}_p(t) = \hat{T}^\dagger(t)\hat{T}(t)/Tr[\hat{T}^\dagger(t)\hat{T}] \tag{61}$$

and:

$$\begin{aligned} &\mathcal{L}(t_1, t_2, ..., t_{16}) \\ &= \sum_{\nu=1}^{16} \frac{[\mathcal{N} \langle \Psi_\nu | \hat{\rho}_p(t_1, t_2, ..., t_{16}) | \Psi_\nu \rangle - n_\nu]^2}{2\mathcal{N} \langle \Psi_\nu | \hat{\rho}_p(t_1, t_2, ..., t_{16}) | \Psi_\nu \rangle}. \end{aligned} \tag{62}$$

This $\mathcal{L}$ function must be minimized (typically by means of a routine in programs such as Mathematica, Matlab, etc.), obtaining this way the values of t_i.

2 For instance:

$$\hat{M}_1 \equiv \frac{1}{2}\begin{pmatrix} 2 & -(1-i) & -(1+i) & 1 \\ -(1+i) & 0 & i & 0 \\ -(1-i) & -i & 0 & 0 \\ 1 & 0 & 0 & 0 \end{pmatrix}.$$

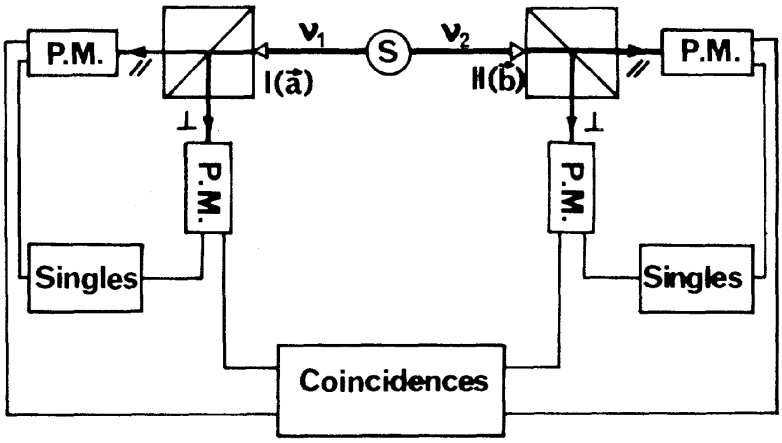

Figure 12: Experimental setup used for the measurement of Bell inequalities [10].

For a higher precision, 36 measurements can be done instead of 16 (all the combinations of $|H\rangle$, $|V\rangle$, $|D\rangle$, $|A\rangle$, $|R\rangle$ and $|L\rangle$) and increase the summatory of equation 62 from 16 to 36.

When dealing with tomography measurements, there is always random electronic noise. The accidental counts (ACC) follow the relation: $ACC = \gamma C_1 C_2/\tau$, where γ is a Poissonian constant (identical for all the combinations), τ is the coincident time window and C_1, C_2 are the single photon counts of the two detectors. This constant γ is calculated by means of the measurement of the coincidences and the detection in each APD without the correct synchronization. Once the value of the constant is obtained, the noise of each measurement of the tomography can be calculated using the counts in each detector with the correct synchronization.

2.1.3.2 *Bell inequalities measurement*

In 1982, Alain Aspect and coworkers managed to do the first measurements on Bell inequalities, using as an initial source a crystal which emitted couples of polarization-entangled photons at a rate of 5×10^7 phot/sec. Figure 12 displays the sketch of their experiment. With four different APDs, all the possible combinations of polarizations were studied simultaneously (HH, HV, VH, VV) and by introducing the experimental coincidences for each combination for various sets of angles (θ_1, θ_2) they found a final value of $S = 2.7 \pm 0.05$, violating Bell's inequalities and proving entangled photons for the first time.

Since Aspect's experiment, the calculation of Bell inequalities has become a mandatory proof of the entanglement in most of the studies. When introducing

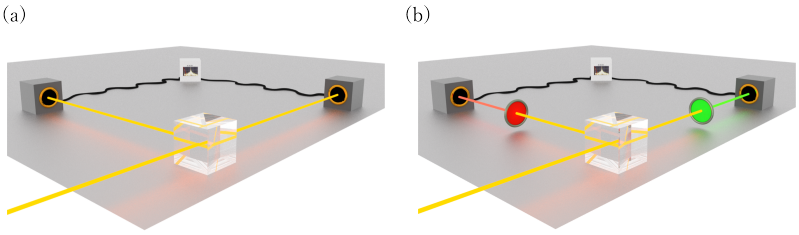

Figure 13: HBT interferometer: (a) No energy discrimination (b) Filters introduced in each branch for energy discrimination

the values of the coincidences in the equations, only 16 values are needed each of them between two photon detectors. To simplify the procedure, only 2 APDs can be used, selecting each of the combinations in each measurement[]. This way, with the measurement of only 16 coincidences the entanglement can be verified reducing the amount of APDs.

2.1.4 *Temporal evolution: the streak camera*

As was explained in Section 1.3, there are various ways of studying photon correlations, of which the most common one is the second-order correlation function $g^{(2)}(\tau)$. The typical setup used for the measurement of this kind of correlation is the HBT interferometer, based on the intensity interferometer designed by Hanbury Brown and Twiss in the 1950s.

The typical HBT interferometer contains one beamsplitter, two single-photon detectors and a photon correlator (see Fig. 13a). The signal emitted by the source is directed to the BS where it is divided into two new beams, each of them sent to an APD. These communicate their detection to a photon correlator, which counts coincidences with temporal delays τ, giving finally the $g^{(2)}(\tau)$ of the source.

These experiments can be made both under pulsed excitation or with continuous-wave (CW) excitations. In the former case, the value $g^{(2)}(0)$ is accessible while in the latter case, also the coherence time τ can be extracted.

Another, more recent, experimental setup used for temporal photon correlations is through a streak camera [11, 28, 37, 120]. This method has started to gain great importance in the last years due to its great efficiency and high temporal resolution.

The streak camera is composed of a photocathode, an oscillatory field and a CCD detector. When the photons arrive to the photocathode, they get to a phosphor screen, which transforms them into photoelectrons. These are sent to the vertically oscillatory field which displaces them as a function of time.

Depending on the moment at which the photoelectron gets to the field, it exits in a different vertical direction towards the camera, translating time to a vertical position on the CCD.

This method was pioneered in 2009 by Wiersig et al. [120]. In their case, this was to study the lasing emission from quantum dots in a micropillar, under pulsed laser excitation out of resonance. With this new method, they managed to overcome the temporal resolution problems found with the APDs and managed to increase it up to 2 ps.

The same year, Assmann (a coauthor of Wiersig's paper) published similar studies, in this case for the emission of exciton-polaritons at $k = 0$ under non-resonant pulsed excitation as a function of the power. With his studies he expanded the method for higher correlation functions at zero delay ($g^{(n)}(\tau = 0)$). It is interesting to notice that polaritons were early candidates for such types of in-depth photon correlations analysises.

The streak camera setup is particularly fit for still another type of photon-correlations, namely, retaining the frequency information of the detected photons, taking the form $g^{(2)}(\omega_1, \omega_2)$ of coincidences of two photons with frequencies ω_1 and ω_2, respectively. The measurement of this function by means of the HBT interferometer is done by introducing filters in each of the branches (see Fig. 13b). Despite the simplicity of this experiment, studies of the 2PS (see section 2.2.2), that will be further studied for an out of equilibrium condensate of exciton-polaritons in chapter 4), imply the measurement for each of the permutations, which extends the experiment and requires an enormous amount of filters [90] (two for each frequency). A new more efficient method for the measurement of both energetic and temporal correlations will be presented in section 4. In next Section, we overview the theory of frequency-resolved photon correlations.

2.2 THEORY

2.2.1 *Frequency-resolved correlations*

The conceptual observable $g^{(2)}(\omega_1, \omega_2)$ of frequency-frequency observable is easy to understand. This is the result of the experiment sketched in Fig. 13(b). Its theoretical computation, however, is far from straightforward. It involved the best efforts of a large number of theorists [34, 36, 71, 88] in the late 90s who arrived, amidst debates and controversy, to the formal definition of a physical two-photon spectrum, that is an extension to two-photon physics of the physical power spectrum advocated by Eberly and Wódkiewicz [40] to supplement the mathematical Wiener-Khintchine theorem. In this approach, a description of the relation between the quantum system that emits light and the

observer that detects it is made by means of the input-output formalism: the photons inside the system (a) are weakly coupled to external continuum of modes (of frequency ω), and ultimately to the detectors, with operators A_ω. The emission of photons with frequency ω_1 at a time T_1 is thus obtained as $S^{(1)}(\omega_1, T_1) = \langle A^\dagger_{\omega_1}(T_1) A_{\omega_1}(T_1)\rangle$. The Energy-Time uncertainty must be taken into account, which is assured by the exponential decays in the Fourier transform of the autocorrelation:

$$\begin{aligned} S^{(1)}_{\Gamma_1} =& \frac{\Gamma_1}{2\pi} \int \int_{-\infty}^{T_1} dt'_1\, dt'_4 e^{-(\Gamma_1/2)(T_1 - t'_1)} e^{-(\Gamma_1/2)(T_1 - t'_4)} \times \\ & \times e^{i\omega_1 (t'_4 - t'_1)} \langle a^\dagger(t'_1) a(t'_4)\rangle \,, \end{aligned} \tag{63}$$

where Γ_1 is the linewidth of the detector A_{ω_1}.

This result extended to two photons (and, in this case, involving two possibly different filters), still with special attention to the time and normal ordering of the operators, leads to an extension of Eq. 63 in the form of:

$$\begin{aligned} S^{(2)}_{\Gamma_1\Gamma_2} =& \frac{\Gamma_1\Gamma_2}{(2\pi)^2} \int \int_{-\infty}^{T_1} dt'_1\, dt'_4 e^{-(\Gamma_1/2)(T_1 - t'_1)} e^{-(\Gamma_1/2)(T_1 - t'_4)} \\ & \int \int_{-\infty}^{T_2} dt'_2 dt'_3 \times e^{-(\Gamma_2/2)(T_2 - t'_2)} e^{-(\Gamma_2/2)(T_2 - t'_3)} \times \\ & \times e^{i(\omega_1 (t'_4 - t'_1))} e^{i\omega_2 (t'_3 - t'_2)} \langle \mathcal{T}[a^\dagger(t'_1) x a^\dagger(t'_2)] \mathcal{T}[a(t'_3) a(t'_4)]\rangle \,, \end{aligned} \tag{64}$$

where $\mathcal{T}_\pm$ are the time ordering operators, such that the leftmost one corresponds to the latest time. By normalizing equation 64, the frequency-resolved second-order correlation function is obtained as:

$$g^{(2)}_{\Gamma_1\Gamma_2}(\omega_1, T_1; \omega_2, T_2) = \frac{S^{(2)}_{\Gamma_1\Gamma_2}(\omega_1, T_1; \omega_2, T_2)}{S^{(1)}_{\Gamma_1}(\omega_1, T_1) S^{(1)}_{\Gamma_2}(\omega_2, T_2)} \,. \tag{65}$$

This quantity, now formally defined (in the integral form of Eqs. 63 and 64), is however exceedingly complicated to compute, even numerically. Drastic approximations have been made even when tackling the simplest problems and recent efforts from [20] for exact numerical results only accessed trivial regimes. When turning to reach higher orders or correlation ($g^{(N)}_{\Gamma_1 \ldots \Gamma_N}$), it becomes quickly impossible to even write down the formal integral to be computed, and new theoretical methods are needed. Such methods have been introduced in 2012 by E. del Valle *et al.* [115], who found an efficient procedure for the exact calculation of these high-order correlation functions which can be extended to all types of open quantum system Q (cf. Fig. 14). These N-photon correlations were obtained introducing N "sensors" to the dynamics of the quantum system. Each of these consists, in the simplest approach, of a two-level system

(2LS) with a different frequency of resonance ω_i, corresponding to the one to be probed, and a linewidth Γ_i (and lifetime $1/\Gamma_i$) corresponding to the spectral window of detection. The N sensors are coupled to the system Q with a vanishing coupling $\epsilon_i \to$, that in practice is kept low enough to leave the system unaffected. In particular, $\langle n_i \rangle = \langle \sigma_i^\dagger \sigma_i \rangle \ll 1$, with σ_i the annihilation operator of the ith sensor. The main result of [115] is to show that the N-photon correlation as defined by the integrals given above can be computed by means of the considerably simpler intensity-intensity correlations between sensors:

$$g^{(N)}_{\Gamma_1 \dots \Gamma_N}(\omega_1, T_1; \dots; \omega_N, T_N) = \lim_{\epsilon_1 \dots \epsilon_N \to 0} \frac{\langle n_1(T_1) \dots n_N(T_N) \rangle}{\langle n_N(T_1) \rangle \dots \langle n_N(T_N) \rangle} \tag{66}$$

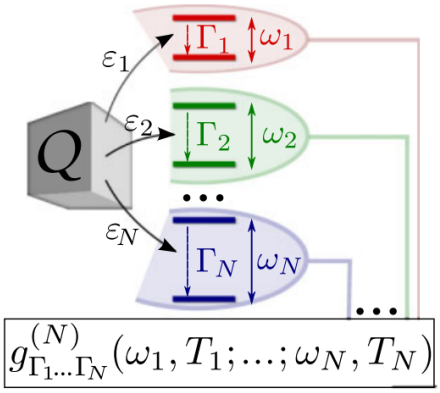

Figure 14: Quantum system (Q) weakly coupled to N detectors (2LS) of different frequencies of resonance and width, that correspond to the filters placed before the detectors.

2.2.2 *Two-photon spectrum*

The efficient method for the calculation of energy-resolved second order correlation functions by means of weakly coupled filters allows to compute a new type of observable, the so-called *Two-photon correlation spectrum* (2PS), that consists in a 2D map of all the possible combinations $g^{(2)}(\omega_i, \omega_j)$. This unravels a rich landscape of correlations otherwise hidden when omitting energy discrimination and goes far beyond the power spectrum when retaining it but at the single-particle level. In 2013, A. Gonzalez-Tudela *et al.* [52] calculated the theoretical 2PS for a large variety of fundamental systems. Such is the novelty of this observable that their characterization needed to consider in their full-right the trivial systems that are the harmonic oscillator (HO) and the Two-level system

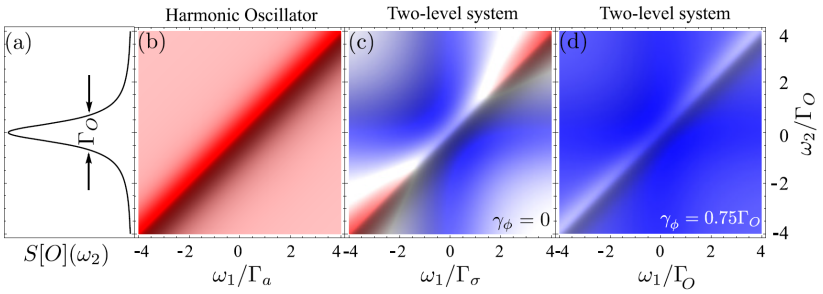

Figure 15: (a) Spectrum of the single-mode emitter. The other 3 panels show the 2PS for a HO (b), 2LS with no dephasing (c) and 2LS with dephasing γ_ϕ. Three different colors are found in the 2PS: red for $g^{(2)} > 0$, white for $g^{(2)} = 1$ and blue for $g^{(2)} < 1$.

(2LS). At the single-particle level, their spectral profile (S) consists solely in one peak with a linewidth Γ_0, and is identical. At the two-particle level (but unfiltered), the $g^{(2)}$ is already different, being respectively, under conditions of incoherent pumping, 2 and 0. Figure 15 depicts their 2PS with the color-code (that we will keep for the rest of the thesis) of "red" for bunching ($g^{(2)} > 1$), "white" for uncorrelated/coherent ($g^{(2)} = 1$) and blue for antibunching ($g^{(2)} < 1$). The figure shows the HO on the left and two different 2LS, without (center) and with (right) pure-dephasing (γ_ϕ). The main features of these figures is the diagonal, that corresponds to autocorrelations when $\omega_1 = \omega_2$. Also of notice is the butterfly shape of antibunching in the 2LS, with smaller antibunching (even rising up to bunching) on the diagonal, and the fact that pure dephasing is enhancing the antibunching. The diagonal feature follows from the known tendency of bosons to clutter together and will be the subject of detailed investigation in Chapter 4 where the fundamental physics at play here will be observed experimentally, thanks to polaritons.

The above cases are extremely fundamental and their structure is in fact as simple as could be. For more complex systems, new and richer patterns appear in the 2PS. Figure 16 shows the case where the HO and the 2LS are coupled together. In this case, the Jaynes–Cummings dynamics takes over and one gets propelled with a simple linear-coupling constant from trivial correlations to extremely complex ones. A small extract is shown in Fig. 16 as a function of increasing coupling between the 2LS and HO (corresponding for instance to a quantum dot in a single-mode microcavity). One observes at low pumping (panel (a)) the Purcell enhanced single-photon source, similar to Fig. 15(b), followed by the emergence of dressed states with the Rabi doublet in the power spectrum and a square lattice of butterflies in the 2PS, with stronger cross-

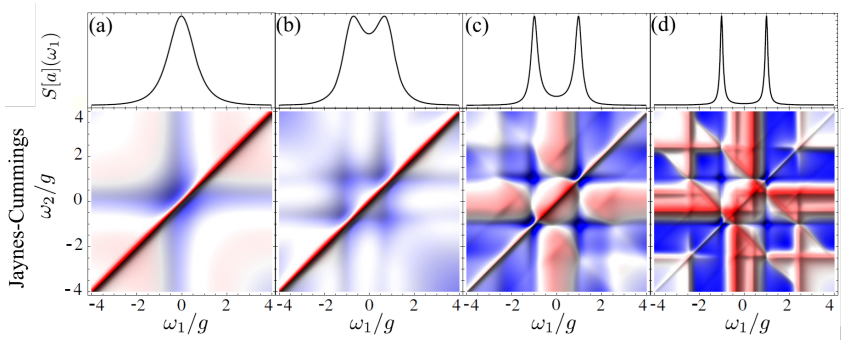

Figure 16: 2PS for a Jaynes-Cummings increasing the coupling (from left to right) leading to merely a splitting in the spectrum but to a rich panel of two-photon correlations in the 2PS.

correlations between the peak as undisturbed by the diagonal bunching. At higher coupling strenghts, (c), the quantum dynamics becomes dominant and triggers a new class of processes, completely transparent in the the power spectrum, but already neatly visible in (c) as diagonals parallel to the bunching one, and also antidiagonals. The structure becomes compelling in very strong-coupling, panel (d), where also other horizontal and vertical patterns emerge, that correspond to transitions high in the Jaynes-Cummings ladder, absent in the single-photon spectrum, but revealed in the 2PS. The (anti)diagonals correspond to transitions involving virtual processes, and while of considerable importance for future quantum technologies (e.g., their Purcell enhancement by [96] leads to a new type of quantum source), they are beyond the scope of this thesis where the source will be limited to microcavity polaritons with bosonic-like excitons rather than two-level emitters that generate such virtual quantum states. The reader interested in this direction is referred to recent experimental works by Peiris *et al.* [90] who considered such configurations. In the following, we will limit ourselves to the case of polaritons, with no strong intrinsic quantum-nonlinearities.

2.3 NUMERICAL METHODS

2.3.1 *Theoretical simulation of photon emission*

Between the theoretical modelling of photon-correlations as provided by master equations, integrals of photo-detection theory or from the sensor methods, and the experimental measurements with APDs placed on both arms of a beam-splitter, lies an intermediate case of increasing importance given the preponder-

ance of computers, namely: computer experiments. In this approach, one use a mixture of theoretical and computer simulations to study a system. In our case, belonging to a quantum optical framework, numerical simulations follow from the "Quantum Monte Carlo" method [47]. This method consists in evolving the wavefunction of the system with a discretization of time in steps δt. For each δt, the chances of obtaining a quantum jump are decided by random sampling. If there is no jump, the system evolves with an effective Hermitian hamiltonian (H_{eff}). Otherwise, the wavefunction is "collapsed". The procedure is the following: we define a probability for each term ($\mathcal{O}$) in H_{eff} that is susceptible of an observation:

$$\Delta P_{\mathcal{O}} = \gamma_{\mathcal{O}} \langle \Psi | \mathcal{O}^\dagger \mathcal{O} | \Psi \rangle \ , \tag{67}$$

where $\gamma_{\mathcal{O}}$ is the decay rate that can provoke the collapse. In the cases of the HO, the system is given by $H_{\text{eff}} = H - i\hbar\frac{\gamma}{2} a^\dagger a - i\hbar\frac{P}{2} a a^\dagger$, where H is XXX, $a^\dagger a$ is associated to the decay of the HO excitations and $a a^\dagger$ to their creation by an incoherent pumping at the rate P. Once these probabilities are computed from the current state of the wavefunction, a random number $r_{\mathcal{O}}$ between 0 and 1 is sampled for each term, for each time-step of the simulation. To decide whether there is a jump or not, the values of $r_{\mathcal{O}}$ and $\Delta P_{\mathcal{O}}$ are compared. If $r_{\mathcal{O}} < \Delta P_{\mathcal{O}}$, there is a jump (which in the HO case corresponds either to a loss of a photon due to the decay or to the increase given by the pumping, depending on which $\mathcal{O}$ is considered). The effect of this jump is to replace (collapse) the wavefunction according to:

$$|\Psi\rangle \to \left|\Psi_{\text{jump}}\right\rangle = \frac{\mathcal{O}|\Psi\rangle}{\langle\Psi|\mathcal{O}^\dagger\mathcal{O}|\Psi\rangle^{1/2}} \, . \tag{68}$$

The evolution given by a jump for the decay and pumping terms are thus given by:

$$|\Psi\rangle \to \left|\Psi_{\substack{\text{after}\\\text{decay}}}\right\rangle = \frac{a|\Psi\rangle}{\langle\Psi|a^\dagger a|\Psi\rangle^{1/2}} \, , \tag{69a}$$

$$|\Psi\rangle \to \left|\Psi_{\substack{\text{after}\\\text{excitation}}}\right\rangle = \frac{a^\dagger|\Psi\rangle}{\langle\Psi|aa^\dagger|\Psi\rangle^{1/2}} \, . \tag{69b}$$

On the other hand, for most of the cases for which all the values of $r_{\mathcal{O}}$ are greater than their corresponding $\Delta P_{\mathcal{O}}$, no jump is observed and the evolution is the one of standard Schrödinger equation:

$$|\Psi\rangle \to \left|\Psi_{\text{NO jump}}\right\rangle = \frac{e^{-\frac{i}{\hbar}\delta t H_{\text{eff}}}|\Psi\rangle}{\sqrt{\langle\Psi| e^{\frac{i}{\hbar}\delta t H_{\text{eff}}} e^{-\frac{i}{\hbar}\delta t H_{\text{eff}}}|\Psi\rangle}} \, . \tag{70}$$

For our simple HO case in which the terms are precisely the ones of decay and pumping, Eq. (70) reads:

$$|\Psi\rangle \to \left|\Psi_{\text{NO jump}}\right\rangle = \frac{\{1 - \delta t(i\frac{H}{\hbar} + \frac{\gamma}{2}a^\dagger a + \frac{P}{2}aa^\dagger)\}|\Psi\rangle}{\sqrt{1 - \Delta P_\gamma - \Delta P_P}}\,. \tag{71}$$

For the purpose of our computer simulations, each jump is recorded as a photon emission from the cavity (modelled as an HO). The times of such detections are stored in a file for post-processing, for instance to calculate the second order correlation function, just as it would be done in the laboratory of an actual experiment.

This quantum Monte Carlo method is equivalent to the master equation, although instead of computing directly averages, one gets access to raw data over which to compute such averages. This can be seen in the following way: taking into account that the evolution must depend on all the possible jumps (with probabilities $\Delta P_{\mathcal{O}}$) and the evolution corresponding to the absence of jumps:

$$\begin{aligned}|\Psi(t)\rangle\langle\Psi(t)| \to |\Psi(t+\delta t)\rangle\langle\Psi(t+\delta t)| = \\ = \sum_{\mathcal{O}} \Delta P_{\mathcal{O}} \left|\Psi_{\mathrm{jump}_{\mathcal{O}}}\right\rangle\left\langle\Psi_{\mathrm{jump}_{\mathcal{O}}}\right| + \\ + (1 - \sum_{\mathcal{O}} \Delta P_{\mathcal{O}}) \left|\Psi_{\text{NO jump}}\right\rangle\left\langle\Psi_{\text{NO jump}}\right|\,.\end{aligned} \tag{72}$$

Given that $\rho = |\Psi\rangle\langle\Psi|$ and assuming small values of $\gamma_{\mathcal{O}}$, the previous equation leads to:

$$\frac{d\rho}{dt} = -\frac{i}{\hbar}[H,\rho] + \sum_{\mathcal{O}} \frac{\gamma_{\mathcal{O}}}{2}\left[2\mathcal{O}\rho\mathcal{O}^\dagger - \mathcal{O}^\dagger\mathcal{O}\rho - \rho\mathcal{O}^\dagger\mathcal{O}\right]\,. \tag{73}$$

which is the master equation.

All these "clicks" obtained from the jumps allow to obtain by computer experiments the final value of the correlation function, obtained directly from Eq. 73. There are advantages and inconvenient to this approach. One inconvenient is that the theoretical observable is approached noisily and one needs a lot of signal for accurate results. An inconvenient is that this noise contains itself much information, for instance on fluctuations, bi-modality of the signal, etc. Studies on post-processing methods are developed in Chapter 3.

3 STUDIES OF PHOTON CORRELATIONS

In this Chapter, we discuss both experimental and theoretical methods for the computation and study of photon correlations. In particular, we undertake computer numerical experiments by generating photon clicks from a Quantum Monte Carlo procedure to study how photon correlations $g^{(2)}(t_1;t_2)$ are affected by various factors which arise in real experimental measurements and that we can keep under control with the computer simulations. These involve deficiencies such as non-stationary signals, noise, imperfect detectors, etc. Whenever possible, this analysis is backed-up by a pure theoretical modeling. Ways to circumvent most limitations are discussed.

3.1 INTRODUCTION

We have already said that one of the key observables in quantum optics is the statistics of photon detections, $g^{(n)}$. The case $n = 2$ has been by far the most investigated since it is the simplest and it makes the distinction between classical and quantum optics. Its definition has been given in Eq. (20) based on amplitudes of the electric field. In order to make it easier to manipulate in the following discussion, we will rewrite it directly as a function of the intensities:

$$g^{(2)}(t_1;t_2) = \frac{\langle I(t_1)I(t_2)\rangle_f}{\langle I(t_1)\rangle_f \langle I(t_2)\rangle_f}\,, \tag{74}$$

where $\langle\rangle_f$ denotes the average over the several measurements required to build up a statistics. Each such measurement will be called a "frame", since in our experimental implementation, it corresponds typically to one snapshot with the streak camera, that accumulates several such frames. The function defined by Eq. (74) is often described in the literature as related to the probability of the two-photon detection event, at the times t_1 and t_2. We will discuss more accurately the exact physical meaning of $g^{(2)}$ (it is clearly not directly a probability since it is unbounded). Eq. (74) is written for the general case. The quantity typically makes more physical sense in terms of a running time t and a correlation time $\tau = t_2 - t_1$:

$$g^{(2)}(t,\tau) = \frac{\langle I(t)I(t+\tau)\rangle_f}{\langle I(t)\rangle_f \langle I(t+\tau)\rangle_f}\,. \tag{75}$$

In the case of stationary signal, where only the time difference $\tau = t_2 - t_1$ matters, the photon statistics becomes a function of a single variable:

$$g^{(2)}(\tau) = \frac{\langle\langle I(t)I(t+\tau)\rangle\rangle_{f,t}}{\langle\langle I(t)\rangle\rangle_{f,t}\langle\langle I(t+\tau)\rangle\rangle_{f,t}}\,, \tag{76}$$

with the zero-delay value, $g^{(2)}(0)$, as the most important quantity, since, as was explained in section 1.3.2, it is the one that most strongly qualifies the character of light, i.e., with $g^{(2)}(0) < 1$ corresponding to a subpoissonian distribution, $g^{(2)}(0) = 1$ to a poissonian distribution and $g^{(2)}(0) > 1$ to a superpoissonian one. In any case, for a stationary signal, photons should not be correlated at infinite time and therefore one should always find that:

$$g^{(2)}(\infty) = 1\,. \tag{77}$$

Experimentally, such photon-correlation functions are typically obtained by photon coincidence experiments, such as the original HBT experiment explained previously (Section 2.1.4).

The guiding approach of the rest of this chapter is to rely on photon clicks generated by a Quantum Monte Carlo procedure, reviewed in section 2.3.1, to undertake numerical experiments that are fully under our control, and in which one can introduce various complications of relevance in actual experiments, where they are, on the opposite, often difficult to identify or set apart from the signal itself. This includes effects such as stationarity of the signal, noise, various imperfections of the detecting devices, etc.

To perform photon correlations, one must first collect the data from photon detection, which, at the simplest level, consist in the times of arrival in the selected modes. Not every emitted photon is duly recorded by the detector. There are basically two types of detector that can register light at the single-photon level: APDs (avalanche photodiodes) and a streak camera. They do not perform equally. We now briefly discuss their advantages and inconvenients. APDs are of great importance for single-photon detection. The most frequently used detectors for detection of low-intensity light are photomultiplier tubes (PMTs), but their quantum efficiency is small (smaller than 0.5). For this reason APDs are used, which have an additional gain mechanism: the 'avalanch effect'. With the APDs, a stable gain on the order of 10^2 to 10^3 can be achieved, which is still too low to detect single photons. For this purpose, the APDs must be used in the 'Geiger mode' [61]. These single-photon avalanche photodiodes (SPADs) have a high detection efficiency and low dark count rates, but they are slow and with a big temporal uncertainty (typically $300-400$ ps, although they can be found of 35 ps [54]). To multiply the signal, they use semiconductor materials. Depending on these materials, the APDs operate in different frequency windows between 550 and 1550 nm. Another source of noise characteristic of

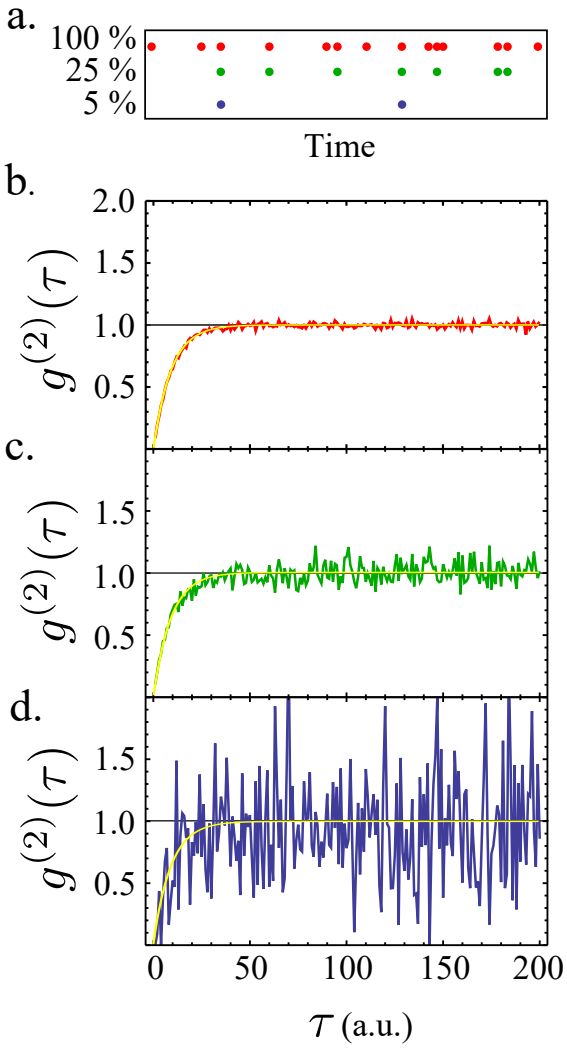

Figure 17: a: detection of photons with time. The red spots correspond to the signal without losses, the green one loses 75 % of the signal and the blue one loses 95 %. b, c and d are the statistics for the same system with different detection efficiencies (red = perfect detection, green = 75% losses and blue = 95%). The yellow curve corresponds to the theoretical results. It is clear how the statistics is the same regardless of the efficiency.

APDs is the afterpulsing, which can limit the count rate [122]. *Streak cameras*, on the other hand, have low detection efficiency but allow for a resolution of the order of the ps. They operate in frequency windows of $300 - 1700$ nm, depending once again on the material used for the photocathode.

3.2 EFFICIENCY OF THE DETECTOR

Given that the streak camera is so inefficient, a first question arises as to whether it is useful for photon correlations. It is well known in the quantum optics literature (see, e.g., Ref. [15]) how only a coherent signal can pass linear optical element without being spoiled, and that subpoissonian or superpoissonian signals will always get closer to Poissonian distributions, e.g., by passing through beam-splitters. This, however, refers to the noise of the signal rather than to its statistics. Such a closeness to a Poissonian distribution is typically measured by the Fano factor, which relates the width of the input distribution to the expected one for a Poissonian distribution with the same average number:

$$\mathrm{Fano} = (\langle n^2\rangle - \langle n\rangle^2)/\langle n\rangle\,. \tag{78}$$

Therefore, as the Fano factor grows linearly from 0, corresponding to the Number state distribution, to 1, corresponding to the Poisson distribution, as the probability to loose any one photon of the input beam is increased, the statistics as measured by $g^{(2)}(0)$ remains constant, equal to that of the ideal signal. This is clear on physical grounds since removing photons to an antibunched signal cannot create bunching. What is spoiled is the signal, which can however be compensated by longer integration times. The loss is therefore in quantity, not in quality. This is illustrated in Fig. 17 (a–d), where this time the photons clicks originate from a two-level system, *in a similar one as detailed above for the HO*. The corresponding $g^{(2)}(\tau)$ is shown for three cases of photon efficiency (100%, 25% and 5%). The respective Fano are 0.83, 0.96 and 0.99. The best fit to the data always provide the same value of antibunching. Only the noise is increased.

3.3 STATIONARITY OF THE SIGNAL

Under CW excitation, one is usually in presence of a stationary signal, i.e., one which, on average, does not depend on time. As a consequence, time-dynamics is in the autocorrelation time. When considering any particular case, there are fluctuations, which are however averaged out by considering multiple realizations or integrating over time. Any of these two procedures results in the same

time-independent average value, a property which is known as the ergodic hypothesis [53]. The two possible types of averaging are defined as:

$$\langle \mathcal{A}(t,\tau)\rangle_t = \frac{\int_0^{t_{max}-\tau} \mathcal{A}(t,\tau)\,dt}{\int_0^{t_{max}-\tau} dt}\,, \tag{79}$$

over time for each value of τ and:

$$\langle \mathcal{A}(t,\tau)\rangle_f = \frac{\sum_{f=1}^{F} \mathcal{A}(t,\tau)_f}{F}\,, \tag{80}$$

over realizations (f), with $\mathcal{A}(t,\tau)_f$ the value of the function $\mathcal{A}(t,\tau)$ for each measurement. We use f as the label in this case referring to a "frame" of the streak camera that provides a given realization. F corresponds to the total number of frames.

For a stationary signal, by definition, the following computation provides the same result regardless of the order of frames and time averages:

$$\widehat{g^{(2)}}(\tau) = \frac{\langle\langle I(t)I(t+\tau)\rangle_f\rangle_t}{\langle\langle I(t)\rangle_f\rangle_t\langle\langle I(t+\tau)\rangle_f\rangle_t} = \frac{\langle\langle I(t)I(t+\tau)\rangle_t\rangle_f}{\langle\langle I(t)\rangle_t\rangle_f\langle\langle I(t+\tau)\rangle_t\rangle_f}\,. \tag{81}$$

There are also other ways to obtain a $g^{(2)}(\tau)$ curve from an underlying $g^{(2)}(t,\tau)$ that is averaged. That is, one averages the ratio rather than making the ratio of the averages as in Eq. (81). There are, again, two possible averages:

$$\overline{g^{(2)}}(\tau) = \langle \frac{\langle I(t)I(t+\tau)\rangle_f}{\langle I(t)\rangle_f\langle I(t+\tau)\rangle_f}\rangle_t\,, \tag{82}$$

by averaging $g^{(2)}(t,\tau)$ over time, and

$$\widetilde{g^{(2)}}(\tau) = \langle \frac{\langle I(t)I(t+\tau)\rangle_t}{\langle I(t)\rangle_t\langle I(t+\tau)\rangle_t}\rangle_f \tag{83}$$

by calculating first $g^{(2)}(\tau)$ in each frame and averaging afterwards over all of them. We will now compare these three approaches, Eqs. (81), (82) and (83).

In an actual experiment, the signal might not be ideally stationary. For instance there might be a small drift in time due to misalignment of the apparatus or slowing changing external parameters. Another cause for non-stationary signals, that is both relevant and difficult to perceive, comes from the use of a "chopper". This is a device that intermittently obstructs the exciting laser, to avoid heating of the sample. This produces sequences of heating and cooling that can leave the one-photon properties unaffected but lead to errors in photon correlations.

To consider the effect of non-stationarity of a signal and the response of the various ways to compute $g^{(2)}$ out of them, we start with an uncorrelated signal, corresponding to coherent emission. The theoretical $g^{(2)}$ in this case is simple:

$$g^{(2)}(t,\tau) = 1\,. \tag{84}$$

We show that the selection of the method to use is not trivial, but depends on the conditions of the experiment. In general the first method ($\widehat{g^{(2)}}(\tau)$) can always be used, but it implies a larger amount of calculations, since it contains 6 averages instead of 4 like the other two methods. Therefore, we study two different limits in order to find the ideal limit for each of the definitions. In the case in which the number of frames (F) is greater than the length of each of them (p), i.e. $F \gg p$, the average should first be done over all the frames (obtaining $g^{(2)}(t,\tau)$), and finally over all the times, hence the third method ($\overline{g^{(2)}}(\tau)$) can be used. In the opposite limit, in which the size of the frames (p) is bigger than the number of frames (F), the third method ($\widetilde{g^{(2)}}(\tau)$) should be applied. That is to say, when dealing with 4 averages instead of 6 the first averages should always be done over the variable with more signal (time in each frame in the first case, and frames in the second one). Otherwise, the first average taken with such a low signal would lead to normalization problems in the final $g^{(2)}(\tau)$. Fig 18 shows the results obtained in both limits using the general formula, which gives well normalized curves for both cases and the two methods. This simulation was done with uncorrelated clicks, hence the statistics is coherent and the $g^{(2)}$ should be one for all times, as we said. But it is clear that the behaviour is not always the predicted one if the method is not selected correctly, leading to wrong normalizations expressed as vertical shifts of the curves.

It should also be pointed out that in the cases in which F and p are not in one of the two limits, the selection of one of the two methods is not trivial. The results of the two studies should be compared, and in some limits extra normalizations may be needed to recover the expected behaviour.

This study was for an ideal signal, for which only the algorithm of computation was altered. In a real context, one is interested in actual alterations on the signal itself. Even with the correct order of the averaging, one can observe a signal not being normalized properly, i.e., for which even $g^{(2)}(\infty) \neq 1$. This is typically caused by non-stationarity.

3.3.1 *Chopper and drift*

Let us consider the most common case: the use of a chopper to avoid warming up the sample (similar to the effect of using pulses instead of continuous

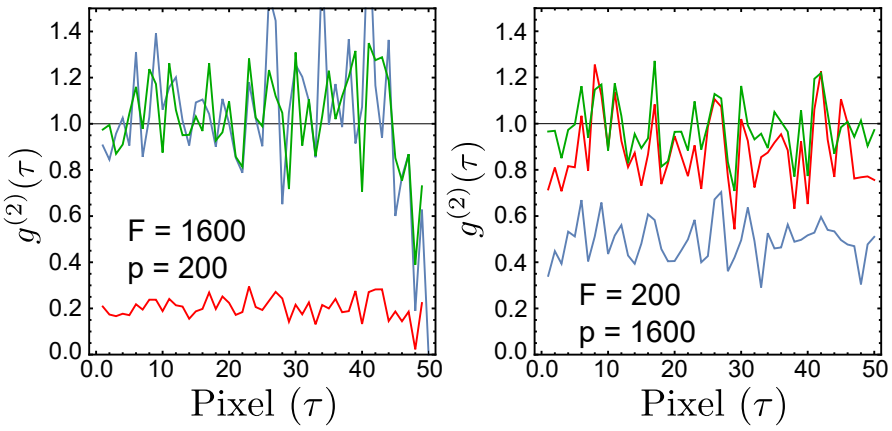

Figure 18: Correlations depending on the proportions between the number of frames and their length. Uncorrelated detections ($g^{(2)} = 1$ expected). Green, blue and red correspond to Eqs. (81), (82) and (83). Left: $F \gg p$, either Eq. (81) or (82) should be used. Right: $p \gg F$, either Eq. (81) or (83) should be used. In order to simplify the color notation along the chapter, all the curves of $\widehat{g^{(2)}}(\tau)$ will be represented in green colors, $\overline{g^{(2)}}(\tau)$ in blue colors and $\widetilde{g^{(2)}}(\tau)$ in red.

signal [77]). Our first purpose is to simulate this experimental set-up: a laser going through a chopper 1:2 (i.e. 50% of the time open).

Two different functions are used to act as the modulation ($\mathcal{F}(t)$): a square wave and a sine square such that it oscillates between 0 and 1. For small frequencies the chopper affects the modulation, but no new correlations are created. On the other hand, as the frequency is increased the effect is clear, not only on the normalization but also on the statistics. These changes can be identified in Fig 19 (a–b), being blue the coherent signal with square wave modulation and light blue the same signal with sinusoidal modulation. When the frequency is such that the oscillations are not appreciated in the individual frames, acting locally as a constant modulation, there is a coherent behaviour multiplied by a factor $\mathcal{C}$. This is given by:

$$g^{(2)*}(\tau) = \frac{\langle I(t)^* I(t+\tau)^* \rangle_{f,t}}{\langle I(t)^* \rangle_{f,t} \langle I(t+\tau)^* \rangle_{f,t}}, \tag{85}$$

where the relation between $I^*(t)$ and $I(t)$ is given by $I^*(t) = \mathcal{F}(t)I(t)$. Taking into account the fact that the modulation and the coincidences are uncorrelated, $\langle I(t)^* \rangle_{f,t} = \langle \mathcal{F}(t) \rangle_{f,t} \langle I(t) \rangle_{f,t}$ and substituting these relations in Eq. (85):

$$g^{(2)*}(\tau) = \mathcal{C} g^{(2)}(\tau), \tag{86}$$

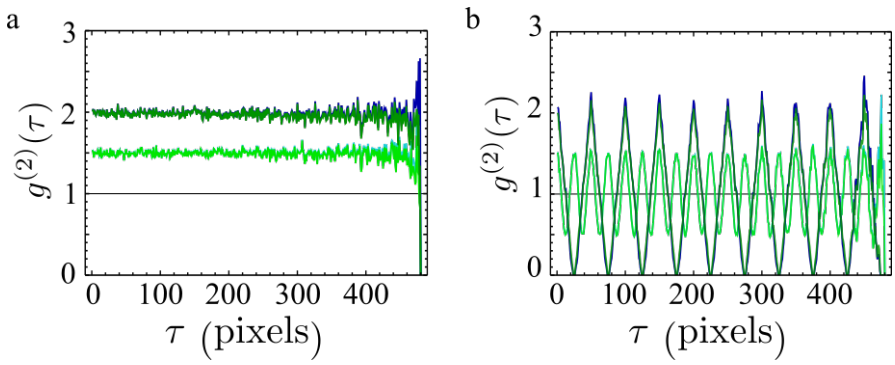

Figure 19: Effects of the modulation. a and b: Slow (left) and fast (right) choppers. Light green and blue correspond to a sinusoidal modulation while dark green and blue correspond to a squared modulation. As in the previous figure, green colors correspond to Eq. (81) ($\widehat{g^{(2)}}(\tau)$) and blue to Eq. (82) ($\overline{g^{(2)}}(\tau)$).

being $\mathcal{C} = \langle \mathcal{F}(t)^2 \rangle_t / \langle \mathcal{F}(t) \rangle_t^2$. For the modulations studied in this paper (chopper 1:2), $\mathcal{C}_{squared} = 2$ and $\mathcal{C}_{sine^2} = 1.5$

On the other hand, when the oscillations take place in each individual frame, the coherent behaviour disappears and the $g^{(2)}(\tau)$ oscillates, which can be seen as a signal with infinite coherence time [81]. These oscillations in the correlations are sinusoidal between 0.5 and 1.5 in the case of sinusoidal modulations, and a triangular wave between 0 and 2 for the square wave modulation. Figure 19 (b) shows the tremendous change in the behaviour of the $g^{(2)}(\tau)$ as the frequency increases. These results can also be obtained when calculating the second-order correlation function for a squared wave [81].

Now we move to a different experiment in which the signal instead of being a normal laser (coherent) shows bunched or antibunched correlations. Once again, these signals are modulated (in this case only the square modulation is considered). Since experimentally the modulation due to the chopper is slower than the time of a frame, we center our studies on slow squared modulations.

Fig. 20 (a–b) presents the results of the simulations. The left panel depicts the effect on the antibunched signal, and in the right panel is the one on the bunched signal. In each figure four curves are identified: yellow, purple, green and blue. The purple curves correspond to the signal without modulations and the green and blue are the same signal with a slow square wave modulation studied by means of $\widehat{g^{(2)}}(\tau)$ and $\overline{g^{(2)}}(\tau)$.

As it was previously shown, a modulation multiplies the original second-order correlation function by a factor $\mathcal{C}$. In this case, we can see how by dividing

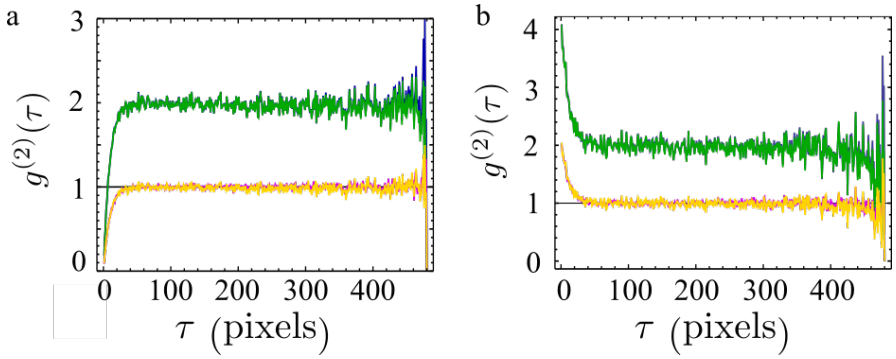

Figure 20: Effects of the modulation. a and b: Antibuched (left) and bunched (right) signals with slow choppers. Purple corresponds to the signal without modulation, green and blue correspond to modulated signals calculated by $\widehat{g^{(2)}}(\tau)$ and $\overline{g^{(2)}}(\tau)$. Yellow correspond to the normalized modulated signal.

the blue curve over 2 ($\mathcal{C}_{squared} = 2$), we recover the original results (yellow curve).

3.3.2 *Effect of modulations on the stationarity*

In the previous section we have studied the effect of a chopper on a signal, assuming that it does not affect the stationarity. This must be checked before continuing with our studies. As can be seen in Fig. 21 (a–b), there is a dependence between the stationarity of the signal and the dephasing of the modulation between frames. If the modulation is such that it has the same phase in all the frames (black curve), the stationarity disappears and the average intensity oscillates. This is because in this case the times with zero intensity are the same ones for all the frames and the values of $\langle I(t)\rangle_f$ are zero for these times. In the cases where there is phase difference between frames (red curve) the average intensity is constant, i.e. the signal is stationary. This dependence on the phase difference between frames must be taken into account when selecting the speed of the chopper (usually slower than a frame, in which case the modulation would not change the stationarity of the system).

Up to this point, we have always found that the results of the $g^{(2)}$ obtained for stationary signals by means of $\widehat{g^{(2)}}(\tau)$ and $\overline{g^{(2)}}(\tau)$ are the same in the limit $F \gg p$. To study the effect of nonstationarity we have applied two different modulations to the same coherent signal. The first one (red curve figure 21c) with a frequency of $\omega = 2\pi/(p+2)$ and the second one (blue curve figure 21c) with a frequency $\omega = 2\pi/p$. Although the difference between these two

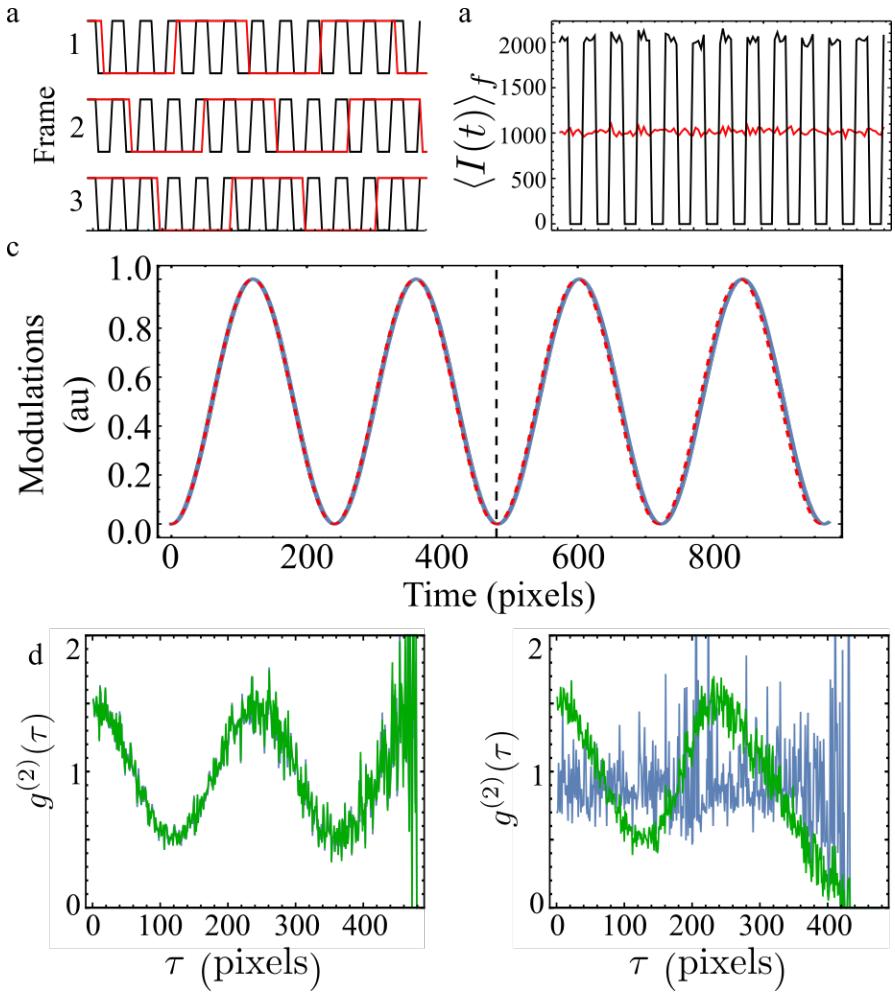

Figure 21: a: modulation in three different frames. Black: no dephasing between frames, red: phase difference between frames. b: stationarity of the modulations of a. c: Modulations of the form $\sin(\omega t)^2$ with small dephase between frames, the dashed line denotes $\mathrm{time} = p$. d: $g^{(2)}(\tau)$ for stationary modulated signal. Both methods overlap. e: $g^{(2)}(\tau)$ for nonstationary modulated signal. In d and e, green corresponds to $\widehat{g^{(2)}}(\tau)$ and blue to $\overline{g^{(2)}}(\tau)$.

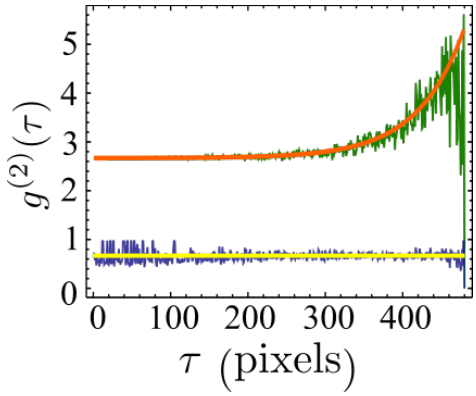

Figure 22: $g^{(2)}(\tau)$ for a Fock state N=3. Green and represent the simulated and the analitical results for $\widehat{g^{(2)}}(\tau)$, Blue and orange yellow represent the simulated and analitical results for $\overline{g^{(2)}}(\tau)$.

modulations is almost neglectable, the first one will correspond to an stationary signal (since there is a phase difference between frames) and the second one to a non-stationary signal. When the value of $g^{(2)}(\tau)$ is calculated, a clear effect appears: while in the stationary limit both methods overlap (figure 21d), in the nonstationary limit (figure 21e) the two methods diverge. In this case, while the green curve ($\widehat{g^{(2)}}(\tau)$) keeps the behavior of the stationary limit up to high τ, the blue curve ($\overline{g^{(2)}}(\tau)$) loses the stationary behavior.

In order to obtain more precise results on nonstationarity a second system was studied: the spontaneous emission of a N=3 Fock state (see figure 22). The theory predicts a value of $g^{(2)}(0) = 1 - 1/N$ for an N Fock state, but it is clear from figure 22 how the blue curve does not satisfy this condition. Unlike in the previous case of nonstationarity, in this case only the definition $\overline{g^{(2)}}(\tau)$ gives the predicted result. Figure 22 also depicts the analitical equation for both definitions: orange for $\widehat{g^{(2)}}(\tau)$ and yellow for $\overline{g^{(2)}}(\tau)$. This result is explained in more detail forward in this chapter in section 3.5.

With these two results in hand, there is not a precised way of defining the "correct" method. Yet, by knowing the expected value at $\tau = 0$ and the one of the two methods, it is easy to identify which is the adequate one for the system.

3.4 EFFECT OF NOISE AND IMPERFECT DETECTORS

For this section we center our studies on a specific set-up explained in section 2.1.4: the streak camera [37]. These devices are of great temporal precision

(temporal distance between pixels = $\Delta t \sim$ ps), which gives any source of noise a stronger effect.

There are three different kinds of noise [12, 107] that must be taken into account when using a streak camera. The first one is the "random noise", which describes the dark counts that appear when the detector produces uncorrelated non-existing counts. The second one is the "gravity peak", induced when the streak camera counts one detection twice and the third one is the "timing jitter" [83], which gives a temporal uncertainty.

In this section we study the effect of these three types of noise on the statistics on bunched and antibunched systems.

3.4.1 *Random noise*

In a streak camera, the signal that arrives to the detector should belong to the photoelectrons created by the source being studied. In some cases, some clicks appear totally uncorrelated to the source. For example, carriers can be created thermally (dark counts) [107], or in some cases, some external signal due to a laser [121] can get inside the streak camera. All these detections uncorrelated with the source cause the so-called "random noise".

If we call $I(t)$ the intensity of clicks for the source and $I'(t)$ the one of the random added clicks, the total final intensity is given by:

$$I^*(t) = I'(t) + I(t) \tag{87}$$

Uncorrelated signals (in this case the source and the random noise) follow the following relation:

$$\langle I(t)I'(t)\rangle_{f,t} = \langle I(t)\rangle_{f,t}\langle I'(t)\rangle_{f,t} \tag{88}$$

Taking ξ as the proportion of the initial signal included with random clicks, the initial and random signals are related by : $\langle I'(t)\rangle_{f,t} = \xi\langle I(t)\rangle_{f,t}$. To calculate the second-order correlation function for a source with random noise we will have to substitute all these previous relations in $g^{*(2)}(\tau)$:

$$g^{*(2)}(\tau) = \frac{\langle I^*(t)I^*(t+\tau)\rangle_{f,t}}{\langle I^*(t)\rangle^2_{f,t}} \tag{89}$$

Including first the definition given by Eq. (87) and the relation of Eq. (88), the previous equation becomes:

$$g^{*(2)}(\tau) = \frac{\langle I(t)I(t+\tau)\rangle_{f,t} + \langle I(t)\rangle_{f,t}\langle I'(t+\tau)\rangle_{f,t}}{(1+\xi)^2\langle I(t)\rangle_{f,t}^2} + \frac{\langle I'(t)\rangle_{f,t}\langle I(t+\tau)\rangle_{f,t} + \langle I'(t)\rangle_{f,t}^2}{(1+\xi)^2\langle I(t)\rangle_{f,t}^2} \tag{90}$$

This way we obtain the following formula that relates the statistics with noise and the one without noise:

$$g^{*(2)}(\tau) = \frac{1}{(1+\xi)^2}\left(g^{(2)}(\tau) + 2\xi + \xi^2\right) \tag{91}$$

As it was shown in the first section, if instead of having bunched or antibunched signals we have a random set of data, the curve should be one for all times, as in the green and blue curves on Fig. 18 (a). Hence, we would expect this extra random signal in a bunched or antibunched set of clicks to shift the $g^{(2)}(\tau)$ to one. This is verified and shown in Fig. 23 (a–b), in which the values of $g^{(2)}(\tau \ll \tau_c)$ move towards one as the proportion of random noise increases. In the same curve we can also see the comparison of the results obtained with the simulations (continuous lines) and the ones with Eq. (91), which clearly match the Monte Carlo results.

One important characteristic of this noise is that it will shift the curves to one, but it will never transform bunching behaviours into antibunching and vice versa [110]. It also has no effect on the coherence time (the time necessary for the correlation to converge to one is independent of the percentage of noise).

3.4.2 *Gravity peak*

Typically, when a photoelectron arrives to the detector, since its size is bigger than one pixel, it should only excite the one at which the center of gravity of the photoelectron is found. Sometimes this selection process is not efficient enough, and more than one pixel are excited by just one detection [12]. This spreading of one photoelectron over several pixels gives rise to the so-called "gravity peak".

Although the effect of introducing clicks changes the entire statistics, these modifications can be neglected for the entire correlation except for the temporal delays of the order of the distance between real and fake detections (Fig. 23 (c–d)). To avoid this effect, it is possible to group these real photodetections with their fake detections and consider them just one click. This way, the fake coincidences at short time delay due to the gravity peak are avoided. On the other hand, this also makes real consecutive arrivals disappear, affecting the correlations at small temporal delays. Typically the size of one photoelectron is such

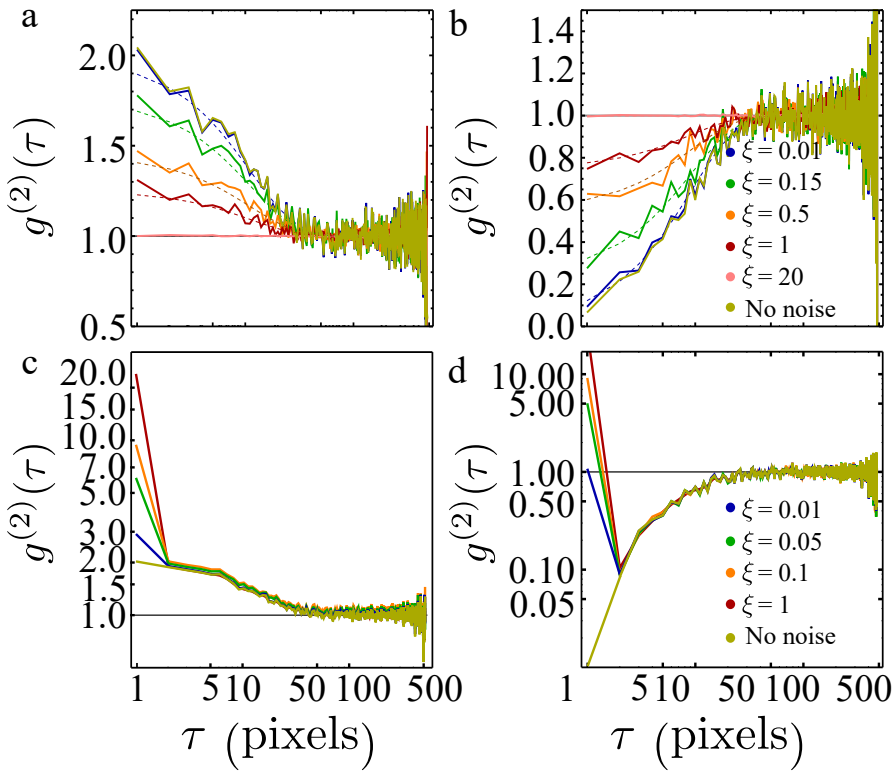

Figure 23: Random noise and gravity peak as an increase of the percentage of noise. a–b: random noise applied to a bunching and antibunching signal. c–d: gravity peak at a bunched and antibunched signal.

that it excites two consecutive pixels (with a temporal difference of Δt). Hence, we limit our studies to the effects of two-pixel width photoelectrons.

To eliminate the effect of this binning process, we have defined a mathematical relation between the obtained results $g^{(2)*}(\tau = \Delta t)$ and the ones expected without noise $g^{(2)}(\tau = \Delta t)$ for the most common case at which one photoelectron excites two pixels. To understand the coincidences we can consider an initial set of 3 clicks at $t = 0$, $t = \Delta t$ and $t = 3\Delta t$, leaving only one coincidence with $\tau = \Delta t$ between the first two clicks. The effect of the gravity peak on the second photon would create two additional coincidences with $\tau = \Delta t$: one between the original second click and the new one and another one between the new click and the one at $t = 3\Delta t$, which initially was at $\tau = 2\Delta t$ from the click with gravity peak. With this in hand, the $g^{(2)*}(\tau = \Delta t)$ can be recalculated including the two new sources of coincidences:

$$g^{(2)*}(\Delta t) = \frac{\langle I(t)I(t+\Delta t)\rangle_{f,t} + \xi\langle I(t)\rangle_{f,t} + \xi\langle I(t)I(t+2\Delta t)\rangle_{f,t}}{(\langle I(t) + \xi I(t)\rangle_{f,t})^2}, \quad (92)$$

being $\langle I(t)\rangle$ the average number of detections per pixel at time t, $\langle I(t)I(t+\tau)\rangle$ the average number of coincidences at τ and ξ the proportion of photoelectrons with gravity peak. This equation takes into account the three sources of coincidences at $\tau = \Delta t$. The first term are the original coincidences without gravity peak (first term). The next one is the one due to the fact that each detected photon with gravity peak will have a coincidence (the real click with the fake click) at $\tau = \Delta t$, so the total number of these coincidences will be given by the total number of added clicks, $\xi\langle I\rangle$. Finally, the ones created between the new detection (at $\tau = \Delta t$) and the original detections at $\tau = 2\ \Delta t$ are given by the third term. The last two terms depend on the proportion of photodetections with gravity peak (ξ). The increase of the number of detections also affects the normalization, that is the reason why the increase of the number of clicks depends on ξ and is included in the denominator.

Taking into account the definition of the second-order correlation function and the fact that, since the signal is stationary $\langle I(t+\tau)\rangle = \langle I(t)\rangle$ the previous equation becomes:

$$g^{(2)*}(\Delta t) = \frac{\langle I(t)I(t+\Delta t)\rangle_f, t + \xi\langle I(t)\rangle_f, t + \xi\langle I(t)I(t+2\Delta t)\rangle_f, t}{((1+\xi)\langle I(t)\rangle_f, t)^2}, \quad (93)$$

which finally gives the relation between the original $g^{(2)}$ and the one with the gravity peak:

$$g^{(2)*}(\Delta t) = \frac{1}{(1+\xi)^2}\left(g^{(2)}(\Delta t) + \frac{\xi}{\langle I(t)\rangle} + \xi g^{(2)}(2\ \Delta t)\right) \quad (94)$$

For our simulations we are always studying two types of signal. The first one is a bunched signal ($g_+^{(2)}$, which corresponds to classical systems, in our case an harmonic oscillator incoherently pumped). The other one is an antibunched one ($g_-^{(2)}$), which corresponds to quantum systems, in our case a two-level system). The correlation function for these two sources is given by:

$$g^{(2)}(\tau)_\pm = 1 \pm e^{-\gamma|\tau|}, \quad (95)$$

where $\gamma = (\gamma_a \mp P_a)$, γ_a corresponds to the decay rate of the harmonic oscillator and P_a is the incoherent pumping rate. Applying these curves in Eq. (94) and considering $\langle I(t)\rangle = n_a\gamma_a\Delta t$, (being n_a the average number of excitations) we arrive to the following formula:

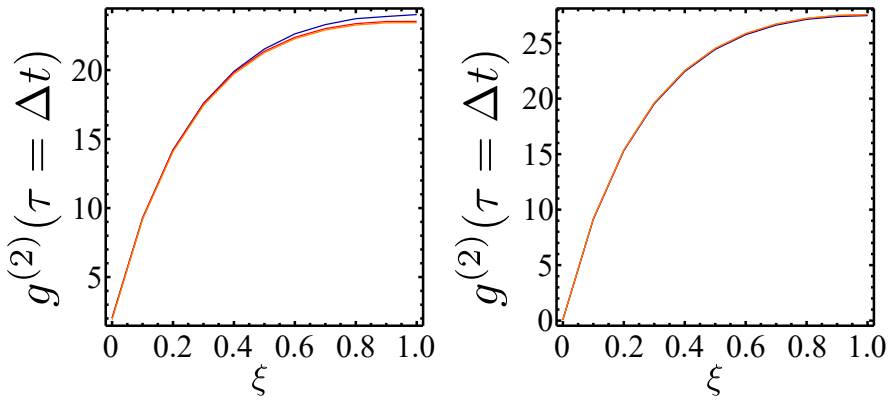

Figure 24: Comparison of the value of $g^{(2)}(\tau = \Delta t)$ with gravity peak as the percentage of photodetections with gravity peak increases. Blue: simulation including a detection after the ξ proportion of the total detections. Red: curve obtained by means of formula $\widehat{g^{(2)}}(\tau)$. Orange: curve obtained by means of formula $\overline{g^{(2)}}(\tau)$. The curves on the left correspond to a bunching signal, and the ones on the right to an antibunching signal.

$$g^{(2)*}(\Delta t)_{\pm} = \frac{1}{(1+\xi)^2}\left(1 \pm e^{-\gamma \Delta t} + \frac{\xi}{n_a \gamma_a \, \Delta t} + \xi(1 \pm e^{-2\gamma \Delta t})\right) \tag{96}$$

Figure 24 shows a comparison of the results obtained by means of the simulation, Eq. (94) and Eq. (96) for the calculation of $g^{(2)*}(\Delta t)$.

3.4.3 *Timming jitter*

$g^{(2)}(\tau)$ measurements suffer from an unavoidable uncertainty in the arrival time of photons to the detector, θ. Although, typically, this does not imply acquiring information about their frequency, it is linked to the uncertainty in frequency Γ as $\sigma = 1/\Gamma$ ($\hbar = 1$) in accordance with Heisenberg principle. The frequency information is erased in the sense that photon counting is performed with all photons, regardless of their frequency.

Experimentally, a jitter is the probability of finding a shift on the temporal detection and is given by a square-normalised ($\int_{-\infty}^{\infty} dt\, [J_\sigma(t)]^2 = 1$) symmetric distribution J. In our case, we study three possible shapes of the jitter: an

exponential decay $P_\sigma(t) = \sqrt{\frac{1}{2\sigma}} e^{-|t|/2\sigma}$, a Heavy-side step-function $H_\sigma(t) = \sqrt{\frac{1}{2\sigma}}\theta(-t+\frac{1}{\sigma})\theta(t+\frac{1}{\sigma})$ and a Gaussian noise one $N_\sigma(t) = \sqrt{\frac{1}{\sigma\sqrt{2\pi}}} e^{-(t/2\sigma)^2}$ [113].

Now we are going to show the steps to follow to arrive to the equation of the second-order correlation function with temporal jitters. Let us start with the physical spectrum of emission, defined as [40]

$$S_\Gamma^{(1)}(\omega, T) = \frac{1}{2\pi}\iint_{-\infty}^{\infty} dt_1\, dt_2 J_\Gamma(T-t_1) J_\Gamma(T-t_2) \\ e^{i\omega(t_2-t_1)}\langle a^\dagger(t_1)a(t_2)\rangle \quad (97)$$

for a particular filtering function F (square-normalised, $\int_{-\infty}^{\infty} dt\,[J_\Gamma(t)]^2 = 1$). Integrating this in the frequency variables leads to

$$S_\Gamma^{(1)}(T) = \langle n_J(T)\rangle = \int_{-\infty}^{\infty} dt J_\Gamma^2(T-t)\langle a^\dagger a\rangle(t)\,. \quad (98)$$

This convolution is the population of the detector or filtering system at a given time T. In a typical spectrometer (Fabry-Perot type) F is an exponentially decaying function $E_\Gamma(t) = \sqrt{\Gamma}\theta(t)e^{-\Gamma t/2}$. This represents, when evaluated at $T-t$, a decaying probability that a photon was emitted at time t before its measurement at time T. This type of delay in detection could be due to the electronics involved in the detection of a photon *after* its arrival.

If the signal is in a steady state where $\langle a^\dagger a\rangle(t) = n_a$ is time-independent, the integral is further simplified to the mean total emitted (or detected) intensity: $S_\Gamma^{(1)} = n_F = n_a$.

An equivalent treatment can be applied to the second order coherence function, resolved in time and frequency [115]:

$$S^{(2)}_{\Gamma_1\Gamma_2}(\omega_1, T_1; \omega_2, T_2) = \frac{\Gamma_1\Gamma_2}{(2\pi)^2}\iiiint_{-\infty}^{\infty} dt_1\, dt_2\, dt_3\, dt_4 \\ J_{\Gamma_1}(T_1-t_1)J_{\Gamma_1}(T_1-t_4)J_{\Gamma_2}(T_2-t_2)J_{\Gamma_2}(T_2-t_3) \\ e^{i\omega_1(t_4-t_1)}e^{i\omega_2(t_3-t_2)}\langle \mathcal{T}_-[a^\dagger(t_1)a^\dagger(t_2)]\mathcal{T}_+[a(t_3)a(t_4)]\rangle\,. \quad (99)$$

with $\mathcal{T}_\pm$ meaning time-reordering of the operators so that the first time is to the far right/left. The frequency-integrated quantity reads (with the same uncertainty for both detections $\Gamma_1 = \Gamma_2 = \Gamma$):

$$S_\Gamma^{(2)}(T_1; T_2) = \langle : n_J(T_1)n_J(T_2) :\rangle \\ = \iint_{-\infty}^{\infty} dt_1\, dt_2 J_\Gamma^2(T_1-t_1)J_\Gamma^2(T_2-t_2) \\ \langle \mathcal{T}_-[a^\dagger(t_1)a^\dagger(t_2)]\mathcal{T}_+[a(t_2)a(t_1)]\rangle\,. \quad (100)$$

This is the intensity-intensity correlations between the output of the two filtering functions, with : meaning normal ordering of the operators. We can separate these integrals in two regions, $t_1 > t_2$ and $t_2 > t_1$, to express them in terms of the standard $G^{(2)}(t,\delta)$ of the system where $\delta = |t_1 - t_2|$ and $t = \min(t_1, t_2)$:

$$S_\Gamma^{(2)}(T_1;T_2) = \int_0^\infty d\delta\, G^{(2)}(t,\delta) \int_{-\infty}^{\infty} dt[J_\Gamma^2(T_1-t)J_\Gamma^2(T_2-t-\delta) + J_\Gamma^2(T_1-t-\delta)J_\Gamma^2(T_2-t)]\,. \quad (101)$$

The normalised second-order correlations read:

$$g_\Gamma^{(2)}(T_1;T_2) = \frac{S_\Gamma^{(2)}(T_1;T_2)}{S_\Gamma^{(1)}(T_1)S_\Gamma^{(1)}(T_2)}\,, \quad (102)$$

Assuming that there is a steady state, $T_1 = 0$, $T_2 = \tau \geqslant 0$, we have $G^{(2)}(t,\delta) = G^{(2)}(\delta)$ and further simplifications:

$$S_\Gamma^{(2)}(\tau) = \int_0^\infty d\delta\, G^{(2)}(\delta) \int_{-\infty}^{\infty} dt[J_\Gamma^2(-t)J_\Gamma^2(\tau-t-\delta) + J_\Gamma^2(-t-\delta)J_\Gamma^2(\tau-t)]\,, \quad (103)$$

with normalised value $g_\Gamma^{(2)}(\tau) = S_\Gamma^{(2)}(\tau)/[S_\Gamma^{(1)}]^2$ finally leads to:

$$g_\sigma^{(2)}(\tau) = \int_0^\infty d\delta\, g^{(2)}(\delta) \int_{-\infty}^{\infty} dt[J_\sigma^2(-t)J_\sigma^2(\tau-t-\delta) + J_\sigma^2(-t-\delta)J_\sigma^2(\tau-t)]\,, \quad (104)$$

By means of Eq. (104), we have been able to calculate the second-order correlation function for the three types of jitter for a bunched (+) and antibunched (-) source:

$$g_{P_\sigma\pm}^{(2)}(\tau) = \frac{e^{-\frac{\tau}{\sigma}}(\pm 2e^{\tau(\frac{1}{\sigma}-\gamma)} + 2e^{\frac{\tau}{\sigma}}(-1+\gamma^2\sigma^2)^2}{2(-1+\gamma^2\sigma^2)^2} \pm \frac{\gamma(-\tau+\sigma(3+\gamma^2\sigma(\sigma+\tau)))}{2(-1+\gamma^2\sigma^2)^2}\,, \quad (105)$$

$$g^{(2)}_{H_{\sigma}\pm}(\tau) = \pm\frac{1}{4\sigma^2}(\pm 4\sigma^2 + \frac{e^{-2\gamma(\sigma+\tau)}(e^{\gamma\tau}(-1+e^{2\gamma\sigma})^2}{\gamma^2} + \frac{e^{\gamma(2\sigma+\tau)}(-e^{2\gamma\sigma}+e^{\gamma\tau}(1+2\gamma\sigma-\gamma\tau))\Theta[2\sigma-\tau]^2}{\gamma^2}) + \frac{e^{\gamma(2\sigma+\tau)}(-e^{2\gamma\sigma}+e^{\gamma\tau}(1+2\gamma\sigma-\gamma\tau))\Theta[2\sigma-\tau]}{\gamma^2} \frac{\Theta[-2\sigma+\tau]+(-1+e^{\gamma(-2\sigma+\tau)}+2\gamma\sigma-\gamma\tau)}{\gamma^2} \frac{(\Theta[2\sigma-\tau]+\Theta[2\sigma-\tau,-2\sigma+\tau])}{\gamma^2}), \quad (106)$$

$$g^{(2)}_{N_{\sigma}\pm}(\tau) = \frac{1}{2}(2 \pm e^{\gamma(\gamma\sigma^2-\tau)}\operatorname{erfc}\left(\gamma\sigma - \frac{\tau}{2\sigma}\right) \pm e^{\gamma(\gamma\sigma^2+\tau)}\operatorname{erfc}\left(\gamma\sigma + \frac{\tau}{2\sigma}\right)). \quad (107)$$

Figure 25 depicts the changes on the correlations as the size of a gaussian jitter increases for both a bunching (left) and an antibunching (right) source. We can see both the Monte Carlo simulations (continuous lines) and the curves obtained by means of the previous formula (dashed). A total agreement between both results is observed. The same behavior is found when using an exponential or a heavy-side ("constant") jitter. The zero delay values tend to one as the size of the jitter increases, since increasing σ means time uncertainty, which destroys the correlations on the signal.

3.5 SPONTANEOUS EMISSION

The spontaneous emission we have studied corresponds to the effect of having a fock state ($|N\rangle$) in a microcavity with a decay γ without any additional pumping. The emission of the system is measured for a time "p" (which corresponds to the size of what we have been refering to as a frame).

Initially, at $t = \tau = 0$, the second order correlation function is given by:

$$g^{(2)}(0,0) = \frac{\langle\Psi|\, a^\dagger a^\dagger a a\,|\Psi\rangle}{\langle\Psi|\, a^\dagger a\,|\Psi\rangle} = 1 - \frac{1}{N}. \quad (108)$$

Since we are dealing with a well-studied non-stationary system, its study can be of great assistance for the comparison of equations $\widehat{g^{(2)}}(\tau)$ and $\overline{g^{(2)}}(\tau)$. The value of $g^{(2)}(t,\tau)$ will be the same for both cases with the form:

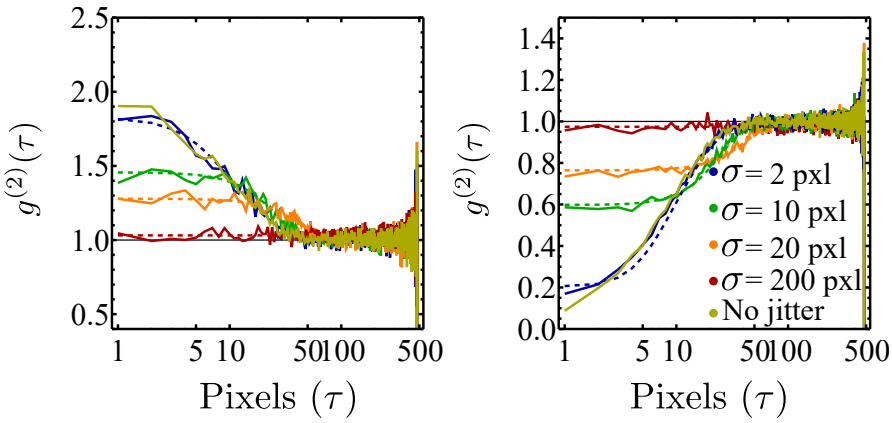

Figure 25: Effect of a gaussian jitter on a bunching (left) and antibunching (right) signals.

$$\begin{aligned} g^{(2)}(t,\tau) &= \frac{\langle a^\dagger(t)a^\dagger(t+\tau)a(t+\tau)a(t)\rangle}{\langle a^\dagger(t+\tau)a(t+\tau)\langle a^\dagger(t)a(t)\rangle} \\ &= \frac{\langle e^{-\gamma(2t+\tau)}n(n-1)\rangle_t}{\langle e^{-\gamma t}n\rangle_t\langle e^{-\gamma(t+\tau)}n\rangle_t}\,. \end{aligned} \tag{109}$$

At this point, the procedure used for the calculation of the average over time will give the difference between the two definitions. Applying Eq. (79) to calculate the averages, two different results are obtained:

$$\widehat{g^{(2)}}(\tau) = \frac{\frac{n-1}{2n}\gamma p(1-e^{-2\gamma(p-\tau)})}{(1-e^{-\gamma p})(1-e^{-\gamma(p-\tau)})}\,, \tag{110}$$

and

$$\overline{g^{(2)}}(\tau) = 1 - \frac{1}{n}\,. \tag{111}$$

The green curve on Fig. 3.3 d corresponds to the results obtained by applying Eq. $\widehat{g^{(2)}}(\tau)$ to the Monte Carlo simulation of this system, and the blue one corresponds to definition $\overline{g^{(2)}}(\tau)$ for N = 3 and p = 480 pixels, i.e. $p = 480\Delta t$. The orange and yellow lines correspond to Eqs. (110) and (111). At this non-stationary limit the two definitions diverge. Although by definition in the stationary limit $\widehat{g^{(2)}}(\tau)$ is considered to be the correct definition of the $g^{(2)}(\tau)$, with this equation the theoretical behavior of $g^{(2)}(0) = 1 - 1/n$ is not found. On the other hand, we can see in the figure that for the $\overline{g^{(2)}}(\tau)$ the initial value does follow the expected value.

3.6 COMPUTATIONAL CALCULATION

Typically experimental measurements are done with stationary signal at the limit $F \gg p$, for which we have shown that two definitions of the $g^{(2)}(\tau)$ are possible: $\widehat{g^{(2)}}(\tau)$ and $\overline{g^{(2)}}(\tau)$. Out of these two, the second one has proven to be the most efficient, reducing the amount of calculations. In this section we introduce the steps for the analysis of the clicks following $\overline{g^{(2)}}(\tau)$.

First the clicks must be obtained by means of the method introduced in section 2.3.1. The obtained data will be a vector in which each value corresponds to the time of arrival of a photon T_i. The highest T_i will be the total time of meassurement T_{total}. For the analysis of these results, the number of t_i per frame (p) must be set. With this set of clicks the steps to follow are:

Step 1 Divide the clicks into F frames. For this, being T_i the value of the click, the quotient of T_i/p will be the frame (f) and the remainder will be the time of arrival *inside* the frame (t_i). The frame of the last click (T_{total}) will be the total number of frames F.

Step 2 Calculate *for each* frame all the combinations t_i, t_j, and for each of them all the combinations t_i, τ, being $\tau = t_j - t_i$.

Step 3 A new vector is defined which contains the previous combinations and the amount of frames which have each of them ($N_{t_i,\tau}$):
$VectorA = t_i, \tau, N_{t_i,\tau}$. This vector will contain all the necessary values for step 5.

Step 4 Define a new vector $I(t_i)$that contains the number of times each t_i is found. The division of each element over F will correspond to $\langle I(t_i)\rangle_F$.

Step 5 Calculate for each combination of t_0, τ: $\langle I(t_i)I(t_i+\tau)\rangle_F = N_{t_i,\tau}/F$.

Step 6 With the last two steps, we can obtaing $g^{(2)}(t_i,\tau) = \frac{\langle I(t_i)I(t_i+\tau)\rangle_F}{\langle I(t_i)\rangle_F\langle I(t_i+\tau)\rangle_F}$, which we will need to average over t_i.

Step 7 For the final average, we must calculate for each τ: $g^{(2)}(\tau) = \frac{\sum_{t_i} g^{(2)}(t_i,\tau)}{p-\tau}$

This last average is based on the definition given at Eq. (79), but since it is not a continuous time, the integral has been substituted by a sum.

Figure 26 depicts the results obtained by calculating the $g^{(2)}(\tau)$ with this method (blue) for a set of clicks obtained by the monte carlo method of section 2.3.1. The system studied is a harmonic oscillator. The red curve corresponds to the theoretical $g^{(2)}(\tau) = 1 + e^{-\gamma\tau}$.

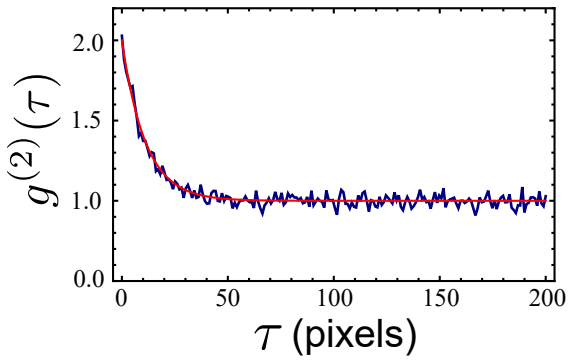

Figure 26: Simulated (blue) and theoretical (red) $g^{(2)}(\tau)$ for a harmonic oscillator.

3.7 CONCLUSIONS

When we are dealing with experimental results, unexpected behaviors may be explained taking into account the presented studies. In the case of an extremely noisy curve, the deficiency on the measurements can be the source of the problem, and it can be reduced by changing detectors; when the final results do not tend to 1 for $\tau \to \infty$ in an stationary signal, the effect will probably be due to external modulations and an additional normalization can be done to return the original values; fast modulations will cause an apparent infinite lifetime which can be fixed slowing down the modulation; if the value of $g^{(2)}(0)$ is very close to 1, some background noise or a big timming jitter can be ruining the real behavior, which can be dealt with experimentally by increasing the isolation and by using detectors with higher temporal precision. Finally, in the case of an abrupt unexpected bunching/superbunching behavior, the gravity peak will most certainly be the problematic point of the experiment, and although that can not be modified experimentally, a theoretical model to recover the original values has been given.

4

THE COLORED HANBURY BROWN–TWISS EFFECT

4.1 THE TEXTBOOK HANBURY BROWN–TWISS EFFECT

As has been introduced in Chapter 1, the Hanbury Brown–Twiss effect is a fundamental manifestation of bosonic particles (mainly, photons) that tend to clutter in their detection time. The setup first built to observe the effect and use it in practical (radio-astronomy) applications also goes by the name of HBT and is nowadays popular to characterize quantum light in the form of antibunching. Since the HBT effect can be understood as a bosonic manifestation, following from their indistinguishability that causes constructive interferences from a wave-like manifestation of light, it may be a bit unsettling that the HBT setup can also capture a classical character of bosons, in the form of coherent light (with no such bosonic tendency to clutter and arrive together on the detector) and even a fermionic character of bosons, in the form of antibunching of a single-photon source. This is because the light that does not exhibit the HBT effect in the HBT setup is not light at equilibrium, but instead light which has been given a proper dynamics, due to interaction with quantum auxiliaries, or from collective effects syncing photons together, such as in a lasing cavity. In this Chapter, we will show that even structureless light, with no imposed dynamics from an external agent, and that should therefore exhibit the bunching $g^{(2)} = 2$ as explained by Purcell from boson-indistinguishability, can also depart from this paradigm and uncorrelated or even bunched, merely from tagging the detected photons with their frequency. In this Section, we will show both theoretically and experimentally that the Hanbury Brown–Twiss experiment of frequency-resolved photon correlations discloses a fundamental structure that brings together bunched, coherent and antibunched light, depending on whether the detected photons are indeed identical or as distinguishable as can be.

4.2 THE STATISTICS OF POLARITONS

Our observation is made with a condensate of microcavity polaritons. Their $g^{(2)}$ has been studied by several groups and in different ways [1, 11, 64] prior to our study, always giving a bunching behavior, with a tendency of reaching unity (coherence) with the onset of condensation. Indeed, such a behaviour has been regarded as one way to evidence polariton condensations. In this case,

deeper information can be reached by adding discriminations on the correlation function such as polarization or position. Here, we consider the problem at a further level, by performing frequency (i.e., energy through $E = h\nu$) discrimination. This is a characterization of a different type than position of polarization, since time and frequency are conjugate variables.

The usual method used to compute the photon correlations $g^{(2)}(\omega_1, \omega_2; \tau)$ is by means of a HBT interferometer with interferencial filters (selecting ω_1 and ω_2) in each of the branches (see section 2.1.4). Although the measurement of one combination (ω_1,ω_2) can be measured easily with this simple setup (see Fig. 13), it is inefficient when mapping over all the combinations (ω_1,ω_2) to calculate the 2PS, implying one measurement for each point of the map [90]. In order to make efficient measurements of temporal and frequency correlations between two photons, a new experimental method is used instead, composed of a monochromator and a streak camera (see figure 27): the signal of the source is first sent to the monochromator, where it is opened horizontally into energies with the grating. That way, the horizontal position of the beam determines the energy of the photon. This energy-distinguished photon goes to the streak camera that sends it to a CCD camera (charge-coupled device), in a specific vertical position that determines the time of arrival. When adding these two parts of the setup, the signal that gets to the camera will have the form of a vertical thick line (see figure 27), in which the vertical pixel includes the time of arrival, and the horizontal one gives the energetic information. Not only this, to optimize the experiment, an additional horizontal slow sweep is given to the CCD. That way, for each horizontal sweep (which we will refer to as a *frame*, which has a duration of 200 ns) various vertical (now diagonal on the camera) sweeps are found, giving up to 8 times the amount of information found without horizontal movement (see figure 28).

The camera is used in the single-photon detection mode, such that for each horizontal sweep only the coordinates of each detection are recorded, diminishing the amount of data to store for the final analysis.

The streak camera is not only used for its efficiency in the 2PS measurements, but also for the high temporal resolution. In these experiments, we are dealing with lifetimes of the order of 150ps, which can only be observed with the precision given by a streak camera. The price to pay for this high precision is the detection efficiency, which is far lower than the average one of an APD. Of course, this time-signal efficiency compromise can be modified depending on the mode used in the streak camera. In this specific case, the signal for each frame was of the order of 1.69 clicks/sweep, requiring long measurements to increase the statistics, recording up to 350000 frames.

As has been previously explained, the (x,y) coordinates on the CCD provide all the information needed to calculate each combination $g^{(2)}(\omega_i, \omega_j; \tau)$. The

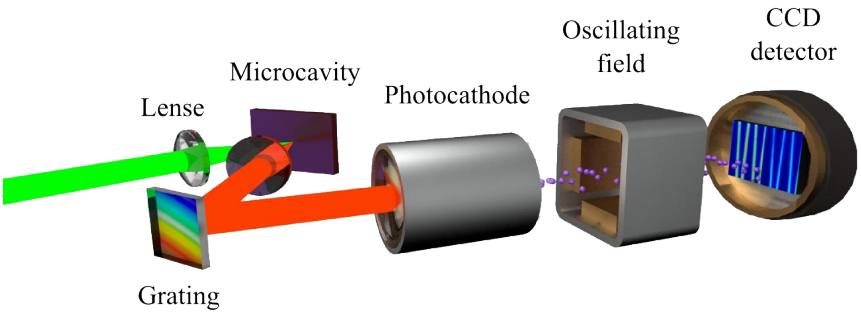

Figure 27: Sketch of the experiment: the reflected light from a microcavity is dispersed onto a streak camera detecting at the single-photon level and stored in individual frames, whose post-processing allows to build photon-correlation landscapes.

energy step between two pixels is of $\Delta E = 10.6\mu eV$ and the temporal step between two vertical pixels is of $\Delta t = 3.2$ ps. To get rid of effects such as the excitation of two pixels by just one photon (see gravity peak in Section 3.4.2), a binning is done, both horizontal and vertically, averaging over groups of 3 vertical pixels and of 7 horizontal ones. This way, the final resolution of the setup is of 10 ps and 70 µeV. Each of these horizontal binnings are considered to be of constant energy and refered to as *subsweeps*.

4.2.1 *Calculation of the correlations*

After the experiment, the data is stored in a .dpc file in which all the (x,y) coordinates of the detections are recorded, with the x-coordinate the energy, and the y-coordinate the time of detection. In this specific case, the sweep was of 40 pixels width. The steps followed for the calculation of these subsweeps were the following:

Step 1 We plot all those points in an array, revealing the diagonals due to the sweep of the signal around the camera.

Step 2 We select each of the sweeps, i.e., select the (x,y) values that belong to the experiment (see figure 29a) and divide them into sets, each of them corresponding to one sweep.

Step 3 We divide each of these sweeps into steps of 1 pixel-width, i. e. subsweeps of constant energy (see figure 29c).

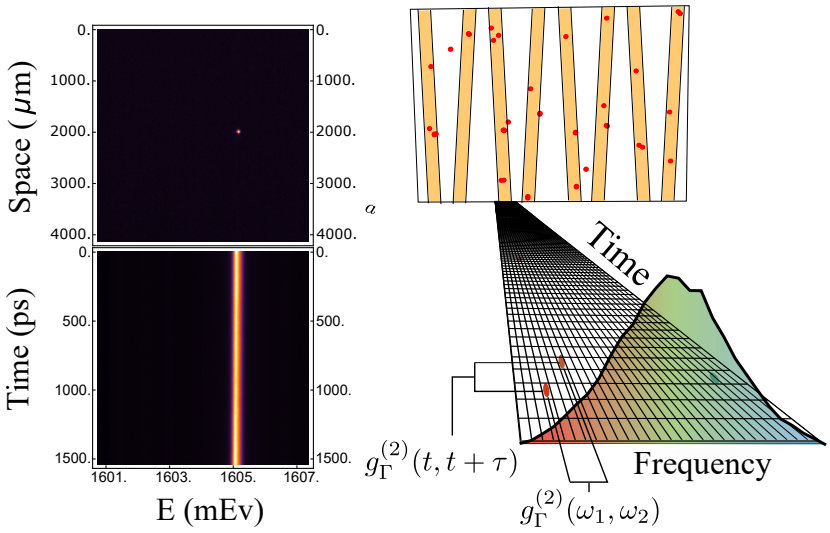

Figure 28: (a) Emission of the condensate of polaritons seen on the CCD camera. (b) Image on the detector due to the vertical sweep of the streak camera. (c) sketch of the results on the CCD: for each frame when the horizontal movement is included, a few photons are detected (red dots). When the measurement is integrate over the order of 350000 frames, 8 oblique lines ("sweeps") are distinguished due to the sweep of the condensate. In each line the horizontal pixel corresponds to the frequency and the vertical one to the time of arrival.

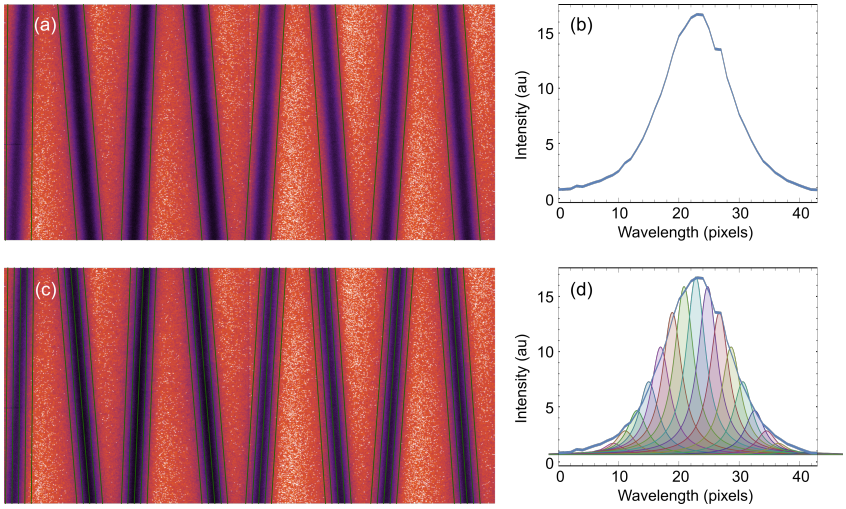

Figure 29: (a) Image on the CCD of the superposition of 350000 frames. The green lines delimit the sweeps. (b) Profile of the emission of the condensate. (c) Selection of subsweeps (in this figure the step has been done bigger than 1 pixel in order to make it easier to appreciate). (d) Sketch of the filtering of the emission. Each filled gaussian corresponds to a subsweep. Each of them is centered at a different energy, overlapping with the neighbor subsweeps.

Step 4 We do the binning with these 1 pixel-width subsweeps (see figure 29d). The procedure used for this binning is explained above.

The binning was done by overlapping 7 pixels-width subsweeps, i.e., we join to each subsweep i the previous three and the following three subsweeps. Of course, the vertical position must never be modified, since this is the procedure done for the energetic binning. The new subsweeps can be defined as:

$$\begin{aligned} \omega_i &= [x_{i-3}, x_{i+3}], \\ \omega_{(i+1)} &= [x_{(i+1)-3}, x_{(i+1)+3}]. \end{aligned} \tag{112}$$

In section 3.3, the stationarity was studied, and proven that the order of the averages depends on the experiment. In this case, the number of frames was of the order of 350 000 frames with 480 pixels per frame, hence the Eq. (82) was applied for the analysis.

4.3 DYNAMICS OF AN OUT-OF-EQUILIBRIUM POLARITON CONDENSATE.

As the source to be spectrally resolved for its two-photon correlations, we use an out of equilibrium condensate of exciton-polaritons. Theoretically, this cor-

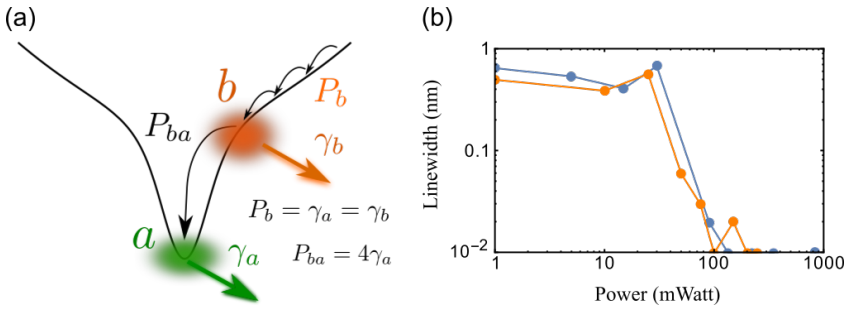

Figure 30: (a)Theoretical model of the polariton condensation: and incoherent pumping (P_b) creates a bath of excitons b with a lifetime γ_b. These excitons condense to the minimum of the branch (P_{ba}) creating the condensate a with a lifetime given by γ_a. (b) Changes on the linewidth of the emission with the pumping power.

responds to the spontaneous emission from a state whose coherence depends on the degree of condensation, as described by the following master equation:

$$\partial_t \rho = i[H, \rho] + [\frac{\gamma_a}{2}\mathcal{L}_a + \frac{\gamma_b}{2}\mathcal{L}_b + \frac{P_b}{2}\mathcal{L}_{b^\dagger} + \frac{P_{ba}}{2}\mathcal{L}_{a^\dagger b}]\rho\,, \tag{113}$$

in which a and b represent two harmonic modes that correspond to the BEC and the exciton reservoir, respectively. There are four mechanisms taken into account in the above equation: two being the loses of the particles a and b, with a decay rate $\gamma_{a/b}$ described by the Lindblad terms $\frac{\gamma_{a/b}}{2}\mathcal{L}_{a/b}\rho$, where $\mathcal{L}_O(\rho) = 2O\rho O^\dagger - O^\dagger O\rho - \rho O^\dagger O$. The third term corresponds to the incoherent injection of excitons to the reservoir at a rate P_b. Finally the last term represents the relaxation transfer of particles from the reservoir to the condensate. Fig. 30 shows a simple scheme of the elements taken into account in this model for the definition of the condensate, where the orange colors correspond to the exciton reservoir, and the green ones to the condensed polaritons.

4.4 2PS IN AN OUT-OF-EQUILIBRIUM CONDENSATE OF EXCITON-POLARITONS

The above setup allows us to measure the 2PS of an out-of-equlibrium condensate, achieved with a non-resonant single-mode pumping in reflection mode on a high quality factor microcavity (Q-factor 100 000) of GaAs/AlGaAs containing 12 GaAs quantum wells placed at three anti-node positions of the electrical field. The front (back) mirror consists of 34 (40) pairs of AlAs/$Al_{0.2}Ga_{0.8}As$ layers. The microcavity was inserted in a cryostat at 5K. Initially a chopper was introduced before the excitation to avoid possible heating of the sample, but

this modulation on the excitation spoiled the normalization of the correlation function ($g^{(2)}(\tau \to \text{inf}) > 1$), as explained in Section 3.3.1.

To achieve condensation, the power was increased slowly (see figure 30b) until the threshold was reached. Although at that power the system is an out-of-equilibrium condensate, increasing the power until reaching the total condensation provokes a shrinking of the linewidth of the emission, arriving to a size of the order of the energy-binning used, making it impossible to calculate a complete 2PS.

The emission of the condensate of polaritons was sent to the setup described previously (see Fig. 27) and integrated for 5-8 hours. Although other studies [11, 120] have been done with far smaller integration times, when distinguishing energies the signal for each subsweep is very small, and such long measurements are necessary to get enough signal for the statistics. Once the measurements were done, all the (ω_i, ω_j) combinations were calculated by means of the method detailed in Section 4.2.1 in order to build the entire map $g^{(2)}(\omega_i, \omega_j; 0)$. Figure 31(a) shows the experimental measurements of the polariton condensate 2PS. Three regions are identified, with the same color code as already introduce for the theoretical 2PS previously discussed: red, white and blue. The red one corresponds to bunching behavior, white to coherent and blue to antibunching. A clear structure is revealed: there is manifest bunching along the diagonal where $\omega_i = \omega_j$, and, even more interestingly, an antibunching when correlating opposite regions of the emission $\omega_i = -\omega_j$. On the other hand, Fig. 31(b) shows the corresponding theoretical calculation for $g^{(2)}(\omega_1, \omega_2; 0)$ by means of the procedure explained in Section 2.2.1 for the system defined by Eq. (113). Almost a perfect agreement theory-experiment can be observed, with the same three regions. The temporal evolution for three different regions of the map is also shown, both theoretically and experimentally. Once again, an almost perfect agreement is found. A clear evolution of the correlations from bunching ($g^{(2)}(0; \omega, \omega) \approx 1.5$ in region 1) to antibunching ($g^{(2)}(0; \omega, -\omega) \approx 0.7$ in region 3) is observed.

One of the strong prediction of the theory of frequency-resolved photon correlations [115] is that the result depends sensibly on the filters width. With increasing size of the filters, the value of $g^{(2)}(\omega_1, \omega_2; \tau)$ must tend to the value of the second-order correlation function without energy discrimination:

$$g^{(2)}(\omega_1, \omega_2; \tau) \xrightarrow[\Gamma \to \infty]{} g^{(2)}(\tau)\,. \tag{114}$$

To study this property experimentally, we simply increase the amount of pixels used for the linewidth of each ω_i (i.e., the horizontal binning) and study the temporal evolution of the correlations of the new collections of photon detections. This shows again the tremendous flexibility of the streak camera setup, that allows such post-processing of the data in a way that is tentamount of

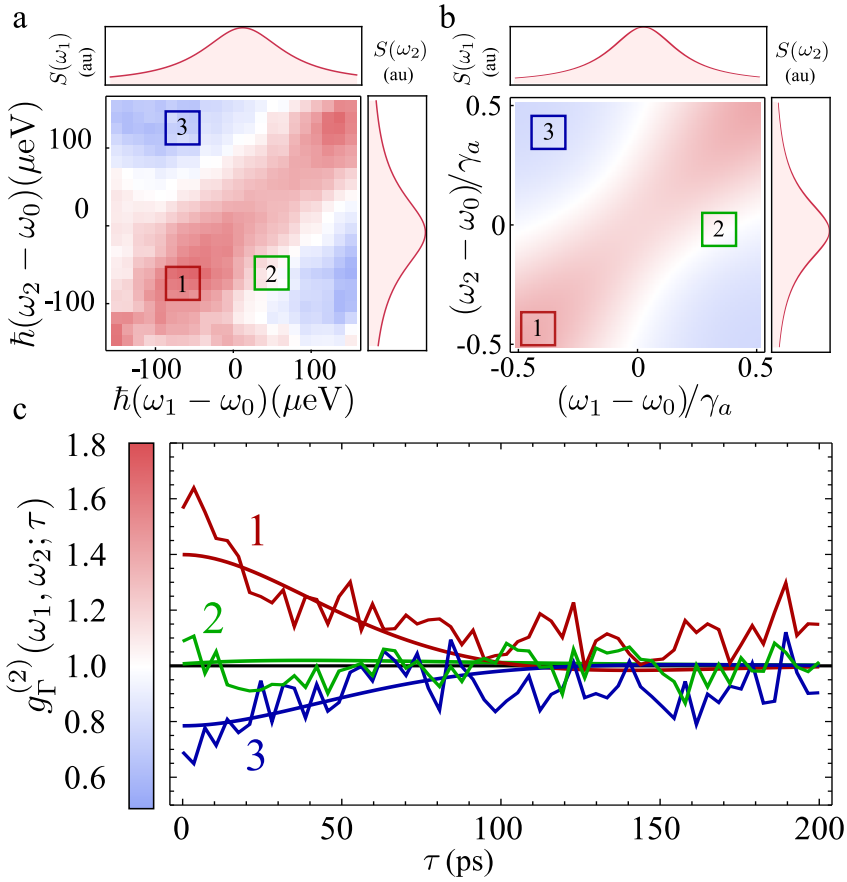

Figure 31: (a) Experimental observation of $g^{(2)}_\Gamma(\omega_1,\omega_2;0)$ for the spontaneous emission from a steady-state of polaritons. (b) Theoretical calculation of $g^{(2)}_\Gamma(\omega_1,\omega_2;0)$ from the model of condensation of polaritons sketched in Fig 30, showing a remarkable agreement. (c) Time-resolved correlation for the three regions marked in the color map: (i) on the diagonal ($\omega_1=\omega_2$) exhibiting bunching, (ii) in the region of transition with no correlation, (iii) correlating opposite elbows, exhibiting antibunching.

doing a new experiment. The upper part of Fig. 32 shows three 2PS with binnings of 7, 13 and for the entire set of pixels, respectively. It is evident how the initial characteristic pattern of Fig. 31 disappears as the linewidth is increased, to reduce in the extreme case of $\Gamma \to \infty$ to a single number, and therefore a single color for the 2PS. The bottom panel shows the temporal evolution of $g^{(2)}(\omega_1, \omega_2; \tau)$ in the orange, blue and green squares cut in the above 2PS. All these squares are centered at a set of frequencies (ω_1, ω_2) in which, when filtering in small frequency windows, there is antibunching. It is clear how, as the size of the filters is increased, the antibunching is washed out until it reaches the size of the entire spectrum (blue square) to become a bunched signal with a zero-delay value $g^{(2)}(0) = 1.15$, which matches with the values reported in previous studies from other groups [11, 13, 64]. Increasing the size of the filters also increases the amount of signal in each frequency, diminishing the noise found when calculating the correlation function. This is also clearly observed in the figure, in which the noise in the red curve (1 pixel binning) is far higher than in the blue one. The curves of the bottom right panel are the theoretical correlation functions expected as increasing the filters, that also display a great agreement with the experimental ones on the left. The 2PS described above are the first ones ton have been measured in any system, and, shortly afterwards, the quantum-optical group of A. Muller reported the 2PS of resonance fluorescence [90].

4.5 2PS FROM A FREE BOSON FIELD

We now discuss the physical meaning of the polariton condensate 2PS. Although the bunching in the diagonal line (corresponding to filters of equal frequency) is expected from the cases already discussed in Section 2.2.2, and is in fact also a well known feature of spectral filtering from a single peak [87], the butterfly shape of the 2PS, that is otherwise expected for a two-level system, comes as not trivial. We now proceed to explain its origin and why it should, in fact, be expected as the fermionic shadow to be found in any bosonic phenomenology. The HBT effect is rooted in both classical and quantum physics, and we will therefore discuss this observation from these two complementary viewpoints.

From a classical point of view, this can be undestood with the particular case of a quasi-monochromatic field $E(t)$ that has a finite bandwidth given by a phase diffusion process:

$$E(t) = E_0 e^{i[\omega_0 t + \phi(t)]}, \tag{115}$$

where $\phi(t)$ is a stochastic function that evolves, for instance, according to a random walk (see fig. 33a). When dealing with the frequency-resolved second-

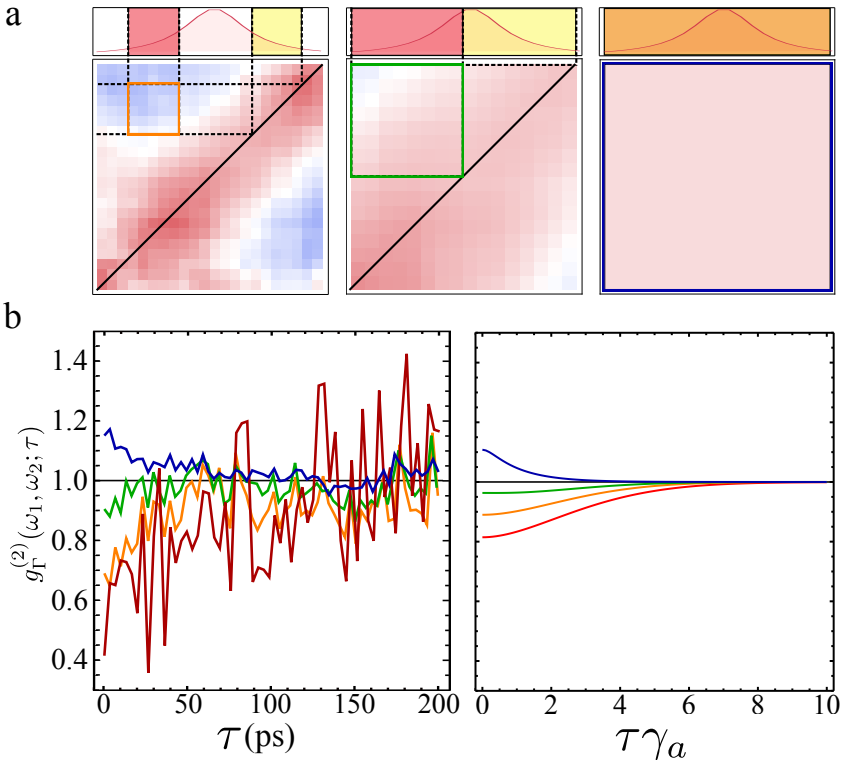

Figure 32: Two-photon correlation landscapes $g^{(2)}(\omega_1, \omega_2; 0)$ as a function of the filter width, from a fraction of the peak, 74.1 μeV (left), roughly half-peak width, 158.8 μeV (center), to full peak filtering, corresponding to standard autocorrelations. The position of the two filters is shown explicitly on the spectral line as the red and yellow windows (orange when overlapping). Bottom left and right panels describe the experiment and the theory from the condensation model, respectively.

order correlation function, the effect of the filters must be introduced in the definition, leading to:

$$g^{(2)}_{\Gamma}(\omega_1,t_1;\omega_2,t_2)=\frac{\langle:\mathcal{T}\left[\prod_{i=1}^{2}\hat{E}_{\omega_i,\Gamma}(t_i)\hat{E}^{+}_{\omega_i,\Gamma}(t_i)\right]:\rangle}{\prod_{i=1}^{2}\langle\hat{E}_{\omega_i,\Gamma}(t_i)\hat{E}^{+}_{\omega_i,\Gamma}(t_i)\rangle}, \tag{116}$$

where:

$$\hat{E}_{\omega_i,\Gamma}(t_i)=\frac{\Gamma}{2}\int_0^{\infty}e^{-i\omega_i t}e^{-\Gamma t/2}\hat{E}(t_i-t)\,dt\,. \tag{117}$$

The application of these two relations to Eq. (115) corresponds to the superposition of fields of equal frequency but different phases, analogous to the description of a thermal field. This produces interferences that oscillate in a chaotic intensity profile, such that:

$$\frac{\langle I^2_{\omega}\rangle}{\langle I_{\omega}\rangle^2}>1 \tag{118}$$

This effect of the energetic filtering with equal frequencies is usually interpreted [81] as the tendency of particles to "clump" together, and increase the spacing between their arrival time, giving rise to a bunching effect.

The previous results show how phase noise is turned into intensity noise by frequency-filtering (see fig.33b-c). Yet, the subtler part of these results is the effect of the frequency-filtering when correlating opposite frequencies, which we have shown experimentally to result in an antibunching behavior. These anticorrelations can be interpreted as a consequence of energy conservation: the rate of photons detected with and without filtering must be conserved. Hence, detecting a clump of photons when correlating them with the same energies must diminish the probability of detecting photons at different frequencies in order to preserve the total rate of detected photons. This argument is verified applying Eq. (20) to the field given by Eq. (115), assuming a random walk dynamics for the phase such that $\langle e^{i[\phi(t)-\phi(t-\tau)]}\rangle = e^{-\gamma|\tau|}$ and $\langle e^{2i[\phi(t)-\phi(t-\tau)]}\rangle = e^{-\gamma_2|\tau|}=e^{-4\gamma|\tau|}$. This way, the analytical expression for the frequency resolved correlation function at zero delay can be found exactly:

$$\begin{aligned}g^{(2)}_{\Gamma}(\Delta_1,\Delta_2)=&\frac{\left[\Delta_1^2+(\gamma+\Gamma/2)^2\right]\left[\Delta_2^2+(\gamma+\Gamma/2)^2\right]}{4(\gamma+\Gamma/2)^2}\\&\Re\left\{\frac{2(\gamma+3\Gamma/2)}{(\gamma+i\Delta_2+\Gamma/2)(\Delta_1^2+(\gamma+3\Gamma/2)^2)}+\Gamma\left[f_{\Gamma}(\Delta_2,\Delta_{12}^{-},\Delta_2)\right.\right.\\&+f_{\Gamma}(\Delta_1,\Delta_{12}^{-},-\Delta_2)+f_{\Gamma}(\Delta_1,\Delta_{12}^{+}-i\gamma_2,\Delta_1)+\\&\left.\left.f_{\Gamma}(\Delta_2,\Delta_{12}^{+}-i\gamma_2,\Delta_1)\right]+[\Delta_1\leftrightarrow\Delta_2]\right\}\end{aligned} \tag{119}$$

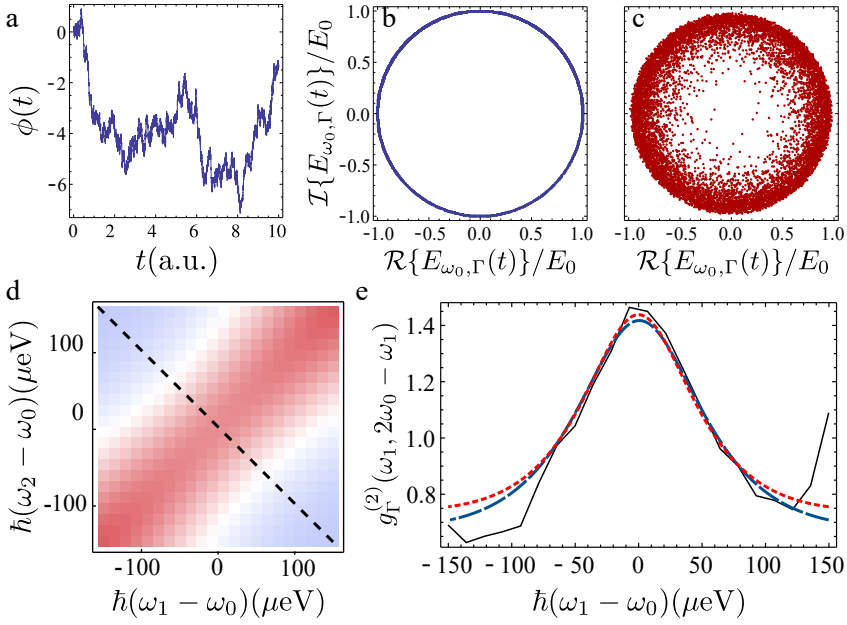

Figure 33: (a) The random-walk evolution of diffusing phase of a field $E(t) = E_0 \exp i[\omega_0 t + \phi(t)]$, with $\langle e^{i(\phi(t+\tau)-\phi(t))}\rangle = e^{-\gamma\tau}$ (b) $E(t)$ in phase space over different times. (c) Phase fluctuations are converted into intensity fluctuations after frequency filtering $E(t)$ (d) Fitting of the experimental 2PS by Eq. ((119)), with fitting parameters $\gamma \approx 193\,\mu eV$, $\Gamma \approx 134\,\mu eV$. The colorscale is that of Fig. 31. (e) 2PS along the dashed line in (d) for the experiment (straight, black), the fitting for the phase diffusing field (long dashed, blue) and the fitting of the form factor $\mathcal{F}_{\Gamma,\gamma,\gamma_\phi}$ (short-dashed, red). Despite not being an exact theoretical description for this experiment, the form factor agrees very well with the data for the parameters $\gamma \approx 99\,\mu eV$, $\gamma_\phi \approx 440\,\mu eV$, $\Gamma \approx 17\,\mu eV$.

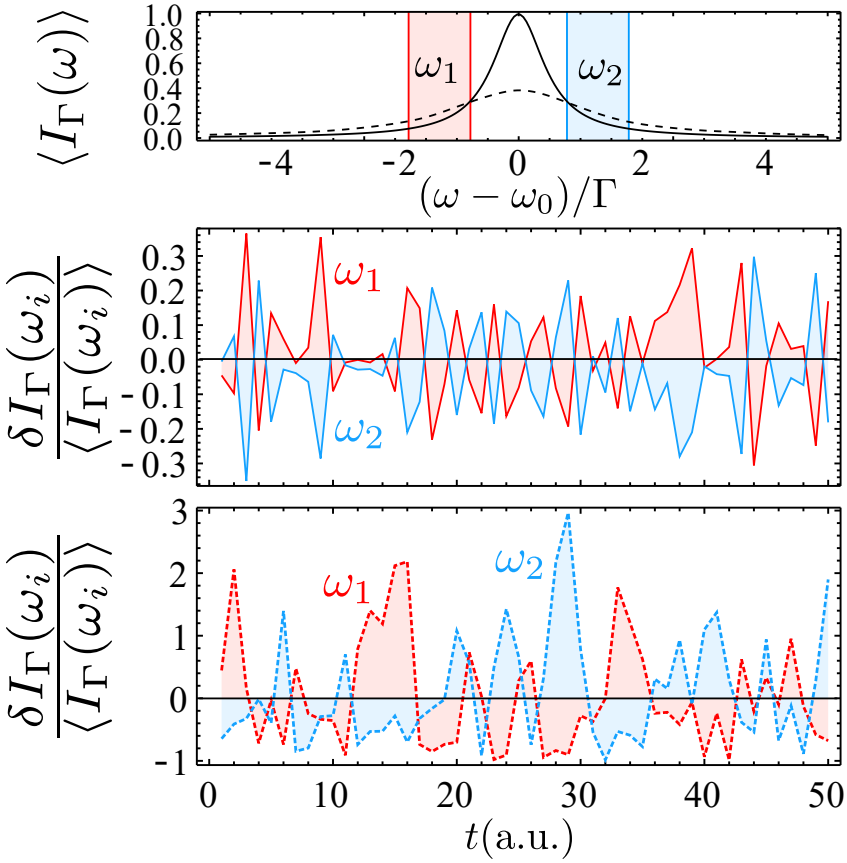

Figure 34: Fluctuations in the intensity of the filtered field $I_\Gamma(\omega_i) = \langle I_\Gamma(\omega_i)\rangle + \delta I_\Gamma(\omega_i)$ for the two frequencies shown at the top panel and two values of γ, $\gamma \approx 8\times10^{-3}\Gamma$ (solid lines, middle panel), and $\gamma \approx 0.8\,\Gamma$ (dashed lines, bottom panel). The corresponding values of $g^{(2)}(\omega_1,\omega_2)$ are 0.97 and 0.65 resp. In the middle-panel case, where $\Gamma \gg \gamma$, the anticorrelations in the noise become exact.

where $\Delta_i \equiv \omega_i - \omega_0$, $\Delta_{12}^- \equiv \Delta_2 - \Delta_1$, $\Delta_{12}^+ \equiv \Delta_2 + \Delta_1$ and:

$$f_\Gamma(\omega_1,\omega_2,\omega_3) = \frac{1}{(i\omega_1+\gamma+\Gamma/2)(i\omega_2+\Gamma)(i\omega_3+\gamma+3\Gamma/2)}\,. \tag{120}$$

Figures 33d-e depict both the 2PS obtained with Eq. (119) and the profile along the antidiagonal. A very good agreement with the experimental results (Fig. 31) is obtained.

For a deeper study of these anticorrelations, Fig. 34 shows the intensity fluctuations after frequency filtering in the phase diffusing field. The curve on the top corresponds to the emission of our source in which two opposite energies of the spectrum ($\omega_1 = -\omega_2$) are selected. The middle panel corresponds to the case in which the linewidth of the filter becomes much larger than the natural linewidth of the field ($\Gamma \gg \gamma$). In this limit, the anticorrelations on the noise become, surprisingly, exact! The smaller fluctuations $\delta I_\Gamma(\omega_i)$ around the mean value tend to become perfectly anticorrelated for frequencies in opposite sides of the spectrum, $\delta I_\Gamma(\omega_0 - \omega) \approx -\delta I_\Gamma(\omega_0 + \omega)$.

This phase-fluctuation model provides a classical point of view of the colored HBT effect. On the other hand, the description from the quantum/particle point of view, also possible, poses some difficulties, but this should not be unexpected as this is exactly the situation with the conventional HBT effect. The conventional second-order correlation function is given by the simple form:

$$g_0^{(2)} = \frac{\sum_{n=0}^{\infty} n(n-1)\langle n|\rho|n\rangle}{(\sum_{n=0}^{\infty} n\langle n|\rho|n\rangle)^2}\,, \tag{121}$$

which only requires the density matrix ρ to be computed. When introducing the resolving in energy, $g^{(2)}(\omega_1, T_1; \omega_2, T_2)$, the time dynamics is necessary even to compute zero-delay coincidences (with $T_1 = T_2$) since one has to integrate over time t (see Eqs. (116) and (117)). Because of this, the frequency information implies the specification of the dynamics of the entire system. We study the simplest situation: an arbitrary quantum state given by the density matrix $\rho(0)$ is left to decay from the source to a continuum of modes under spontaneous emission with a rate γ_a and also with a pure dephasing rate γ_ϕ, thus eliminating every possible dynamics except the essential one that brings the photons from the source to the detector (that performs the frequency-filtering and correlation) and some dephasing mechanism. This is thus described by the following master equation:

$$\frac{\partial \rho}{\partial t} = \left[\frac{\gamma_a}{2}\mathcal{L}_a + \frac{\gamma_\phi}{2}\mathcal{L}_{a^\dagger a}\right](\rho)\,, \tag{122}$$

which can be solved by recurrence, yielding:

$$\begin{aligned}\rho_{n,m}(t) = \sum_{k=0}^{\infty} \rho_{k,m-n+k}(0)\sqrt{\binom{k}{n}\binom{m-n+k}{m}} \\ \left(e^{\gamma_a t} - 1\right)^{k-n} e^{-[\gamma_a(2k+m-n)+\gamma_\phi(n-m)^2]t/2}\,.\end{aligned} \tag{123}$$

Despite the rather complicated form of this general solution, the two-photon correlation that results:

$$g^{(2)}(t) = \frac{\langle a^\dagger a^\dagger a a\rangle(t)}{\langle a^\dagger a\rangle(t)^2} \tag{124}$$

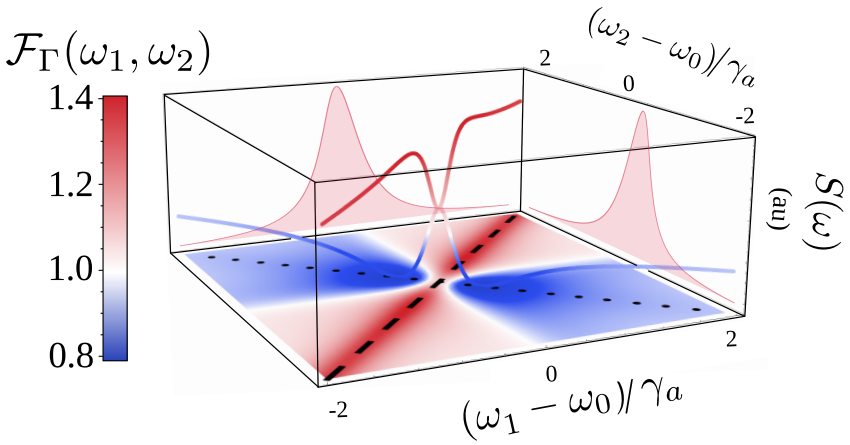

Figure 35: 3D plot of the form factor. On the bottom: 2PS calculated with the form factor. Back and right: emission of the system. 3D curves: $g^{(2)}(\omega_1,\omega_2;0)$ for the diagonal ($\omega_1=\omega_2$) and the antidiagonal ($\omega_1=-\omega_2$).

turns out to provide an even simpler and stronger result:

$$g^{(2)}(t)=g^{(2)}(0)\,. \tag{125}$$

In contrast, the value of $g^{(2)}_\Gamma(\omega_1,\omega_2)$ is found as:

$$g^{(2)}_\Gamma(\omega_1,\omega_2)=g^{(2)}_0\mathcal{F}_\Gamma(\omega_1,\omega_2)\,, \tag{126}$$

with $g^{(2)}_0$ the zero delay second-order correlation function of the initial state and $\mathcal{F}_\Gamma(\omega_1,\omega_2)$ a *boson form factor*, which is independent of the quantum state ρ in which the system is prepared, and depends only on the dynamics of emission and detection (see figures 33 and 35).

This form factor behavior can be found in other simple systems such as the Fock states (which follow $g^{(2)}(0)=1-1/N$), coherent states (for which $g^{(2)}(0)=1$) or thermal states (with $g^{(2)}(0)=2$). Figure 36 shows the antidiagonals of the 2PS for these systems. Two effects are clear: first of all, the behavior of the form factor in all of them with a vertical shift given by the value $g^{(2)}(0)$ and second of all, the loss of the behavior as the filtering is washed out (blue curve).

In general, when the physics goes beyond that of the mere emission from a quantum state ρ, and involves quantum emission, e.g., through virtual processes, dressing of the states, collective emission, stimulated emission and other types of likewise quantum correlations, the standard Glauber's correlation $g^{(2)}_0$ does not simply factorize from $g^{(2)}_\Gamma(\omega_1,\omega_2)$. In such cases, the 2PS offers a

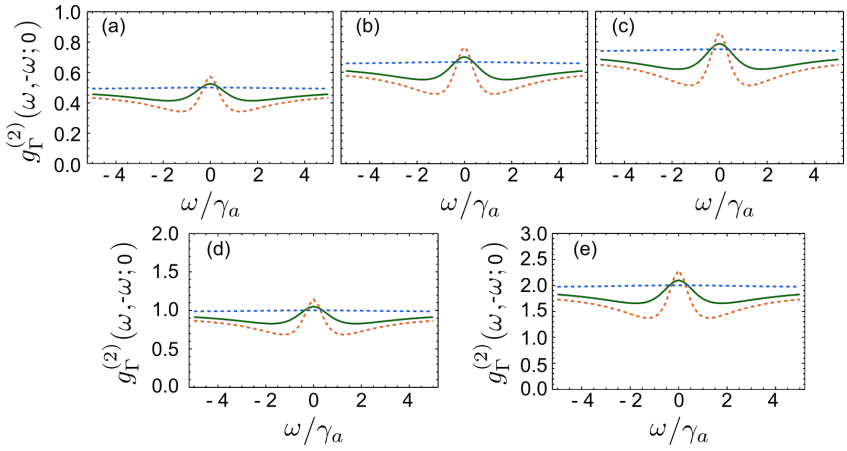

Figure 36: Plot of the $g^{(2)}(\omega_1,\omega_2;0)$ for the antidiagonal ($\omega_1 = -\omega_2$). Three different colors are found: orange for $\Gamma = 0.1\gamma_a$, green for $\Gamma = \gamma_a$ and blue for $\Gamma = 10\gamma_a$. Five different systems are shown: (a) N=2 fock state, (b) N=3 fock state, (c) N=4 fock state, (d) Harmonic oscillator and (e) thermal state.

complex landscape of correlations with strong and characteristic features, as we have already mentionned (cf. Fig. 16).

With this last result, the complete description of the HBT effect is given: classical and quantum analysis, along with the experiment and theoretical characterization of the steady state emission. These results, that generalize the Hanbury Brown–Twiss effect to exhibit correlations of different types depending on the energies— are of fundamental interest, but should also be of technological importance.

4.6 ADDITIONAL MEASUREMENTS AND EXPERIMENTAL DISCUSSIONS

Frequency correlations are not only useful when dealing with single-mode emissions. As it was discussed in Section 2.2.2, this type of analysis can show correlations at the single-particle when dealing with more complicated systems. In particular, we studied correlations in the optical parametric oscillator (OPO) in nanowires. The emission of the OPO (see figure 37) was sent to our setup used, to map all the frequency correlations from an emitter with a stronger quantum character. The 2PS obtained is shown in Fig. 38. In this case, however, no clear pattern is found beyond the diagonal bunching. This absence of clear two-photon correlations is a negative result, that confirms that quantum effects from polariton systems, are difficult to observe, even in configurations that are expected to be strongly quantum, such as dynamics of the OPO that

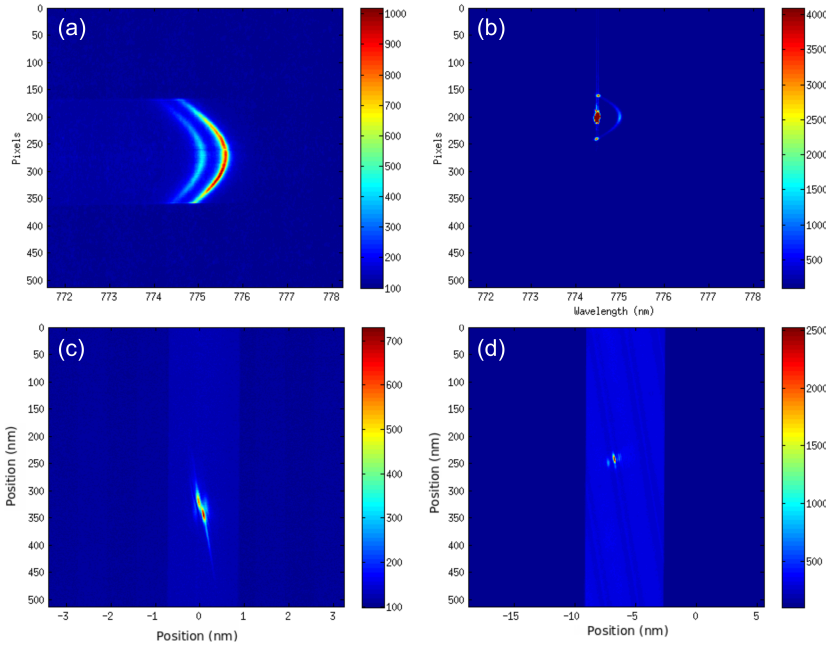

Figure 37: OPO obtained in nanowires. (a) split of the LPB due to the nanowire. (b) OPO seen in the FF, emission at $\pm k$ with an excitation at $k = 0$ in the higher energy branch. (c) OPO seen in the NF with open slits: flow in opposite directions can be seen. (d) Surface of the sample: two nanowires can be distinguished with the spot of the laser on one of them.

include clear two-photon scattering processes. However, even when the polaritonic idler and signal states are parametrically correlated in their one-photon spectra, they fail to shown quantum correlations at the two-particle level. Such a direct observation remains to be made with polaritons. We will show in next Chapter that a genuine non-classical regime can be reached by taking another route towards quantum effects.

Our setup is not only a big advance for studies of frequency-resolved correlation, but is also of great interest when dealing with energetic temporal evolution. While in previous studies [120], the streak camera had been used to study correlations with pulsed lasers, this is the first time that there is also an energetic discrimination by means of the monochromator. With this energy–time resolution, we can also study the behavior of the condensate by means of pulsed excitation. For this, a precise synchronization between the excitation and the sweep of the camera is required: the horizontal velocity must be such that the pulse arrives always to the same vertical position on the CCD camera. For

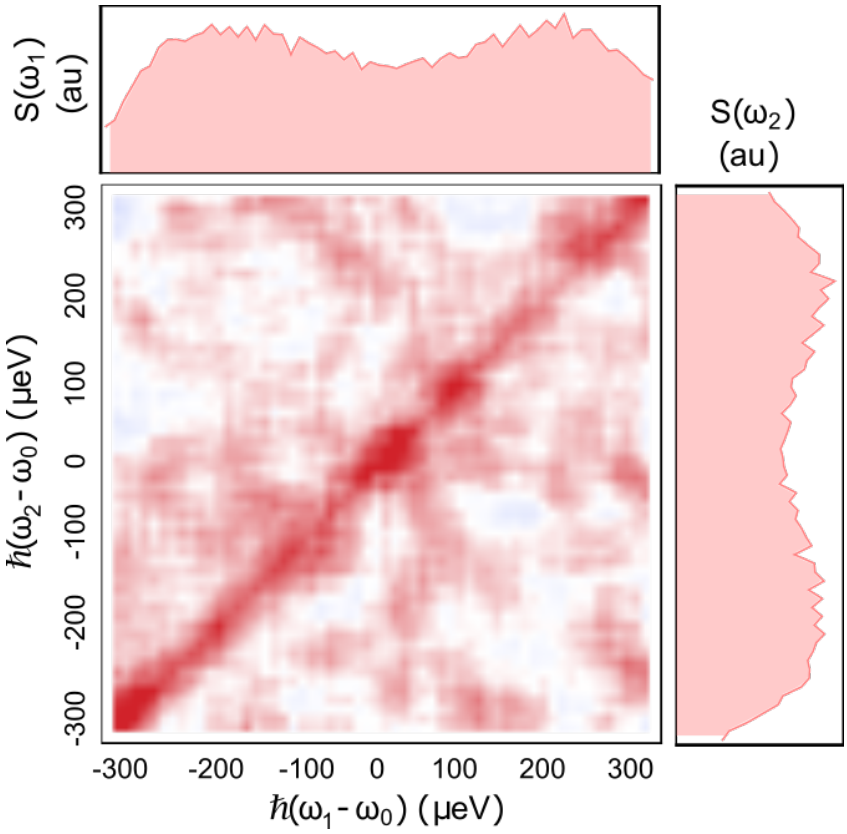

Figure 38: 2PS of the emission of the OPO on the nanowires. No clear patters are found.

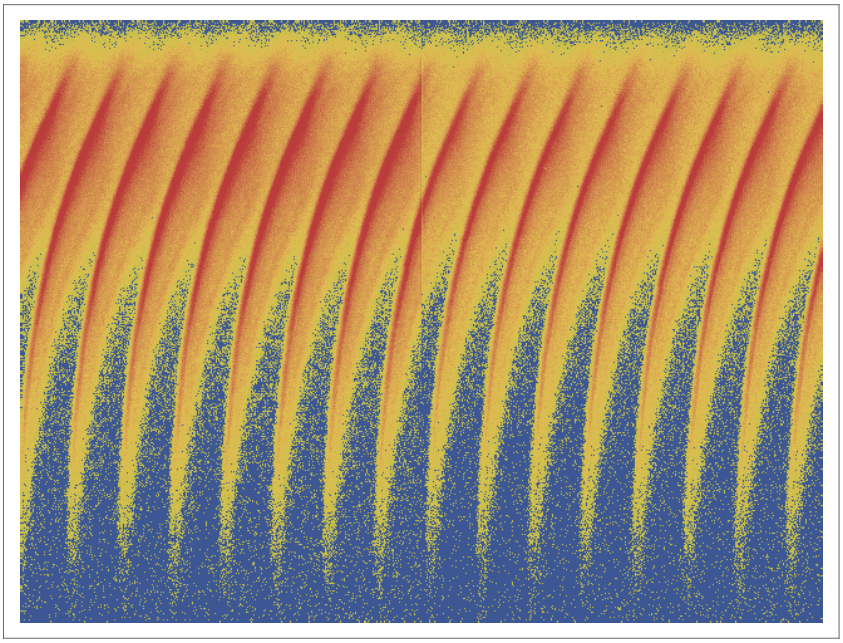

Figure 39: Integrated image on the CCD after 8000 frames. Horizontal sweep of 400 ns. Each curve corresponds to the condensate for one pulse of the laser.

our studies, we excited the sample with a pulsed laser with enough power to create the condensation and redirect that emission towards the setup. Figure 39 shows the detection of the camera: 16 vertical curves are found, each of them corresponding to one pulse of the laser. Unlike in the cases of the CW laser, in which we found straight diagonals, the pulse provokes curves that from top to bottom shift to the left and lose intensity until they disappear. These shift to the left, since we have the monochromator giving the horizontal component an energetic meaning, corresponds to energy loss with time, i.e., it shows how the blueshift due to the decay of the condensate.

4.7 CONCLUSIONS

We have measured the 2PS of a polariton condensate and found that the observed structure manifests a fundamental character of bosons, that exhibit bunching when detected in identical frequency windows (as could be expected and as was even previously reported in some particular cases before), but also, less expectedly, the opposite effect of antibunching when detected in frequency windows siding on opposite sides of the central peak. In order to obtain these

results, a new setup has been developed, that should be of great use not only for the measurement of frequency correlations with high temporal precision and the mapping of 2PS for different emitters, but also for the study of the energetic flow of the signal (illustrated with the pulsed laser evolution of the condensate). In this way, we managed to measure anticorrelations between individual photons for the case of an out-of-equilibrium condensate of exciton polaritons under continuous excitation. This approach can be used in quantum optical systems, with prospects of accessing further classes of quantum correlations [72, 93], optimising those already known [97, 114], or analysing problems such as spectral diffusion at new levels of precision [94].

5 QUANTUM POLARITONS

5.1 WHY QUANTUM POLARITONS?

Since the apparition of quantum physics, enormous efforts have been done to study quantum systems and its always unexpected features. Of all of them, the most counter-intuitive one is the entanglement [59, 101], that violates everything that we can imagine by means of nonlocality and long-distance effects between particles. Of all the possible entangled systems, the most commonly studied because of its easy control are the entangled photons, with which the violation of Bell inequalities has been proven, and with it the quantum behavior [10, 43].

Nowadays, quantum optics is one of the main research lines due to its application to quantum information. The most exciting prospects of these studies are the encryptation, quantum communication and the creation of quantum computers, which should imply a revolution in computation (in fact, it could make nowadays concept of internet crush due to the fast desencryptation it would provide, which would make every server vulnerable). For this, quantum logical gates are necessary. At this point enters the interest on polaritons.

Polaritons are at the meeting point between light and matter [65]. They are a entangled superposition of light and matter: $|U/L\rangle = (\alpha|0_a 1_b\rangle \pm \beta|1_a 0_b\rangle)$, with $|1_a\rangle$ a cavity photon of a single-mode microcavity and $|1_b\rangle$ a Coulomb-correlated electron-hole pair (exciton), giving rise to a one-particle upper (U)-/lower (L) polariton, respectively. It is this mixture of light and matter what makes them more interesting for these purposes, since they combine both worlds keeping the most useful characteristics of each of them: their photonic component gives them a light mass, facilitating the condensation (in fact,condensation-related phenomena in a semiconductor chip up to room temperature [31] have been studied); on the other hand, they present strong nonlinearities which can not be found when dealing with photons. All these characteristics have started giving useful results with future applications in the present-day electronics [16] and are emerging as the future generations of lasers [69, 100].

Although, as it was shown in section 1.1.2, polaritons have both quantum and classical descriptions, this doesn't reduce the importance of finding the quantum limit. With all the future prospects promised by these quasiparticles, enormous efforts to achieve the quantum regime of polaritons have been done,

but even in configurations that are expected to provide strong quantum correlations [9], polaritons have so far remained obstinately classically correlated.

In the last years, several results have been presented such as squeezing of the polariton field [22], studies on polariton blockade [116] and unconventional polariton blockade [17, 78]. Yet, no clear demonstration of quantum regime of exciton-polaritons has been found.

In this studies, we will reach the quantum polariton limit, achieving the single-polariton level by means of single photon excitation and, with it, manage to entangle a photon with a polariton.

5.2 INTRODUCTION TO THE EXPERIMENT

Until now, polaritons had always been achieved exciting a microcavity with a laser (continuous or pulsed) either in or out of resonance, but this method gives no control of the amount of polaritons created. In our experiment the excitation is quantized, allowing the limitation of the number of polaritons down to just one instead of a classical bath.

The experiment necessary to create quantum polaritons is composed of two different parts: the quantic and the polaritonic ones. The first part corresponds to the quantum source of the system, obtained with the sagnac interferometer (see section 2.1.1). As it was previously explained, with this setup couples of polarization-entangled photons are created with a non-linear crystal: the PPKTP. This crystal has a specific wavelength of greater performance for which the two emitted photons are degenerate. Otherwise, their wavelength can be set tuning the temperate, but losing the degeneracy. For our specific case, the wavelength of greater performance of the crystal is 810 nm, but the wavelength necessary for the excitation of the microcavity is between 829 and 830 nm (depending on the experiment). Small shifts of the wavelength can destroy the creation of polaritons, making a precise control of the temperature (and hence wavelength) of the PPKTP mandatory. This was achieved by means of a peltier cooler attached to the mount of the crystal, and to increase the stability the entire Sagnac interferometer was isolated, both thermally and luminously, by introducing it inside of a black box with a constant cold air flow and working in total darkness for all the measurements.

In this specific case, the signal of the emitted photons is of the order of 350000 photons/sec in each stage of the Sagnac interferometer. Figure 40 depicts the emission of the stage of the idler photon, obtained sending the photons through a fiber directly to the monochromator followed by a CCD camera (at -80ºC, with an energy step of 0.03 nm and a pixel size of 13 μm). Long times of integration are necessary to see the emission given the big losses specially on the fiber (40

%) and the monochromator (80 %). The spectrum shows a good gaussian shape with a linewidth of 0.45 nm.

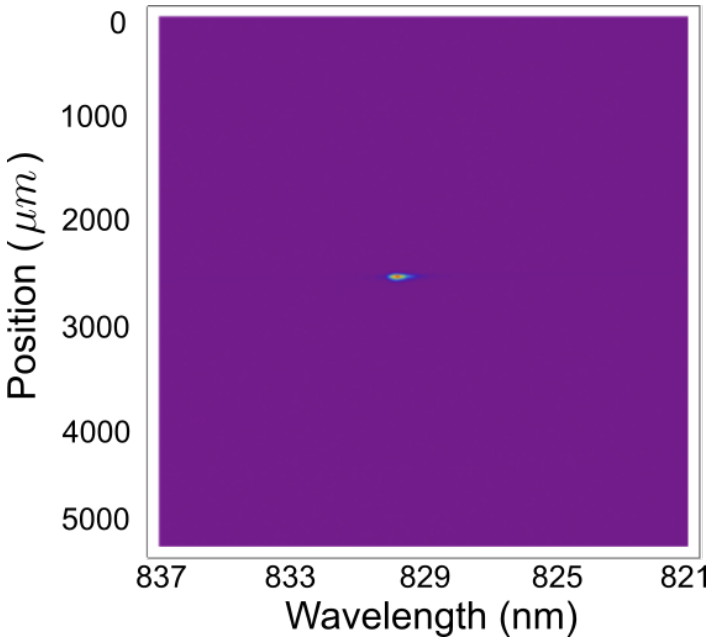

Figure 40: Emission of the SPDC integrated over 6 ms.

The polaritonic part of the experiments is formed by the microcavity (composed of front and back Distributed Bragg Reflectors (DBR) with 37 and 38 pairs, and one $In_{0.05}Ga_{0.95}As$ quantum well) inside a cryostat at temperatures of the order of 17 K and low vacuum (50 mtorr). For this experiment, we work on resonance with the polariton, which decreases the losses. One characteristic of polaritons on resonance excitation is that they are created with the same polarization of the source. Hence, working on transmission is mandatory, otherwise if measuring on reflection mode there would no form of separating the signal given by the polaritons and the one of the laser reflected on the surface of the microcavity. Of course, working on transmission also brings problems, out of which the worst is the percentage of the signal transmitted. When the polariton photons try to exit the microcavity on the second face (we will say that the first one is the one of incidence), they are absorbed mainly by the substrate on top of which the DBRs are grown (in our case GaAs). In this specific case the width of this substrate was of the order of 300 µm, giving a zero transmission (see Fig. 41a). To increase it, the sample was first manually lapped up to 100 µm, still making it impossible to measure any signal after the second face. As

another attempt, holes were chemically dug (wet etching [82]) on the buffer of a radius of the order of 200 μm (see Fig 41b), yet not being enough. Although at this point there are no losses in the substrate, the quality factor Q of the sample was too high, making the photons remain longer inside and "die" inside. To decrease the Q-factor, couples of DBRs were removed from both sides of the microcavity by means of reactive ion etching (RIE) [89] leaving 20 pairs on both faces. Finally, this gave a transmission in the LPB of the 4 %, and of 0.6 % in the UPB which, although very small, was big enough to work with. Of course, this decrease of the Q-factor broadens the branches of the polaritons decreasing, as desired, the lifetime of the polariton.

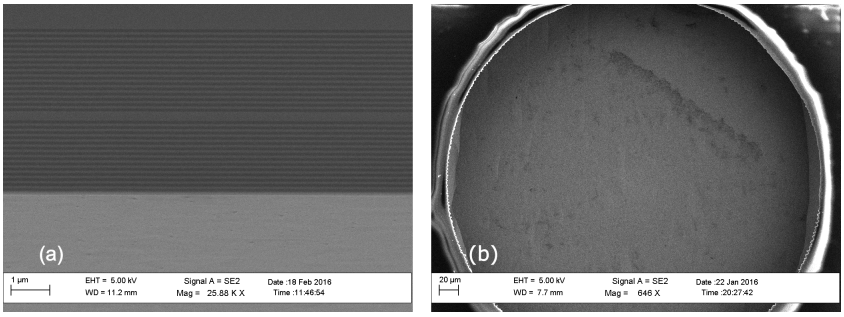

Figure 41: Microcavity used to obtain quantum polaritons. (a) Transverse figure of the microcavity with the substrate. Initially the sample was asymmetric, but the RIE procedure to reduce the Q-factor was done until the amount of DBRs was the same on both faces (20 couples). (b) Hole on the GaAs

When exciting the sample with normal incidence such that $k_x = k_y = 0$, the polaritons component were mainly photonic (photonic fraction of 70%). To modify this and try to get to a limit with exact proportions photon-exciton, the value of k should change. In this case the changes were done on the k_x component by tilting the sample, initially 14°, which gave the opposite limit with an excitonic component of 70%, and finally and angle of 7° at which the detuning was zero. With this tilt on the sample, at the excitation $k_x = 0.92\ \mu m^{-1}$ and $k_y = 0$. All the measurements shown below were done at this limit, with the microcavity tilted 7° and changing only the value of the k_y by modifying the vertical angle of incidence in the cavity, which we will refer to as k.

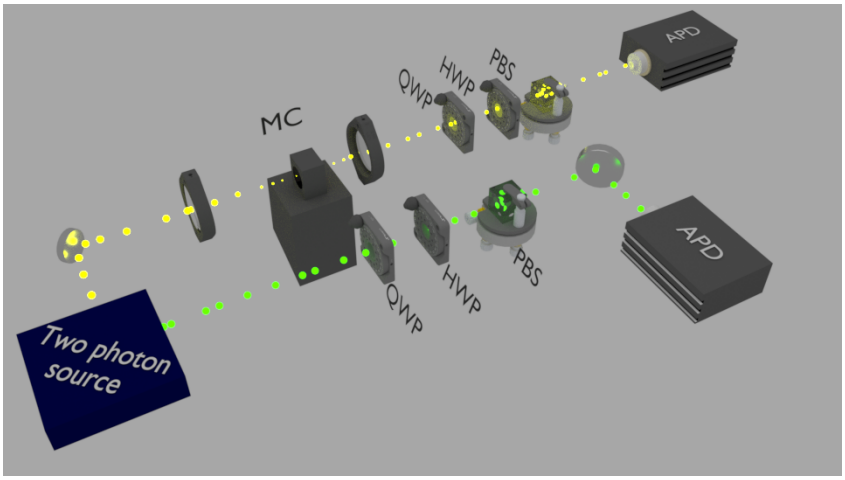

Figure 42: Setup for the creation of the quantum polaritons. The two photon source corresponds to the Sagnac interferometer (see figure 9). The branch of the signal (green) sends the single-photons to a tomography stage while the idler photons (yellow) go to the cryostat with the microcavity (creating the single-polaritons) followed by the second tomography stage.

5.3 SINGLE QUANTUM POLARITON

5.3.1 *Creation of quantum polaritons*

As previously explained, the source of entangled photons is tuned to get the idler photon to be at the energy of the LPB (830 nm), leaving the signal at 790 (see Fig. 43). The latter is sent to a tomography stage, which consists on a QWP followed by a HWP, a PBS and finally detected in an APD. The former photon, instead, was sent to a microcavity sample (Fig. 42). This one will excite resonantly with the LPB a single-polariton that will remain inside the microcavity for the lifetime of the polariton (Fig. 43). Once this photon is re-emitted due to the finite lifetime of the polariton, it will be directed to the other part of the tomography stage.

Of course, the fact that single-photon excitation creates single-polaritons can't be imposed as a general rule, but must be proven. There are several ways of proving quantumness such as antibunching in $g^{(2)}$ measurements (Cauchy-Swarz Inequalities), squeezing (although a classical field can be squeezed in all its directions), polariton blockade, the Wigner function, etc. In our case, we will center our studies on the entanglement, which we will look for between the sig-

nal photon and the single-polariton created by the idler photon. Two different variables were studied: Bell inequalities and concurrence.

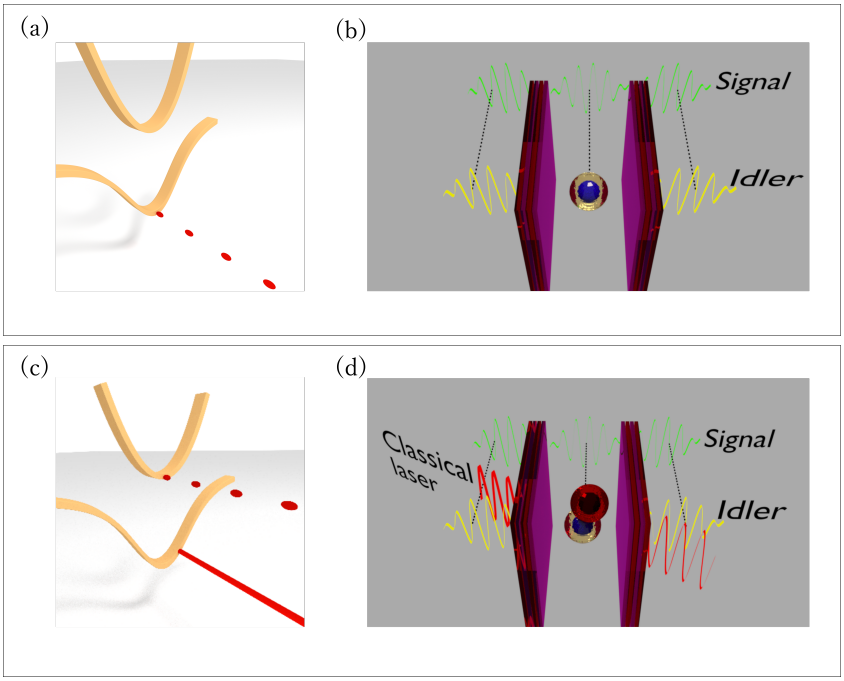

Figure 43: Sketch of the excitations both in the linear and the non-linear experiment. For the linear regime, the LPB at k=0 is excited (a) creating a single-polariton inside the cavity (b). In the non-linear regime, the laser is sent resonantly to the LPB at k≠0 and the single photon to the UPB at k=0 (c), creating a single-polariton inside a bath of polaritons (red) (d).

5.3.2 *Studies on the single polariton: demostration*

5.3.2.1 *Measurement of Bell inequalities*

Any entangled system (and hence in the quantum regime) must violate Bell inequalities. As seen in the theoretical introduction, for entangled systems the rule of locality must be violated, so the paremeter S should be greater than 2. In figure 44 is the representation of Bell curves for $b = 0$ and $b' = \pi/4$. Introducing the values of the points on the curves inside the Eq. (**??**), the calculated value of S was 2.463 ± 0.007, which unambiguously violates the classical CHSH inequality, and proves in this way the non-local character of the photon-polariton system.

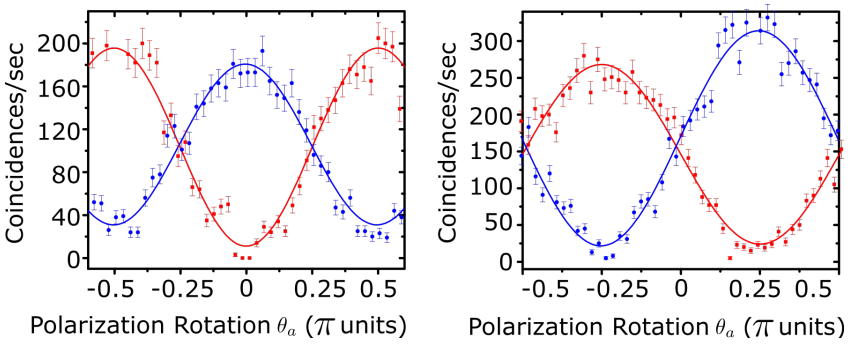

Figure 44: Coincidences as function of polarization between the external photons and the polaritons. Left: Bell curves for a polarization angle $b = 0$. Right: Bell curves for $b = -\pi/4$. Red squares and blue circles denote the $++$ and $+-$ coincidences,respectively

5.3.2.2 *Concurrence conservation*

Another proof of quantumness is obtained by calculating the concurrence of the signal-polariton system by means of tomography measurements. In section 2.1.3.1, three different methods for tomography measurements were explained, for this studies we use the last one, which although longer (36 measurements instead of 16), is the most precise one.

When we did these measurements between the LPB polariton at $k = 0$ and the signal photon, we obtained a concurrence of 0.806, which gives a second proof of the quantumness of these single-polaritons.

To see the effect of the polariton on the initial Bell state, we studied the concurrence and the density matrix both between the two initial photons and between the polariton and the photon. As shown in figure 45, the Bell state is conserved (both density matrix show the same behavior both in the real and imaginary parts). It should also be noted that the imaginary part is barely modified either, meaning that this single polariton doesn't provoke any additional phases on the initial state.

The effect of the polariton on the concurrence is also almost negligible, going from 0.826 ± 0.007 to 0.806 ± 0.006, which is a reduction of only the 2.4%. This proves that the polariton state, that inherited and later passed this information, was itself in a genuine one-particle quantum state, being entangled with the external photon. Namely, we have created the state $|\Psi\rangle = (1/\sqrt{2})(a_H^\dagger p_V^\dagger + a_V^\dagger p_H^\dagger)|0\rangle$, where p_H and p_V are the boson annihilation operators for the horizontally and vertically polarized polaritons, and a_H and a_V for the signal photon.

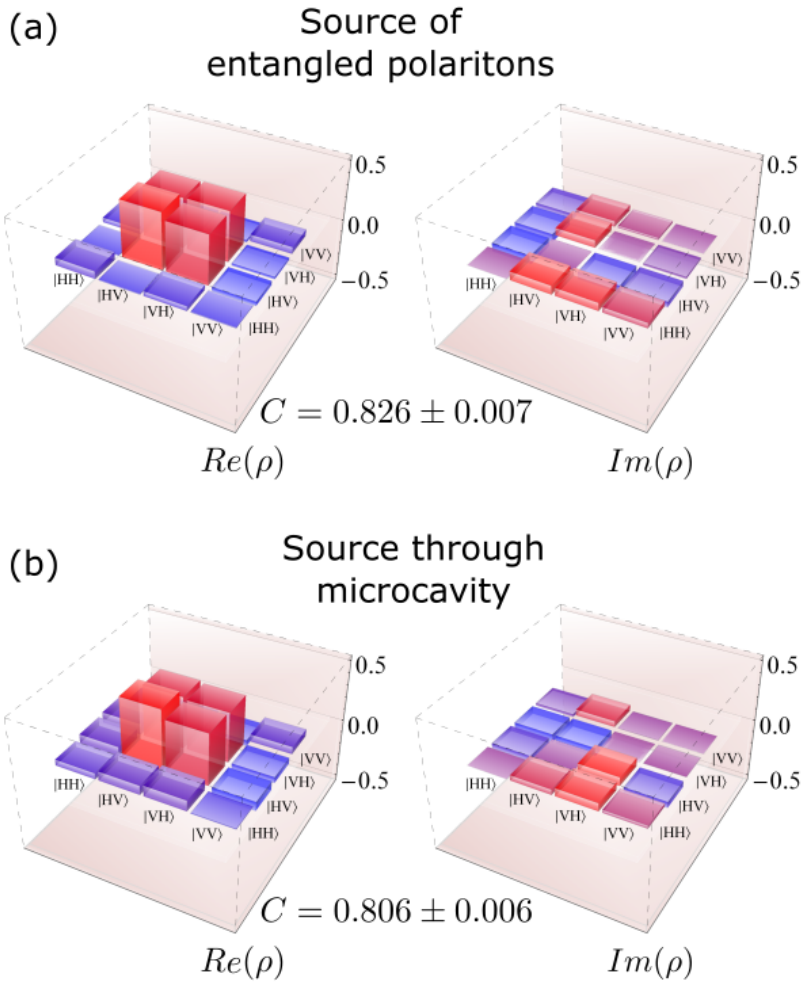

Figure 45: Tomography measured between the signal (external) and idler (LPB polariton) photons. (a) Real (left) and imaginary (right) components of the density matrix for the source of photon-pairs without the sample. The concurrence of 0.826 is not unity due to the operation wavelength that is not the optimum one for the source. (b) Real (left) and imaginary (right) components of the density matrix when passing through the microcavity. The concurrence of 0.806 shows that polaritons retain the entanglement.

5.3.2.3 *Confirmation of polaritonic behavior*

Proving quantumness is not enough though. It must also be proven that we are dealing with polaritons, otherwise we could just see the entanglement between the two initial photons.

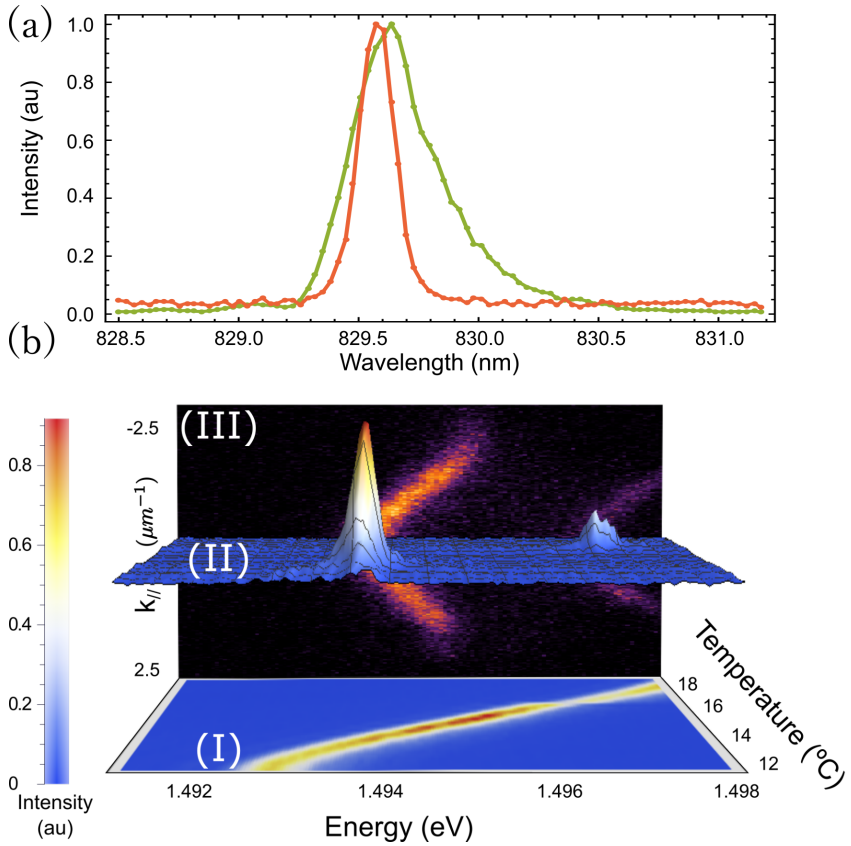

Figure 46: (a) Green: normalized emission of the PPKTP crystal. Orange: normalized transmission of (a) in the LPB. (b) Changes on the resonance as a function of the temperature on the crystal. At the bottom is the 2D map of the emission of the crystal outside of the microcavity. On the back there is the far field of the emission with a non-coherent pumping. Finally, the 3D figure shows the intensity as a function of the energy as the temperature varies. Two peaks can be identified, each of them corresponds to the resonance on one of the polariton branches.

Polaritons are created in the strong coupling regime between the cavity mode of the microcavity and the exciton of the quantum well (see section 1.1.2). Only when the polaritonic regime is achieved, there is a split in the eigenenergies creating 2 modes: LPB and UPB. Hence, only photons that have become polaritons can be emmitted at the wavelength of the LPB or the UPB. In the case of this specific experiment, the LPB was found at 830 nm, and the UPB at 829 (see fig 46).

By changing the temperature of the PPKTP we could sweep in energies from the LPB to the UPB. In the mean time we measured the transmitted signal and saw that (as shown in figure 46), the photons are *only* able to go through the cavity at the energy of the LPB and the UPB, implying that we are dealing with a polariton. There is also a shrink on the spectrum of the photon when it gets in resonance with the polariton branches, meaning that only the part of the emission *exactly inside* of the branch is able to be transmitted.

This way, by means of the entanglement and the transmission on the microcavity, we have demonstrated the creation of quantum polaritons. The lack of effect of the polariton on the initial entangled state and their ability to transfer the quantum state makes them a good candidate for quantum information. This shows in particular that pure dephasing (their capability to interact with photons) is negligible and that their radiative lifetime is not detrimental to quantum coherence.

5.4 POLARITON-POLARITON INTERACTION

Once studied the behavior of the single-polariton in the linear regime, it can be extrapolated to the non-linear regime in which interactions between polaritons is possible at a few particle level.

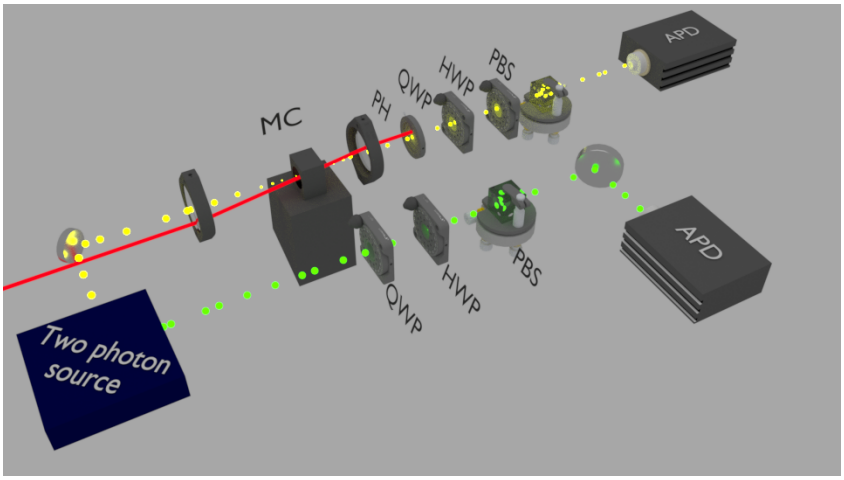

Figure 47: Setup for the study of interaction between polaritons. A great similarity with the setup of figure 42 can be found with and additional laser in the branch of the idler that goes through the microcavity and is covered with a diaphragm (PH).

In this case, the single photons are sent to the microcavity resonantly with the UPB at $k = 0$ and a second laser is sent to the microcavity resonantly with the LPB at a non-zero momentum (See Figs 43,47). This distribution of energies is chosen to avoid any effects of relaxation of the classical source to lower energy states and keep the quantum state easily distinguishable from the classical polaritons. We managed to cover the laser to avoid fake signal in the APDs by means of a closed diaphragm in the Fourier plane of the recollection lense after the microcavity. As discussed previously, the electronic noise in the tomography is calculated by means of a constant parameter γ (see section 2.1.3.1) obtained by means of the detections on both APDs and the coincidences when the temporal delay is modified in such a way that the couples of photons don't arrive together to the correlator. In this case, even with the diaphragm, there is a non-zero probability of finding a signal given by the laser that can provoke polarized additional noise. To get 100% rid of the classical signal, the noise substraction is done for each of the 36 permutations of the tomography independently keeping always the laser and the single photon instead of assuming the existence of a constant γ for the entire experiment.

Before applying any external polaritons with the continuous laser, we must check that the behavior of the quantum state on the LPB is mantained in the UPB, so we also studied the concurrence and state conservation when the single photons are sent to the UPB. In this case, the Ψ^- state is set, and as in the previous case, its conservation is evident (see Fig 45). The concurrence is higher in this case, since the wavelength of the emission (829 nm) is closer to the ideal one of the crystal (810 nm). Also in this case, the loss of concurrence is small, going from 0.884 ± 0.006 to 0.870 ± 0.007, which is a reduction of only the 1.5%.

With the new continuous pumping we manage to create a bath of polaritons in the microcavity. Both the laser and the single photon are sent to the same spatial point of the sample, that way the polaritons of this bath will interact with the single-polariton created by the entangled photon. To avoid damaging the sample and other nonlinear effects such as blueshift, the power of the laser was always kept very low, reaching a maximum density of 0.003 polaritons/μm^2. Despite this low densities, when the single photon arrives to the microcavity there will always be a non-zero chance of finding a polariton given by this bath with which it can interact. This interaction will have an effect on the concurrence of the initial entangled photons, which suffer a slow degradation as the amount of polaritons in game increases, that will be increased by raising the pumping of the laser.

Figure 49 shows both the the experimental (dots) and theoretical concurrences as the number of polaritons in the bath increases. As can be seen, the concurrence remains almost constant as the number of polaritons created by the laser increases until it reaches to 1 polariton. At that point the two polari-

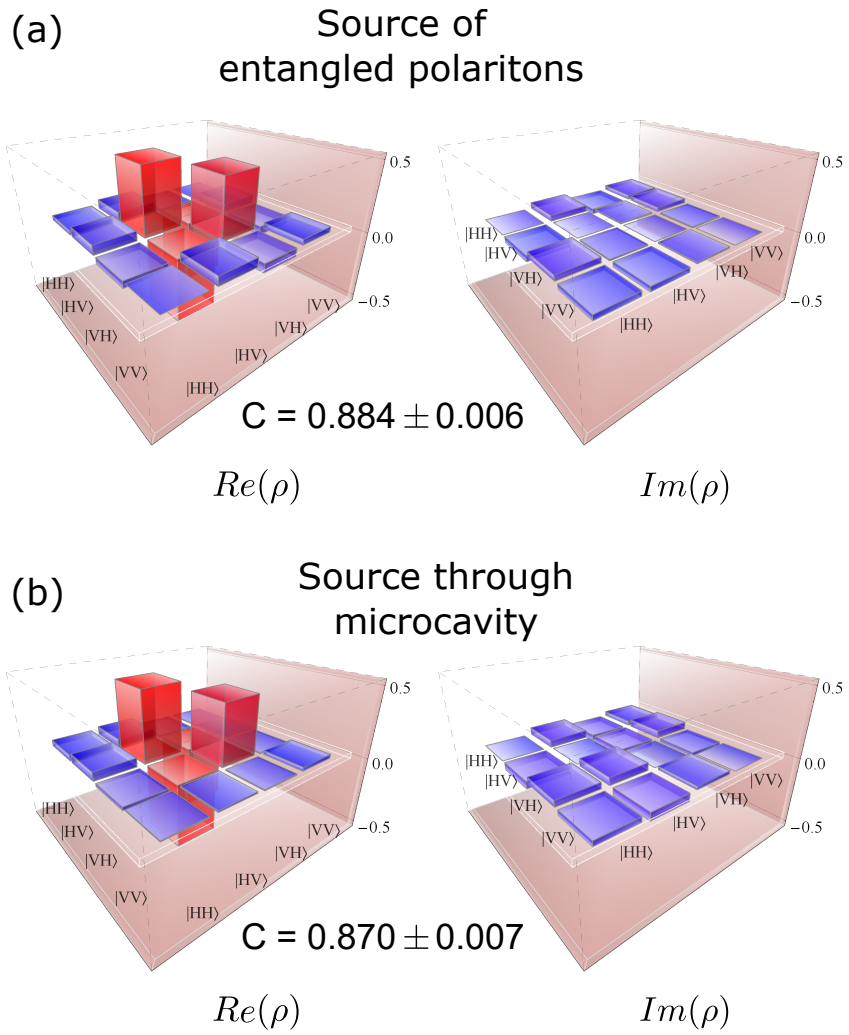

Figure 48: Tomography measured between the signal (external) and idler (UPB polariton) photons. (a) Real (left) and imaginary (right) components of the density matrix for the source of photon-pairs without the sample. The concurrence of 0.884 increases respect to the one of the LPB, since the energy is closer to the one of maximum efficiency of the PPKTP. (b) Real (left) and imaginary (right) components of the density matrix when passing through the microcavity. The concurrence of 0.870 shows that polaritons also retain the entanglement in the UPB.

tons start interacting and the polariton entangled to the signal photon becomes

dephased from it as it suffers the effects of its interacting peers while in the cavity. As a result, once reverted to a photon, the system is found in a degraded situation of indistinguishability where the polariton that interacted lost its quantum link with the photons that went straight to the detector.

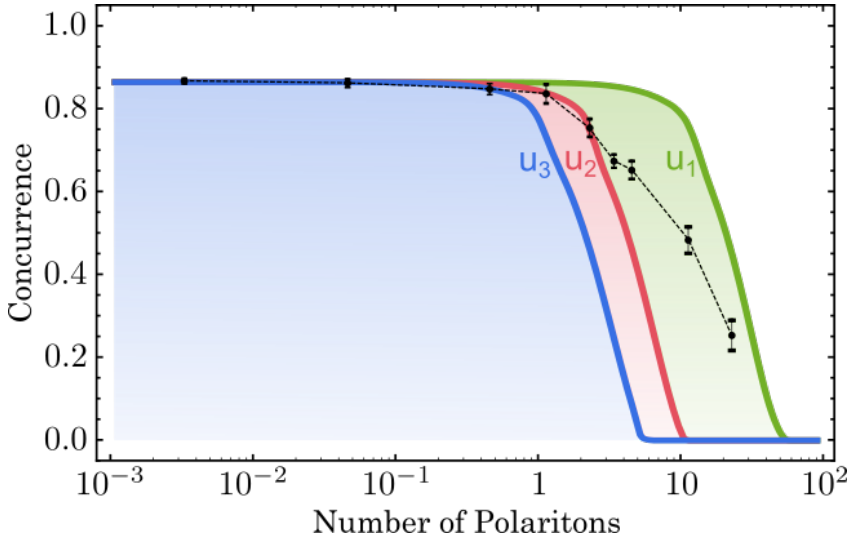

Figure 49: The concurrence $\mathcal{C}$ between the external photon and the polariton inside the microcavity as a function of the mean number of polaritons present in the sample (x axis) from a classical laser. The black points correspond to the experimental results obtained by means of the measurement of the tomography. A dashed line is introduced as a guide. The solid lines are theoretical simulations for a the model of interacting polarized polaritons explained in the text. Three different values are studied: for values of $u_1 = 0.1$ (blue), $u_2 = 0.05$ (red) and $u_3 = 0.01$ (green), where $u_i = U_1/\gamma_{pol}$ is the unitless polariton interaction normalized to their decay rate. An excellent agreement between the experimental results and the theoretical prediction is found.

This effect on the concurrence can be simulated taking into account the interacting polaritons (which is independent of the polarization), the decays (γ) and the pumping (P) on the microcavity. Eq. (127) is the master equation of the system.

$$\partial_t \rho = i[H, \rho] + \sum_{k=V,H} \frac{\gamma_k}{2} \mathcal{L}_{p_k} \rho + \frac{P}{2} \mathcal{L}_{d^\dagger} \rho \tag{127}$$

With Liouvillian in the Lindblad form $\mathcal{L}_c \rho = 2c\rho c^\dagger - c^\dagger c\rho - \rho c^\dagger c$, and $d^\dagger = (a_H^\dagger p_V^\dagger + a_V^\dagger p_H^\dagger)/\sqrt{2}$. H corresponds to the Hamiltonian of interaction of polaritons, which includes a term given by the interaction between polaritons as a

function of their polarization interaction strength (U). The Hamiltonian of the system is given by:

$$\begin{aligned} H =& \omega_p(p_V^\dagger p_V + p_H^\dagger p_H) + 2U_1 p_H^\dagger p_H p_V^\dagger p_V + \Omega(p_V^\dagger + p_V) + \\ &+ \frac{U_1 + U_2}{2}(p_H^\dagger p_H^\dagger p_H p_H + p_V^\dagger p_V^\dagger p_V p_V) - \\ &- \frac{U_1 - U_2}{2}(p_H^\dagger p_H^\dagger p_V p_V + p_V^\dagger p_V^\dagger p_H p_H) \end{aligned} \tag{128}$$

where ω_p is the free polariton energy, Ω is the intensity of a laser driving coherently vertically polarized and U_1 (U_2) is the interaction strength between parallel (antiparallel) spins. Typically the polariton interaction is strongly anisotropic, such that $|U_1| \gg |U_2|$, so that the assumption that $U_2 = 0$ can be done without a big effect on the results.

If figure 49 is studied carefully a mismatching between the experimental and theoretical slopes is clear. This difference is expected to be due to the assumption of null antiparallel interaction.

5.5 OTHER STUDIES

5.5.1 *Pulsed excitation*

The first studies for the creation of single-photons for the single-photon excitation were done by means of BBOs with a pulsed laser. The BBOs were bought at 830 nm, in order to achieve degenerate photons at the wavelength of resonance.

The setup was the following: a pulsed laser of 133 fs with repetition rate of 50 Hz was sent at 830 nm to a second harmonic generator (SHG), which converted this signal into a pulsed laser at 415 nm. Although the initial power of the laser was close to 1 Watt, at the exit of the SHG the power was below 100 mW. This new signal was sent to a short-pass filter 450 nm, to select only the second harmonic and get rid of any remaining signal at 830 nm. The filtered signal arrived to the first BBO. Changes on the tilt and the angle on the BBOs change both the radius of the cones of the type-II SPDC and the angle between them. Hence, the crystals were mounted in order to have control over all the possible components. After going through this crystal, the two cones were emitted (see figure 50). Appart from these two phtons at 830 nm, some incident component at 415 nm also managed to go through the crystal, and was suppressed by means of a long-pass filter of 800 nm. After going through one BBO the delay created on each photon is not the same, so a second BBO is introduced to match the temporal delay between both photons. To do so the polarization of the cones had to be rotated by 90°, so a HWP at 45° was inserted between both crystals.

The cones after the second BBO where, were perfectly synchronized. For the porpuse of the experiment, only the point of intersection was necessary, so a pinhole was put right after the first BBO for the spatial selection of the intersection (see figure 50b). The cones expand as they get away from the crystals, so two lenses had to be inserted after the final BBO in order to collilmate the selected region.

This selected region corresponded to two indistinguishable photons (in the case of the figure). There was a big problem in this source: the signal. Being a pulsed laser, the energy spectrum was enormous, with a linewidth of the order of 8 nm, exciting both the LPB and the UPB, which was incompatible with our experiments. Of course, an interferencial filter (IF) could be introduced to select only the region of the polariton branch. On the other hand, this solution was also problematic due to the count rate. The signal, with the entire emission had a rate of 10^3 photons/sec, which was already too small for measurements. If in addition the signal was filtered, the amount of photons was too low, and incompatible to measurements (taking into account that only on the sample, we lost a 96% of the signal.

Due to this incompatibility of the pulsed excitation on the BBOs with the experiment, we decided to use a more efficient source of entangled photons: the sagnac interferometer with a PPKTP crystal.

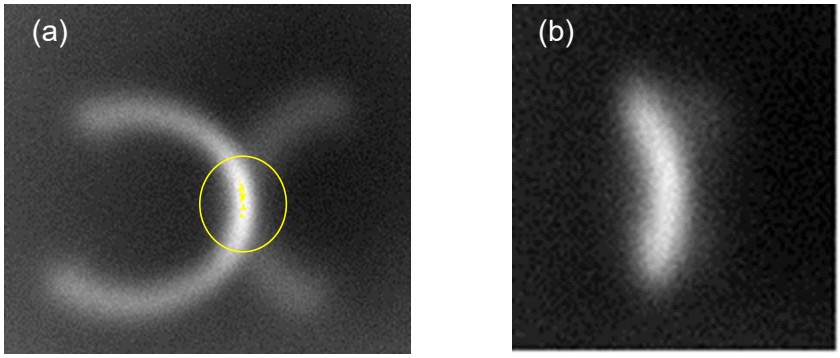

Figure 50: a: Emission of the first BBO seen on a CCD camera. The crystal was set to obtain the two cones in the indistinguishable limit. b: Selected region of the emission.

5.5.2 *Study of classical decoherence*

After studying the efffect of a bath of photons on the concurrence of the entangled polariton, we decided to study the effect of a bath of polaritons on another classical bath of polaritons.

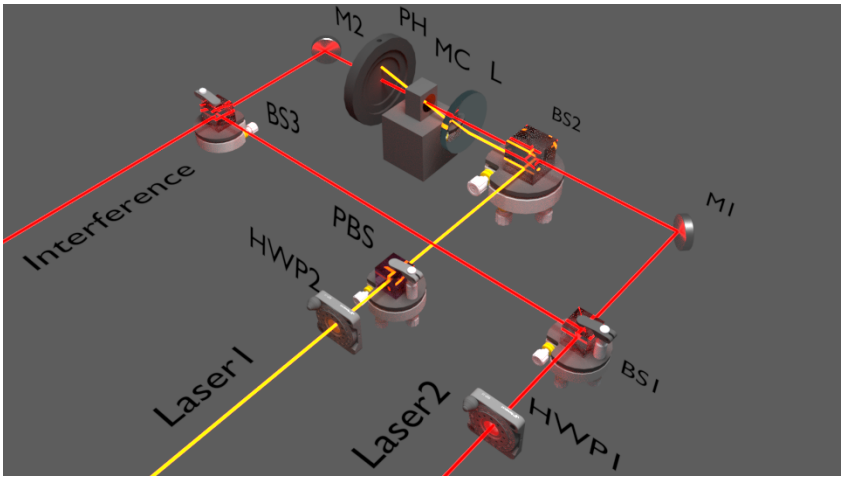

Figure 51: Experimental setup for the measurement of the changes on the $g^{(1)}$ of the polaritons created by laser 2 (red) while the microcavity is excited with another laser (laser 1, yellow) with different powers.

For this experiment two lasers were necessary, one for the bath of polaritons at the LPB, and another one substituting the single-polariton at the UPB (see Fig. 51). The effect of the first laser (yellow) on the polaritons of the UPB (red) was measured by means of the $g^{(1)}$ of the UPB as a function of the power of the first laser. To do so, the second laser was split into two identical beams before the microcavity, and the $g^{(1)}$ was measured by means of the visibility when one of the new beams interfered with the emission of the sample (as in the previous experiments, in transmission mode). Like in the case with single-photon excitation, the laser sent at the LPB had a non-zero momentum in order to cover it in the fourier plane of the detection lens. To change the power of this laser a HWP (HWP2 in the figure) and a PBS were introduced during its path.

There were no effects on the classical coherence when changing the power of the laser on the LPB.

In the case of the single-photon excitation we are always sending $|HV\rangle$ single photons to the microcavity, so playing with the polarization made sense. To do so we included a HWP (HWP1 in the figure) in the path of the second laser (the one substituting the single-photons) and studied the effects on the classical coherence when changing both polarization and power. Once again no changes were found (see Fig. 52).

At first you could consider this lack of effect on the classical coherence a "failure" on the theory or a proof of a "bug" in the experiments, but in fact it was not. Although the effect of the interaction was clear in the case of the

single-photon, they are very fragile systems, and any little interaction has an effect. On the other hand, the condensate is not as fragile and, being so small the interaction between polaritons, the existence of another condensate doesn't affect its classical coherence.

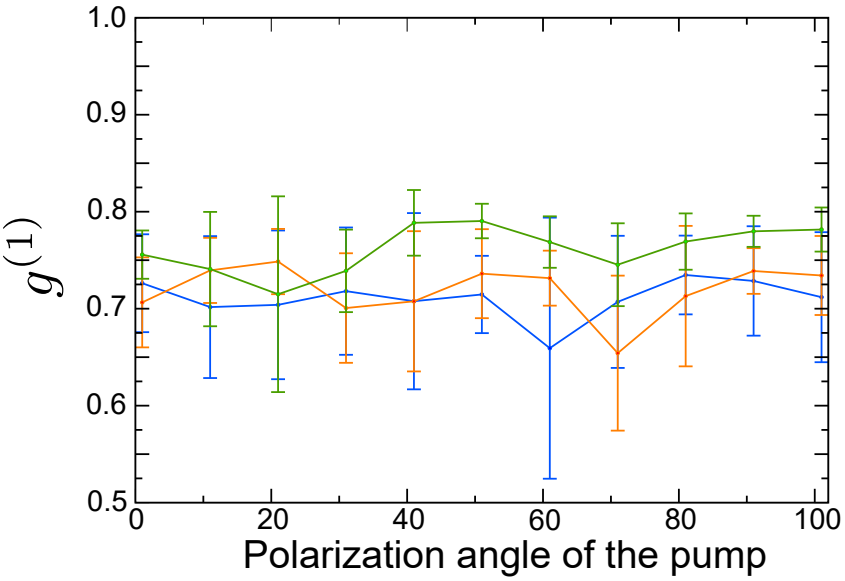

Figure 52: Changes on the $g^{(1)}$ as a function of the polarization of the first laser. Three different powers for laser one were studied: 6 μW (blue), 50 μW (red) and 100 μW (green).

5.6 CONCLUSIONS AND FUTURE PROSPECTS

With these experiments, the quantum behavior of these particles is demonstrated, and with it new gates are opened. Given the ability of polaritons to maintain their state in the single-particle regime, they could be used as single quantum bits transfering unaltered information to an external photon. On the other hand, when a bath of polaritons starts altering the quantum coherence of the state due to polariton-polariton interaction it could be applied for quantum spectroscopy.

Future experiments could be done changing the PPKTP to work with fock states of N>1. Initially 2 single photons could be sent to one branch (taking the wavelength of degeneracy of the crystal equal to the one of the polariton branch). If the wavelength of the PPKTP is taken in between the LPB and UPB,

one polariton could be created in each of them simultaneously with the correct temperature.

Another way of creating single polaritons could be changing the source for the pumping and using single-photon sources instead of selecting one of the two photons of an entangled couple. Sources such as quantum dots [4, 26] or nitrogen vacancy centers on diamond [3, 14] with an emission at the resonance frequency would be suitable for this work. Of course, the efficiency of these sources should be extremely high. Yet, the measurements instead of entanglement to proof quantumness, should be substituted by second-order correlation function in order to find an antibunching in the photons emitted by the microcavity after the single-photon excitation. The efficiency of this kind of measurement would be higher since the setup would be simpler, substituting the tomography stage (composed of 3 elements) by a HBT one, which only needs a BS. On the other hand, the emission of the QDs should be in exact resonance with the polariton, which closes lots of doors unlike with the PPKTP crystal, in which the wavelength is tuned with temperature.

6 CONCLUSIONS

6.1 CONCLUSIONES (CASTELLANO)

En esta tesis, hemos estudiado a los polaritones desde una perspectiva cuántica, con el incentivo de alcanzar un régimen donde no existe un modelo clásico adecuado para describirlos. Debemos comparar esto con el caso general en el que tal descripción clásica existe, pero es igualmente conveniente, si no más, recurrir a una descripción cuántica equivalente. Este enfoque dual clásico/cuántico comienza con el polaritón en sí mismo, usualmente descrito como la superposición cuántica de luz y materia, y como tal, un estado de Bell máximamente entrelazado. Sin embargo, en el laboratorio, sea en la forma de estados puros o mixtos, los polaritones son estados producto que no muestran ningún entrelazamiento y que pueden ser descritos mediante ecuaciones de Maxwell para campos clásicos. Para observables de una sola partícula, los resultados no dependen de la elección del formalismo. Por lo tanto, para probar el caracter genuinamente cuántico, uno debe fijarse en los observables a dos partículas. Este es el enfoque seguido en esta tesis, usando dos métodos diferentes. Los polaritones emiten luz cuya detección permite reconstruir su dinámica, de modo que su análisis se convierte en un problema de óptica cuántica.

Nuestra búsqueda de los polaritones cuánticos comienza con la relación más importante entre dos partículas: la función de correlación de segundo orden $g^{(2)}(\tau)$, que cuantifica la correlación entre dos partículas. El límite $g^{(2)}(0) < 1$ es una prueba de un comportamiento sub-Poissoniano de el campo y, al igual que la violación de las desigualdades de Schwarz en el tiempo, es una demostración de su comportamiento cuántico. Ha habido numerosos intentos de medir $g^{(2)}(0) < 1$ en la comunidad polaritónica, en particular en la configuración del "bloqueo polaritónico". Sin embargo, todos han llevado a resultados fallidos debido a la gran disipación respecto a la no linearidad de un polaritón en el régimen de partícula única. Aprovechando la reciente teoría de correlaciones entre fotones resueltas en energía, que da una mayor información que la $g^{(2)}$ usando el grado de libertad energético, medimos el espectro de correlaciones a dos fotones del sistema polaritónico estrella: el condensado de polaritones. Para ello, ampliamos una técnica reciente para la medida de la $g^{(2)}(\tau)$ usando una streak camera. Pese a su gran precisión temporal, este método conlleva varias fuentes de ruido que afectan al resultado final. Hemos estudiado el enfoque más eficiente para el análisis de los resultados obtenidos

de esta manera, y analizamos el efecto de varias complicaciones experimentales que pueden afectar a los resultados. Inesperadamente, vimos que componentes tan inofensivos como un chopper pueden destruir la estacionaridad de la señal en el caso de modulaciones rápidas, o arruinar la normalización en el caso de modulaciones lentas. Hemos demostrado que este efecto se puede subsanar con un post-procesado de los datos. Además de el effecto del chopper, estudiamos otros efectos que alteran los resultados, tales como deficiencias de los detectores, que aumentar el ruido sin modificar el comportamiento; ruido externo randómico, como por ejemplo los dark counts, que tienden a destruir las correlaciones; el gravity peak de la streak, que destruye el valor de las correlaciones para bajos valores de τ, provocando falsos comportamientos bunched; y el jitter temporal debido a la resolución temporal y que, al igual que el ruido randómico, randomiza la señal. Teniendo en cuenta estos resultados, diseñamos un experimento para medir la detecciones de fotones con discriminación energética introduciendo un monocromator antes de la streak camera. Este experimento nos permitió estudiar de un modo eficiente todo el mapa de correlaciones fotón-fotón a lo largo de todas las frecuencias de emisión. Además de para este tipo de medida, este nuevo sistema es aplicable al estudio de correlaciones en frecuencia y tiempo, como por ejemplo para la medida de difusión espectral en sistemas cambiantes. En el caso específico de un condensado de polaritones, encontramos una estructura característica formada por correlaciones positivas para las mismas energías y negativas para energías opuestas respecto al máximo de emisión. Puesto que en el caso de un sistema de dos niveles la estructura es similar (bunching para frecuencias iguales debido a la indistinguibilidad y una forma de mariposa debido a el antibunching entre frecuencias opuestas), este resultado parece el primer paso hacia el polaritón único. Sin embargo, no encontramos ninguna violación de desigualdades clásicas o manifestaciones directas de comportamientos no lineales en los polaritones. Por lo tanto, el origen de este comportamiento se debe encontrar en alguna otra parte. Encontramos que, de hecho, es una manifestación de una estructura fundamental de los bosones, que extiende el bien conocido efecto de Hanbury Brown y Twiss. Este último es un pilar de la óptica cuántica, siendo el detonante de su desarrollo teórico. Pone de manifiesto que los fotones de una fuente térmica (o no correlacionadas) tienden a llegar juntas a un detector. Nuestro experimento identifica y mide el *boson form factor*, que describe la correlación en energía de los fotones independientemente de la dinámica de la fuente, que aporta el valor de $g^{(2)}(0)$, tal que el espectro de correlaciones de dos fotones puede escribirse de la forma $g^{(2)}_{\Gamma}(\omega_1, \omega_2) = g^{(2)}(0)\mathcal{F}(\omega_1, \omega_2)$. Dado que $\mathcal{F}$ tiene valores inferiores a uno, en el caso de una fuente coherente en la que $g^{(2)} = 1$, encontraremos zonas de este mapa de correlaciones en las que también su valor sea menor que uno, implicando "photon antibunch-

ing" cuando es detectado con (las apropiadas) frecuencias distintas. Esto revela una simetría fundamental de bosones que postulamos ocurre similarmente, pero rotado, para fermiones, con correlaciones cruzadas positivas y autocorrelaciones negativas. Al igual que en el efecto estándar de Hanbury Brown-Twiss, su versión coloreada tiene dos interpretaciones. Una en términos de la física clásica con interferencias constructivas y destructivas de ondas. En este caso, encontramos unas anticorrelaciones sorprendentemente perfectas para frecuencias simétricas en el límite de filtros infinitamente anchos. La otra interpretación es cuántica y se hace en términos de partículas, envolviendo su (in)distinguibilidad. Ambos aspectos han sido largamente discutidos y contrastados uno con otro. Mientras los hallazgos son de alto interés intrínseco, puesto que proveen un cuadro completo para uno de los efectos más fundamentales en la óptica cuántica, pertenecen precisamente a esta categoría de fenómenos que pueden ser igualmente acomodados en un cuadro clásico o cuántico. Los polaritones han sido usados aquí como una fuente conveniente para tal medida, con un amplio ancho de línea (y por tanto fácil para filtrar) unido a una emisión coherente.

La segunda parte de la tesis presenta un enfoque completamente distinto para alcanzar el régimen de polaritones genuinamente cuántico. Concretamente, en vez de generar el estado cuántico desde dentro de la cavidad, por ejemplo distorsionando un haz láser externo en un estado comprimido gracias a las interacciones polaritónicas, excitamos directamente la microcavidad con luz cuántica. La idea sigue recientes propuestas teóricas sobre la excitación cuántica, tales como la espectroscopía de Mollow, que propone medir pequeñas nolinearidades en sistemas altamente disipativos sondeándolas con todo el abanico de estadísticas fotónicas, desde "antibunched" a "superbunched", como por ejemplo proporciona la luz de el triplete de Mollow. Ya que todavía existen grandes dificultades técnicas para conectar emisores cuánticos (como fuentes) y polaritones en microcavidades (como blancos de la excitación), hemos optado por una variación original que hace uso de un par de fotones entrelazados en polarización. Un fotón es enviado a la microcavidad antes de su llegada a el detector, mientras que el otro es enviado directamente a un segundo detector permitiendo de este modo la medida de la correlación entre éste y el fotón emitido por la microcavidad. Al hacer así en la microcavidad vacía, podemos reconstruir la matriz densidad de la pareja, la cual encontramos muy similar a la original obtenida sin la interrupción de la muestra. Esto significa que en el foton que pasó a través de la cavidad creó un polaritón en el régimen cuántico: un polariton en estado Fock $|1\rangle$; y que este estado no sufrió, o lo hizo muy poco, por esta conversión, ni por su defase en el interior de la cavidad, ni por su reemisión al exterior ni por ningún otro de los factores detrimentales que han frustrado hasta ahora la observación de los polaritones en

genuinos estados cuánticos. Este es un alentador primer resultado para el futuro de la polaritónica cuántica. En este régimen de un solo polaritón, hemos además demostrado la no-localidad del entrelazamiento entre el polaritón y un fotón externo mediante la medición de una fuerte violación de la desigualdad de Bell. Este descubrimiento abre las puertas a numerosos experimentos con polaritones cuánticos, incluyendo su propagación en circuitos y su interacción a nivel de una única partícula. También dimos un primer paso hacia una aplicación útil y original de este régimen estableciento las bases de la espectroscopia cuántica. Concretamente, enviamos un fotón del par entrelazado a una microcavidad que ahora alberga un condensado de polaritones creado por medio de una excitación clásica continua, y observamos los efectos de esta última en el entrelazamiento. Encontramos, de acuerdo con el modelo teórico, que la presencia de condensados interactuando estropea la concurrencia de la pareja de fotones a un ratio que permite medir la fuerza de la interacción. Esta medida es la primera de una nueva generación de experimentos que deberían aprovechar la luz cuántica, y les permite la sustitución de lásers, abriendo una nueva página en la óptica.

Como conclusión, mientras muchas tesis exitosas consiguen empezar y finalizar un problema dado, esta recoge un problema que lleva tiempo abierto y no lo concluye, sino que abre el problema aún más. Creemos que con las páginas de cierre de este trabajo, empezamos una nueva era en la polaritónica cuántica; incluso más que esto, nosotros también empezamos una nueva carrera: aquella hacia los "dispositivos polaritónicos cuánticos". ¡Únanse a la carrera!

6.2 CONCLUSIONS (ENGLISH)

In this thesis, we have studied polaritons from a quantum perspective, with the incentive of reaching a regime where no classical description is suitable to describe them. This is to be contrasted with the general case where such a classical description exists, but it is equally, if not more, convenient to recourse to an equivalent quantum description. Such a dual classical/quantum approach starts with the polariton itself, often described as the quantum superposition of light and matter, and as such, as a maximally entangled Bell state. Nevertheless, in the laboratory, whether in the form of mixed or pure states, polaritons are product states that feature no entanglement and that can be described by Maxwell equations for classical fields. For single-particle observables, results do not depend on the choice of formalism. To prove the genuine quantum character, one must therefore turn to two-particles observables. This is the approach pursued in this thesis, using two different methods. Polaritons emit light whose

detection allow a reconstruction of their dynamics, so their analysis becomes a problem of quantum optics.

Our quest for quantum polaritons starts with the most popular two-particles quantity, the second-order correlation function $g^{(2)}(\tau)$ that quantifies two-particles correlations. The case $g^{(2)}(0) < 1$ proves the sub-Poissonian character of the field and as a violation of Schwarz inequalities in time, also proves its genuine quantum character. There have been numerous prior attempts by the polariton community to measure $g^{(2)}(0) < 1$, in particular in the so-called "polariton blockade" configuration. They have remained so far unsuccessful, due to too large dissipation as compared to the polariton nonlinearity at the single-particle level. Taking advantage of the recently developed theory of frequency-resolved photon correlations, that allows to extract more information from $g^{(2)}$ measurements by retaining the energy degree of freedom, we first measured the two-photon correlation spectrum of the star polariton system: the polariton condensate. To do so, we extended a recent technique for the measurement of $g^{(2)}(\tau)$ by means of a streak camera. This method, although it has a high temporal resolution, suffers from several sources of noise that can affect the results. We studied the most efficient approach for the analysis of the results obtained in this way as well as the effects of various experimental complications that could affect the result. Innocuous components such as a chopper can destroy the stationarity of the signal in the case of fast modulations or ruin the normalization of the correlation function for the opposite case of slow modulations. We have shown how this can be fixed by post-processing of the data. Other sources of alterations of the results that were considered include photon-detection deficiencies, that increase noise but do not alter the behavior, random external noise such as dark counts, which tend to decorrelate the signal, the streak-camera gravity peak, which destroys the value for low τ, creating a fake bunching, and the timing jitter, which accounts for the temporal resolution and, as in the case of the random noise, also randomizes the signal. With the previous results in hand, we designed a setup to empower the photon detection with frequency-discrimination by including a monochromator before the streak camera. This efficient experimental method allowed us to obtain the entire map of photon-photon correlations spanning over all frequencies of emission. This new setup should find further applications for the study of temporal and frequency correlations, for instance for the measurement of spectral-diffusion times when applied to fluctuating systems. In the case of a polariton condensate, we observed a characteristic structure with positive correlations for equal frequencies, and, oppositely, negative correlations for symmetric frequencies with respect to the maximum of emission. This appears to be a first step towards single-polariton effects since the emission of a two-level system has a similar structure, with bunching for equal frequencies

as a result of photon indistinguishability and a characteristic butterfly shape of antibunching for different frequencies. In the case of a polariton condensate, however, we find no violation of classical inequalities and do not find any direct manifestation of polariton nonlinearities. Therefore, the origin of this shape is to be found somewhere else. We find it indeed to be the manifestation a fundamental structure of bosons that extends the well-known Hanbury Brown and Twiss effect. The latter is a pillar of quantum optics and triggered the development of its theory. It states that photons from a thermal source (or from uncorrelated sources) tend to arrive together on a detector. Our experiment identifies and measure the so-called *boson form factor* that specifies how bosons are correlated in frequency regardless of the dynamics of the source, which contributes an overall factor $g^{(2)}(0)$, so that the two-photon correlation spectrum reads $g(2)_\Gamma(\omega_1,\omega_2) = g^{(2)}(0)\mathcal{F}(\omega_1,\omega_2)$. Since $\mathcal{F}$ takes values less than unity, for a coherent source, with $g^{(2)} = 1$, the two-photon spectrum also takes values less than unity, implying photon antibunching when detected with (appropriate) different frequencies. This reveals a fundamental symmetry of bosons that we postulate occurs similarly, but rotated, for fermions, with positive cross-correlations and negative auto-correlations. Just as the standard Hanbury Brown–Twiss effect, its colored version comes with two interpretations: one in terms of classical physics with constructive and destructive interferences of waves. In this case, we find a surprising perfect anticorrelations for symmetric frequencies in the limit of infinitely broad filter widths. The other interpretation is quantum and is made in terms of particles, involving their (in)distinguishability. Both aspects have been discussed at length and contrasted to each others. While the findings are of high intrinsic interest, as they provide the complete picture for one of the most fundamental effect in quantum optics, they belong precisely to this categories of phenomena that can be accommodated equally well in a classical or quantum picture. Polaritons have been used here as convenient source for such a measurement, with a broad lineshape (and therefore easy to filter through) linked to a coherent emission.

The second part of the thesis takes a completely different approach to reach the genuinely quantum regime of polaritons. Namely, instead of self-servicing the generation of a quantum state from within the microcavity, for instance by distorting an external laser beam into a squeezed state thanks to polariton interactions, we excite directly the microcavity with quantum light. The idea follows recent theoretical proposals of quantum excitation, such as Mollow spectroscopy, that offers to measure small nonlinearities in highly dissipative systems by probing them with a full range of photon statistics, from antibunched to superbunched, as is provided for instance by the Mollow triplet. Since there are still major technical difficulties to bring together quantum emitters (as the source) and microcavity polaritons (as the target), we aimed for an original

variation that uses a pair of polarization-entangled photons. One photon is sent to the microcavity before collection, and the other to another detector, that correlates detection with the output from the microcavity. Doing so for the microcavity in vacuum, we reconstruct the correlation matrix of the pair and find it to be very close to that obtained without the intermission of the sample. This means that the one-photon that passed through the cavity created one polariton in the long-sought genuine quantum regime: a polariton Fock state $|1\rangle$, and that this state did not suffer, or very little, from this conversion, from dephasing once inside the cavity, from its re-emission outside and from all the other detrimental factors that have thwarted so far the observation of genuine polariton quantum states. This is an encouraging first result for the future of quantum polaritonic. In this single-polariton regime, we have furthermore demonstrated non-locality of the entanglement between the polariton and the external photon through the measurement of a strong violation of Bell's inequality. This finding opens the road to numerous experiments with quantum polaritons, including their propagation in circuits and their interaction at the single-particle level. We also made a first step towards a useful and original application of this regime by laying the grounds for quantum spectroscopy. Namely, we sent one photon of the entangled pair into a microcavity now hosting a polariton condensate created by means of continuous classical excitation, and we observed the effect of the latter on the entanglement. We find, in agreement with a theoretical model, that the presence of an interacting condensate spoils the concurrence of the photon-pair at a rate that allows to measure the interaction strength. This measurement is a first from a new-generation series of experiments that should take advantage of quantum light and brings them to substitute lasers, opening a new page of optics.

As a conclusion, while many successful Theses manage to start and finish a given problem, this one took on a problem that has been long time opened and did not bring it to its conclusion but widened the problem even more. We believe that with the closing pages of this work, we start a new era of quantum polaritonics, but even more than that, we also start a new race: that towards "quantum polaritonic devices". Join the race!

BIBLIOGRAPHY

[1] Albert F Adiyatullin, Mitchell D Anderson, Pierre V Busi, Hadis Abbaspour, Régis André, Marcia T Portella-Oberli, and Benoit Deveaud. "Temporally resolved second-order photon correlations of exciton-polariton Bose-Einstein condensate formation." In: *Applied Physics Letters* 107.22 (2015), p. 221107.

[2] GS Agarwal. "Vacuum-field Rabi splittings in microwave absorption by Rydberg atoms in a cavity." In: *Physical review letters* 53.18 (1984), p. 1732.

[3] Igor Aharonovich, Chunyuan Zhou, Alastair Stacey, Julius Orwa, Stefania Castelletto, David Simpson, Andrew D Greentree, François Treussart, Jean-Francois Roch, and Steven Prawer. "Enhanced single-photon emission in the near infrared from a diamond color center." In: *Physical Review B* 79.23 (2009), p. 235316.

[4] A Paul Alivisatos. "Semiconductor clusters, nanocrystals, and quantum dots." In: *Science* 271.5251 (1996), p. 933.

[5] A. Amo et al. "Collective fluid dynamics of a polariton condensate in a semiconductor microcavity." In: *Nature* 457 (2009), p. 291. URL: doi:10.1038/nature07640.

[6] A Amo, J Bloch, A Bramati, I Carusotto, C Ciuti, B Deveaud, E Giacobino, G Grosso, A Kamchatnov, G Malpuech, et al. "Comment on "Linear Wave Dynamics Explains Observations Attributed to Dark Solitons in a Polariton Quantum Fluid"." In: *Physical review letters* 115.8 (2015), p. 089401.

[7] Alberto Amo, Jérôme Lefrère, Simon Pigeon, Claire Adrados, Cristiano Ciuti, Iacopo Carusotto, Romuald Houdré, Elisabeth Giacobino, and Alberto Bramati. "Superfluidity of polaritons in semiconductor microcavities." In: *Nature Physics* 5.11 (2009), pp. 805–810.

[8] Alberto Amo, S Pigeon, D Sanvitto, VG Sala, R Hivet, Iacopo Carusotto, F Pisanello, G Leménager, R Houdré, E Giacobino, et al. "Polariton superfluids reveal quantum hydrodynamic solitons." In: *Science* 332.6034 (2011), pp. 1167–1170.

[9] V. Ardizzone, M. Abbarchi, A. Lemaître, I. Sagnes, P. Senellart, J. Bloch, C. Delalande, J. Tignon, and P. Roussignol. "Bunching visibility of optical parametric emission in a semiconductor microcavity." In: *Physical review b* 86 (2012). URL: doi:10.1103/PhysRevB.86.041301.

[10] A. Aspect, P. Grangier, and G. Roger. "Experimental Tests of Realistic Local Theories via Bell's Theorem." In: *Physical review letters* 47 (1981). ASP1, p. 460. URL: doi:10.1103/PhysRevLett.47.460.

[11] M Assmann, F Veit, M Bayer, Mike van der Poel, and Jørn Märcher Hvam. "Higher-order photon bunching in a semiconductor microcavity." In: *Science* 325.5938 (2009), pp. 297–300.

[12] Marc Aßmann, Franziska Veit, Jean-Sebastian Tempel, Thorsten Berstermann, Heinrich Stolz, Mike van der Poel, Jørn M Hvam, and Manfred Bayer. "Measuring the dynamics of second-order photon correlation functions inside a pulse with picosecond time resolution." In: *Optics express* 18.19 (2010), pp. 20229–20241.

[13] Marc Aßmann, Jean-Sebastian Tempel, Franziska Veit, Manfred Bayer, Arash Rahimi-Iman, Andreas Löffler, Sven Höfling, Stephan Reitzenstein, Lukas Worschech, and Alfred Forchel. "From polariton condensates to highly photonic quantum degenerate states of bosonic matter." In: *Proceedings of the National Academy of Sciences* 108.5 (2011), pp. 1804–1809.

[14] Thomas M Babinec, Birgit JM Hausmann, Mughees Khan, Yinan Zhang, Jeronimo R Maze, Philip R Hemmer, and Marko Lončar. "A diamond nanowire single-photon source." In: *Nature nanotechnology* 5.3 (2010), pp. 195–199.

[15] Hans-Albert Bachor and Timothy C Ralph. *A guide to experiments in quantum optics*. Wiley, 2004.

[16] Dario Ballarini, Milena De Giorgi, Emiliano Cancellieri, Romuald Houdré, Elisabeth Giacobino, Roberto Cingolani, Alberto Bramati, Giuseppe Gigli, and Daniele Sanvitto. "All-optical polariton transistor." In: *Nature communications* 4 (2013), p. 1778.

[17] M. Bamba, A. Imamoglu, I. Carusotto, and C. Ciuti. "Origin of strong photon antibunching in weakly nonlinear photonic molecules." In: *Physical review A* 83 (2011), 021802(R). URL: doi:10.1103/PhysRevA.83.021802.

[18] J. J. Baumberg et al. "Spontaneous Polarization Buildup in a Room-Temperature Polariton Laser." In: *Physical Review Letters* 101 (2008), p. 136409.

[19] Gordon Baym. "The physics of Hanbury Brown–Twiss intensity interferometry: from stars to nuclear collisions." In: *arXiv preprint nucl-th/9804026* (1998).

[20] Golan Bel and Frank LH Brown. "Theory for wavelength-resolved photon emission statistics in single-molecule fluorescence spectroscopy." In: *Physical review letters* 102.1 (2009), p. 018303.

[21] David Bohm. *Quantum theory*. Courier Corporation, 1951.

[22] T Boulier, M Bamba, A Amo, C Adrados, A Lemaitre, E Galopin, I Sagnes, J Bloch, C Ciuti, E Giacobino, et al. "Polariton-generated intensity squeezing in semiconductor micropillars." In: *Nature communications* 5 (2014).

[23] Eric Brannen and Harry IS Ferguson. "The question of correlation between photons in coherent light rays." In: (1956).

[24] R Hanbury Brown. *Boffin: a personal story of the early days of radar, radio astronomy and quantum optics*. CRC Press, 1991.

[25] R Hanbury Brown and Richard Q Twiss. "LXXIV. A new type of interferometer for use in radio astronomy." In: *The London, Edinburgh, and Dublin Philosophical Magazine and Journal of Science* 45.366 (1954), pp. 663–682.

[26] Sonia Buckley, Kelley Rivoire, and Jelena Vučković. "Engineered quantum dot single-photon sources." In: *Reports on Progress in Physics* 75.12 (2012), p. 126503.

[27] Tim Byrnes, Kai Yan, and Yoshihisa Yamamoto. "Accelerated optimization problem search using Bose–Einstein condensation." In: *New Journal of Physics* 13.11 (2011), p. 113025.

[28] H Cao, Y Ling, J.Y Xu, and C.Q Cao. "Photon statistics of random lasers with resonant feedback." In: *Physical Review Letters* 86.20 (2001), pp. 4524–4527. URL: doi:10.1103/PhysRevLett.86.4524.

[29] I. Carusotto and C. Ciuti. "Probing Microcavity Polariton Superfluidity through Resonant Rayleigh Scattering." In: *Physical review letters* 93 (2004), p. 166401. URL: doi:10.1103/PhysRevLett.93.166401.

[30] EA Cerda-Méndez, D Sarkar, DN Krizhanovskii, SS Gavrilov, K Biermann, MS Skolnick, and PV Santos. "Exciton-polariton gap solitons in two-dimensional lattices." In: *Physical review letters* 111.14 (2013), p. 146401.

[31] S. Christopoulos et al. "Room-Temperature Polariton Lasing in Semiconductor Microcavities." In: *Physical review letters* 98 (2007), p. 126405. URL: doi:10.1103/PhysRevLett.98.126405.

[32] P Cilibrizzi, H Ohadi, T Ostatnicky, A Askitopoulos, W Langbein, and P Lagoudakis. "Linear wave dynamics explains observations attributed to dark solitons in a polariton quantum fluid." In: *Physical review letters* 113.10 (2014), p. 103901.

[33] David Colas, Lorenzo Dominici, Stefano Donati, Anastasiia A Pervishko, Timothy CH Liew, Ivan A Shelykh, Dario Ballarini, Milena De Giorgi, Alberto Bramati, Giuseppe Gigli, et al. "Polarization shaping of Poincaré beams by polariton oscillations." In: *Light: Science & Applications* 4.11 (2015), e350.

[34] JD Cresser. "Intensity correlations of frequency-filtered light fields." In: *Journal of Physics B: Atomic and Molecular Physics* 20.18 (1987), p. 4915.

[35] Frederick W Cummings. "Reminiscing about thesis work with ET Jaynes at Stanford in the 1950s." In: *Journal of Physics B: Atomic, Molecular and Optical Physics* 46.22 (2013), p. 220202.

[36] J Dalibard and S Reynaud. "Correlation signals in resonance fluorescence: interpretation via photon scattering amplitudes." In: *Journal de Physique* 44.12 (1983), pp. 1337–1343.

[37] Lloyd M Davis and Christian Parigger. "Use of streak camera for time-resolved photon counting fluorimetry." In: *Measurement Science and Technology* 3.1 (1992), p. 85.

[38] SS Demirchyan, I Yu Chestnov, AP Alodjants, MM Glazov, and AV Kavokin. "Qubits based on polariton Rabi oscillators." In: *Physical review letters* 112.19 (2014), p. 196403.

[39] Hui Deng, Hartmut Haug, and Yoshihisa Yamamoto. "Exciton-polariton bose-einstein condensation." In: *Reviews of modern physics* 82.2 (2010), p. 1489.

[40] JH Eberly and K Wodkiewicz. "The time-dependent physical spectrum of light." In: *JOSA* 67.9 (1977), pp. 1252–1261.

[41] A. Einstein. "Über einen die Erzeugung und Verwandlung des Lichtes betreffenden heuristischen Gesichtspunkt." In: *Annalen der Physik* 322 (1905), pp. 132–148. DOI: 10.1002/andp.19053220607.

[42] Albert Einstein, Boris Podolsky, and Nathan Rosen. "Can quantum-mechanical description of physical reality be considered complete?" In: *Physical review* 47.10 (1935), p. 777.

[43] Alessandro Fedrizzi, Thomas Herbst, Andreas Poppe, Thomas Jennewein, and Anton Zeilinger. "A wavelength-tunable fiber-coupled source of narrowband entangled photons." In: *Optics Express* 15.23 (2007), pp. 15377–15386.

[44] H Flayac, DD Solnyshkov, IA Shelykh, and G Malpuech. "Transmutation of Skyrmions to Half-Solitons Driven by the Nonlinear Optical Spin Hall Effect." In: *Physical review letters* 110.1 (2013), p. 016404.

[45] T Gao, E Estrecho, KY Bliokh, TCH Liew, MD Fraser, S Brodbeck, M Kamp, C Schneider, Sven Höfling, Y Yamamoto, et al. "Observation of non-Hermitian degeneracies in a chaotic exciton-polariton billiard." In: *Nature* 526.7574 (2015), pp. 554–558.

[46] Dario Gerace, Hakan E Türeci, Atac Imamoglu, Vittorio Giovannetti, and Rosario Fazio. "The quantum-optical Josephson interferometer." In: *Nature Physics* 5.4 (2009), pp. 281–284.

[47] C. C. Gerry and P. L. Knight. *Introductory Quantum Optics*. Cambridge University Press, 2005.

[48] RJ Glauber. "C. deWitt, A. Blandin, C. Cohen-Tannoudji." In: *Quantum Optics and Electronics, Gordon and Breach, New York* (1964), p. 63.

[49] Roy J Glauber. "Coherent and incoherent states of the radiation field." In: *Physical Review* 131.6 (1963), p. 2766.

[50] Roy J Glauber. "The quantum theory of optical coherence." In: *Physical Review* 130.6 (1963), p. 2529.

[51] Roy J Glauber. "Nobel Lecture: One hundred years of light quanta." In: *Reviews of modern physics* 78.4 (2006), p. 1267.

[52] A. González-Tudela, F. P. Laussy, C. Tejedor, M. J Hartmann, and E. del Valle. "Two-photon spectra of quantum emitters." In: *New journal of physics* 15 (2013), p. 033036. URL: doi:10.1088/1367-2630/15/3/033036.

[53] JW Goodman. *Statistical Optics, ch. 5*. New York: John Wiley and Sons, 1985.

[54] Robert H Hadfield. "Single-photon detectors for optical quantum information applications." In: *Nature photonics* 3.12 (2009), pp. 696–705.

[55] R. Hanbury Brown, R. C. Jennison, and M. K. Das Gupta. "Apparent Angular Sizes of Discrete Radio Sources: Observations at Jodrell Bank, Manchester." In: *Nature* 170 (1952), p. 1061. URL: doi:10.1038/1701061a0.

[56] R. Hanbury Brown and R. Q. Twiss. "A Test of a New Type of Stellar Interferometer on Sirius." In: *Nature* 178 (1956), p. 1046. URL: doi:10.1038/1781046a0.

[57] R. Hanbury Brown and R. Q. Twiss. "Correlation between Photons in two Coherent Beams of Light." In: *Nature* 177 (1956), p. 27. URL: doi:10.1038/177027a0.

[58] R Hivet, H Flayac, DD Solnyshkov, D Tanese, T Boulier, D Andreoli, E Giacobino, J Bloch, A Bramati, G Malpuech, et al. "Half-solitons in a polariton quantum fluid behave like magnetic monopoles." In: *Nature Physics* 8.10 (2012), pp. 724–728.

[59] R. Horodecki, P. Horodecki, M. Horodecki, and K. Horodecki. "Quantum entanglement." In: *Review modern physics* 81 (2009), p. 865. URL: doi:10.1103/RevModPhys.81.865.

[60] Daniel FV James, Paul G Kwiat, William J Munro, and Andrew G White. "Measurement of qubits." In: *Physical Review A* 64.5 (2001), p. 052312.

[61] BE Kardynał, ZL Yuan, and AJ Shields. "An avalanche‐ photodiode-based photon-number-resolving detector." In: *Nature photonics* 2.7 (2008), pp. 425–428.

[62] Torsten Karzig, Charles-Edouard Bardyn, Netanel H Lindner, and Gil Refael. "Topological polaritons." In: *Physical Review X* 5.3 (2015), p. 031001.

[63] J. Kasprzak et al. "Bose–Einstein condensation of exciton polaritons." In: *Nature* 443 (2006), p. 409. URL: doi:10.1038/nature05131.

[64] J. Kasprzak, M. Richard, A. Baas, B. Deveaud, R. André, J.-Ph. Poizat, and Le Si Dang. "Second-Order Time Correlations within a Polariton Bose–Einstein Condensate in a CdTe Microcavity." In: *Physical review letters* 100 (2008), p. 067402. URL: doi:10.1103/PhysRevLett.100.067402.

[65] A. Kavokin, J. J. Baumberg, G. Malpuech, and F. P. Laussy. *Microcavities*. 2nd ed. 2011.

[66] Alexey Kavokin, Guillaume Malpuech, and Fabrice P Laussy. "Polariton laser and polariton superfluidity in microcavities." In: *Physics Letters A* 306.4 (2003), pp. 187–199.

[67] Alexey Kavokin, Jeremy J Baumberg, Guillaume Malpuech, and Fabrice P Laussy. *Microcavities*. Vol. 16. OUP Oxford, 2011.

[68] KV Kheruntsyan, J-C Jaskula, P Deuar, Marie Bonneau, Guthrie B Partridge, Josselin Ruaudel, Raphaël Lopes, Denis Boiron, and Christoph I Westbrook. "Violation of the Cauchy-Schwarz inequality with matter waves." In: *Physical review letters* 108.26 (2012), p. 260401.

[69] S. Kim, B. Zhang, Z. Wang, J. Fischer, S. Brodbeck, M. Kamp, C. Schneider, S. Höfling, and H. Deng. "Coherent Polariton Laser." In: *Physical review x* 6 (2016), p. 011026. URL: doi:10.1103/PhysRevX.6.011026.

[70] M Kira, F Jahnke, Stephan W Koch, JD Berger, DV Wick, TR Nelson Jr, Galina Khitrova, and HM Gibbs. "Quantum theory of nonlinear semiconductor microcavity luminescence explaining "Boser" experiments." In: *Physical review letters* 79.25 (1997), p. 5170.

[71] L Knoll, G Weber, and T Schafer. "Theory of time-resolved correlation spectroscopy and its application to resonance fluorescence radiation." In: *Journal of Physics B: Atomic and Molecular Physics* 17.24 (1984), p. 4861.

[72] M. Koch, C. Sames, M. Balbach, H. Chibani, A. Kubanek, K. Murr, T. Wilk, and G. Rempe. "Three-Photon Correlations in a Strongly Driven Atom-Cavity System." In: *Physical review letters* 107 (2011), p. 023601. URL: doi:10.1103/PhysRevLett.107.023601.

[73] P. G. Kwiat, K. Mattle, H. Weinfurter, A. Zeilinger, A. V. Sergienko, and Y. Shih. "New High-Intensity Source of Polarization-Entangled Photon Pairs." In: *Physical review letters* 75 (1995), p. 4337. URL: doi:10.1103/PhysRevLett.75.4337.

[74] O Kyriienko and TCH Liew. "Exciton-polariton quantum gates based on continuous variables." In: *Physical Review B* 93.3 (2016), p. 035301.

[75] KG Lagoudakis, T Ostatnickỳ, AV Kavokin, Yuri G Rubo, Régis André, and Benoit Deveaud-Plédran. "Observation of half-quantum vortices in an exciton-polariton condensate." In: *Science* 326.5955 (2009), pp. 974–976.

[76] Konstantinos G Lagoudakis, Michiel Wouters, Maxime Richard, Augustin Baas, Iacopo Carusotto, Regis André, Le Si Dang, and B Deveaud-Plédran. "Quantized vortices in an exciton–polariton condensate." In: *Nature Physics* 4.9 (2008), pp. 706–710.

[77] Y Li, G Li, YC Zhang, XY Wang, J Zhang, JM Wang, and TC Zhang. "Effects of counting rate and resolution time on a measurement of the intensity correlation function." In: *Physical Review A* 76.1 (2007), p. 013829.

[78] T. C. H. Liew and V. Savona. "Single Photons from Coupled Quantum Modes." In: *Physical review letters* 104 (2010), p. 183601. URL: doi:10.1103/PhysRevLett.104.183601.

[79] TCH Liew and V Savona. "Multipartite polariton entanglement in semiconductor microcavities." In: *Physical Review A* 84.3 (2011), p. 032301.

[80] TCH Liew, IA Shelykh, and G Malpuech. "Polaritonic devices." In: *Physica E: Low-dimensional Systems and Nanostructures* 43.9 (2011), pp. 1543–1568.

[81] Rodney Loudon. *The quantum theory of light*. Oxford university press, 2000.

[82] MS Minsky, M White, and EL Hu. "Room-temperature photoenhanced wet etching of GaN." In: *Applied physics letters* 68.11 (1996), pp. 1531–1533.

[83] Bruce Moision and William Farr. "Communication limits due to photon detector jitter." In: *IEEE Photonics Technology Letters* 20.9 (2008), pp. 715–717.

[84] C Sánchez Muñoz, Elena del Valle, Carlos Tejedor, and Fabrice P Laussy. "Violation of classical inequalities by photon frequency filtering." In: *Physical Review A* 90.5 (2014), p. 052111.

[85] AV Nalitov, DD Solnyshkov, and G Malpuech. "Polariton Z topological insulator." In: *Physical review letters* 114.11 (2015), p. 116401.

[86] AV Nalitov, G Malpuech, H Terças, and DD Solnyshkov. "Spin-orbit coupling and the optical spin hall effect in photonic graphene." In: *Physical review letters* 114.2 (2015), p. 026803.

[87] R Centeno Neelen, DM Boersma, MP Van Exter, G Nienhuis, and JP Woerdman. "Spectral filtering within the Schawlow-Townes linewidth as a diagnostic tool for studying laser phase noise." In: *Optics communications* 100.1 (1993), pp. 289–302.

[88] Gerard Nienhuis. "Spectral correlations in resonance fluorescence." In: *Physical Review A* 47.1 (1993), p. 510.

[89] SJ Pearton, WS Hobson, FA Baiocchi, AB Emerson, and KS Jones. "Reactive ion etching of InP, InGaAs, InAlAs: comparison of C2H6/H2 with CCl2F2/O2." In: *Journal of Vacuum Science & Technology B* 8.1 (1990), pp. 57–67.

[90] M. Peiris, B. Petrak, K. Konthasinghe, Y. Yu, Z. C. Niu, and A. Muller. "Two-color photon correlations of the light scattered by a quantum dot." In: *Physical review b* 91 (2015), p. 195125. URL: doi:10.1103/PhysRevB.91.195125.

[91] EM Purcell. "The question of correlation between photons in coherent light rays." In: *Nature* 178 (1956), pp. 1449–1450.

[92] Yuri G Rubo. "Half vortices in exciton polariton condensates." In: *Physical review letters* 99.10 (2007), p. 106401.

[93] A. Rundquist, M. Bajcsy, A. Majumdar, T. Sarmiento, K. Fischer, K. G. Lagoudakis, S. Buckley, A. Y. Piggott, and J. Vučković. "Nonclassical higher-order photon correlations with a quantum dot strongly coupled to a photonic-crystal nanocavity." In: *Physical review A* 90 (2014), p. 023846. URL: doi:10.1103/PhysRevA.90.023846.

[94] G. Sallen, A. Tribu, T. Aichele, R. André, L. Besombes, C. Bougerol, M. Richard, S. Tatarenko, K. Kheng, and J.-Ph. Poizat. "Subnanosecond spectral diffusion measurement using photon correlation." In: *Nature photonics* 4 (2010), p. 696.

[95] JJ Sanchez-Mondragon, NB Narozhny, and JH Eberly. "Theory of spontaneous-emission line shape in an ideal cavity." In: *Physical Review Letters* 51.7 (1983), p. 550.

[96] C. Sánchez Muñoz, E. del Valle, A. González Tudela, K. Müller, S. Lichtmannecker, M. Kaniber, C. Tejedor, J.J. Finley, and F.P. Laussy. "Emitters of N-photon bundles." In: *Nature photonics* 8 (2014), p. 550. URL: doi:10.1038/nphoton.2014.114.

[97] C. Sánchez Muñoz, E. del Valle, C. Tejedor, and F.P. Laussy. "Violation of classical inequalities by photon frequency filtering." In: *Physical review A* 90 (2014), p. 052111. URL: doi:10.1103/PhysRevA.90.052111.

[98] D Sanvitto, FM Marchetti, MH Szymańska, G Tosi, M Baudisch, FP Laussy, DN Krizhanovskii, MS Skolnick, L Marrucci, A Lemaitre, et al. "Persistent currents and quantized vortices in a polariton superfluid." In: *Nature Physics* 6.7 (2010), pp. 527–533.

[99] P. G. Savvidis, J. J. Baumberg, R. M. Stevenson, M. S. Skolnick, D. M. Whittaker, and J. S. Roberts. "Angle-Resonant Stimulated Polariton Amplifier." In: *Physical Review Letters* 84 (2000), p. 1547.

[100] C. Schneider et al. "An electrically pumped polariton laser." In: *Nature* 497 (2013), p. 348. URL: doi:10.1038/nature12036.

[101] F. Selleri. *Quantum Paradoxes and Physical Reality*. Springer Netherlands, 1990.

[102] I Shelykh, KV Kavokin, AV Kavokin, Guillaume Malpuech, Pierre Bigenwald, H Deng, G Weihs, and Y Yamamoto. "Semiconductor microcavity as a spin-dependent optoelectronic device." In: *Physical Review B* 70.3 (2004), p. 035320.

[103] M Sich, DN Krizhanovskii, MS Skolnick, Andriy V Gorbach, Robin Hartley, Dmitry V Skryabin, EA Cerda-Méndez, K Biermann, R Hey, and PV Santos. "Observation of bright polariton solitons in a semiconductor microcavity." In: *Nature photonics* 6.1 (2012), pp. 50–55.

[104] J Michael Steele. *The Cauchy-Schwarz master class: an introduction to the art of mathematical inequalities*. Cambridge University Press, 2004.

[105] WL Steiger. "On a generalization of the Cauchy-Schwarz inequality." In: *The American Mathematical Monthly* 76.7 (1969), pp. 815–816.

[106] David Stoler. "Photon antibunching and possible ways to observe it." In: *Physical Review Letters* 33.23 (1974), p. 1397.

[107] Damien Stucki, Grégoire Ribordy, André Stefanov, Hugo Zbinden, John G Rarity, and Tom Wall. "Photon counting for quantum key distribution with Peltier cooled InGaAs/InP APDs." In: *Journal of modern optics* 48.13 (2001), pp. 1967–1981.

[108] C Sturm, D Tanese, HS Nguyen, H Flayac, E Galopin, A Lemaître, I Sagnes, D Solnyshkov, A Amo, G Malpuech, et al. "All-optical phase modulation in a cavity-polariton Mach–Zehnder interferometer." In: *Nature communications* 5 (2014).

[109] D Tanese, H Flayac, D Solnyshkov, A Amo, A Lemaître, E Galopin, R Braive, P Senellart, I Sagnes, G Malpuech, et al. "Polariton condensation in solitonic gap states in a one-dimensional periodic potential." In: *Nature communications* 4 (2013), p. 1749.

[110] Malvin Carl Teich and Bahaa EA Saleh. "Effects of random deletion and additive noise on bunched and antibunched photon-counting statistics." In: *Optics letters* 7.8 (1982), pp. 365–367.

[111] H Terças, DD Solnyshkov, and G Malpuech. "Topological Wigner Crystal of Half-Solitons in a Spinor Bose-Einstein Condensate." In: *Physical review letters* 110.3 (2013), p. 035303.

[112] H Terças, H Flayac, DD Solnyshkov, and G Malpuech. "Non-Abelian gauge fields in photonic cavities and photonic superfluids." In: *Physical review letters* 112.6 (2014), p. 066402.

[113] SM Ulrich, C Gies, S Ates, J Wiersig, S Reitzenstein, C Hofmann, A Löffler, A Forchel, F Jahnke, and P Michler. "Photon statistics of semiconductor microcavity lasers." In: *Physical review letters* 98.4 (2007), p. 043906.

[114] E. del Valle. "Distilling one, two and entangled pairs of photons from a quantum dot with cavity QED effects and spectral filtering." In: *New journal of physics* 15 (2013), p. 025019. URL: doi:10.1088/1367-2630/15/2/025019.

[115] E. del Valle, A. González-Tudela, F. P. Laussy, C. Tejedor, and M. J. Hartmann. "Theory of Frequency-Filtered and Time-Resolved N-Photon Correlations." In: *Physical review letters* 109 (2012), p. 183601. URL: doi:10.1103/PhysRevLett.109.183601.

[116] A. Verger, C. Ciuti, and I. Carusotto. "Polariton quantum blockade in a photonic dot." In: *Physical review b* 73 (2006), p. 193306. URL: 10.1103/PhysRevB.73.193306.

[117] PM Walker, L Tinkler, DV Skryabin, A Yulin, B Royall, I Farrer, DA Ritchie, MS Skolnick, and DN Krizhanovskii. "Ultra-low-power hybrid light-matter solitons." In: *Nature communications* 6 (2015).

[118] Roald K Wangsness. "Electromagnetic fields." In: *Electromagnetic Fields, 2nd Edition, by Roald K. Wangsness, pp. 608. ISBN 0-471-81186-6. Wiley-VCH, July 1986.* (1986), p. 608.

[119] C. Weisbuch, M. Nishioka, A. Ishikawa, and Y. Arakawa. "Observation of the coupled exciton-photon mode splitting in a semiconductor quantum microcavity." In: *Physical review letters* 69 (1992), p. 3314. URL: doi:10.1103/PhysRevLett.69.3314.

[120] J. Wiersig et al. "Direct observation of correlations between individual photon emission events of a microcavity laser." In: *Nature* 460 (2009), p. 245. URL: doi:10.1038/nature08126.

[121] Li Yuan, Zhang Yu-Chi, Zhang Peng-Fei, Guo Yan-Qiang, Li Gang, Wang Jun-Min, and Zhang Tian-Cai. "Experimental study on coherence time of a light field with single photon counting." In: *Chinese Physics Letters* 26.7 (2009), p. 074205.

[122] ZL Yuan, BE Kardynal, AW Sharpe, and AJ Shields. "High speed single photon detection in the near-infrared." In: *arXiv preprint arXiv:0707.4307* (2007).

[123] Y. Zhu, D. J. Gauthier, S. E. Morin, Q. Wu, H. J. Carmichael, and T. W. Mossberg. "Vacuum Rabi splitting as a feature of linear-dispersion theory: Analysis and experimental observations." In: *Physical review letters* 64 (1990), p. 2499. URL: doi:10.1103/PhysRevLett.64.2499.

PUBLICATIONS

[1] Álvaro Cuevas*, Blanca Silva*, Juan Camilo López Carreño, Milena de Giorgi, Carlos Sánchez Muñoz, Antonio Fieramosca, Daniel Gustavo Suárez Forero, Filippo Cardano, Lorenzo Marrucci, Vittorianna Tasco, et al. "Entangling a polariton with one photon: effect of interactions at the single-particle level." In: *arXiv preprint arXiv:1609.01244* (2016).

[2] L Dominici, M Petrov, M Matuszewski, D Ballarini, M De Giorgi, D Colas, E Cancellieri, B Silva Fernández, A Bramati, G Gigli, et al. "Real-space collapse of a polariton condensate." In: *Nature communications* 6 (2015).

[3] Jorge Quereda, Marina Ramón, Blanca Silva, Juan José Hinarejos, José Gabriel Rodrigo, and Daniel Farías. "Calibrating the frequency of tuning forks by means of Lissajous figures." In: *American Journal of Physics* 79.5 (2011), pp. 517–520.

[4] B Silva, RF Luccas, NM Nemes, J Hanko, MR Osorio, P Kulkarni, F Mompean, M Garcia-Hernandez, MA Ramos, S Vieira, et al. "Superconductivity and magnetism on flux-grown single crystals of NiBi 3." In: *Physical Review B* 88.18 (2013), p. 184508.

[5] B Silva, C Sánchez Muñoz, A González Tudela, D Ballarini, G Gigli, KW West, L Pfeiffer, E del Valle, D Sanvitto, and FP Laussy. "The colored Hanbury Brown–Twiss effect." In: *Accepted in Scientific Reports* (2016).

FORMATION AND RESEARCH ACTIVITIES

TALKS

- **Italian National Conference on Condensed Matter Physics (FisMat 2015), Palermo** Talk titled *"Measuring photon correlations simultaneously in time and frequency "*.
- **International Conference on the Physics of Semiconductors (ICPS 2014), Austin (Texas)** Talk titled *"Propagation of polariton wavepackets"*.
- **International Conference on Physics of Light-Matter Coupling in Nanostructures (PLMCN 2014), Montpellier** Talk titled *"Photon antibunching from a condensate of exciton-polaritons"*.

POSTERS

- **Third International Conference on Quantum Technologies (ICQT 2015), Moscow** Poster presentation titled *"Measuring photon correlations in time and frequency"*
- **International Conference on the Physics of Semiconductors (ICPS 2014), Austin (Texas)** Poster presentation titled *"Colored photon antibunching from a condensate of exciton-polaritons"*.

TEACHING

- 12 hours teaching the lessons of "Técnicas experimentales" ("Experimental techniques") for students on first year of chemistry.